Localized turbulence in pipe flow

Localized turbulence in pipe flow

PROEFSCHRIFT

ter verkrijging van de graad van doctor
aan de Technische Universiteit Delft,
op gezag van de Rector Magnificus prof. ir. K.C.A.M. Luyben,
voorzitter van het College voor Promoties,
in het openbaar te verdedigen op dinsdag 6 december 2011 om 10:00 uur

door

Dirk Jan KUIK
ingenieur luchtvaart en ruimtevaart
geboren te Franeker.

Dit proefschrift is goedgekeurd door de promotor:
Prof. dr. ir. J. Westerweel

Samenstelling promotiecommissie:

Rector Magnificus,	voorzitter	
Prof. dr. ir. J. Westerweel,	Technische Universiteit Delft,	promotor
Prof. dr. rer. nat. B. Eckhardt,	Universität Marburg,	promotor
Prof. dr. ir. F. Scarano,	Technische Universiteit Delft	
Prof. dr. J.G.M. Kuerten,	Technische Universiteit Eindhoven	
Prof. dr. ir. W. van der Water,	Technische Universiteit Eindhoven	
Prof. dr. A. Doelman,	Universiteit Leiden	
Prof. dr. D. Barkley,	University of Warwick	

This work is part of the research programme of the Foundation for Fundamental Research on Matter (FOM), which is part of the Netherlands Organisation for Scientific Research (NWO).

Contents

Summary

Localized turbulence in pipe flow In many industrial applications the main process is an interlinked set of pipes through which the processing fluids are flowing. The pipes are used to transport liquids from one place to another, to mix and separate fluids or heat the fluid. The efficiency of these processes depends strongly on the flow state in the pipe. To transport a certain amount of liquid in the laminar flow state is less energy demanding than transporting the same amount of fluid at turbulent flow conditions. On the other hand, heat transfer is much more efficient in the turbulent regime.

The transition from one state to the other in pipe flow is one of the long lasting questions in research. Since the first systematic and clearly described experiments by Reynolds (1883), much research has been dedicated to this subject. Mathematical analysis of the governing equations has led to the belief that the laminar velocity profile is linearly stable (Drazin and Reid 2004). This statement has been proven to hold up to $Re = 10^7$ by a numerical simulation (Meseguer and Trefethen 2003). Nevertheless, in most practical situations transition to turbulence is already observed around $Re \approx 2000$. However, by carefully designing the flow facility, the flow in a pipe can be kept laminar up to very high Reynolds numbers ($Re = O(10^5)$, Draad (1996)). This confirms that a finite amplitude disturbance is required to trigger the transition to turbulence and that the flow becomes more sensitive to perturbations as the Reynolds number is increased. When a carefully designed flow facility is used, i.e. a flow facility is used in which the natural transition to turbulence is postponed beyond $Re = O(10^4)$, the facility can be used to investigate the transition to turbulence. Darbyshire and Mullin (1995) and Hof et al. (2003), amongst others, used such a facility to investigate the minimum amplitude necessary to trigger the transition to turbulence. This critical amplitude decreases with increasing Reynolds number. How the applied localized disturbance develops downstream depends on the Reynolds number. The initiated turbulent region can remain localized, break up in multiple patches or grow continuously downstream.

This study focuses on the regime where a large amplitude localized disturbance, which is applied for a very short duration, results in a single localized turbulent patch. This localized turbulent patch is known as a puff. At low Reynolds numbers puffs are able to survive over a limited distance. As the Reynolds number increases, the characteristic lifetime of these puffs increases. The scaling of the lifetime with Reynolds number gives an indication whether the turbulent flow state can be considered a repeller or an attractor. When the turbulent flow state would be an attractor, the flow is not able to return to the laminar flow state naturally. However, when the

turbulent flow state would be a repeller, the flow will eventually return to the laminar flow state. This difference has an enormous impact on the possibility for flow control of turbulent pipe flow. When the turbulent flow state is a repeller, only a minor modification of the turbulent flow state can force it on a trajectory towards the laminar flow state. Hence, the options for flow control are much more promising than when the flow state would be a turbulent attractor.

To determine the proper scaling of the transition to turbulence a large number of experiments were conducted. In the first set of experiments the flow was perturbed and then the flow state was determined at different downstream locations. The resulting statistics were then used to determine the proper lifetime scaling. One of the major issues with the methods used so far was that it was unknown whether the disturbance was successfully applied. Moreover, the flow state was often determined by *visual* inspection of the flow. Therefore the results might be influenced by the observer. In order to remove this uncertainty, a different method has been used to determine the lifetime of each individual observation.

Pressure drop measurements were used to detect the presence of a puff. The presence of a puff causes a slightly larger pressure drop when present in the section covered by the pressure transducers. If the puff decays within the section covered by the pressure transducers, the pressure level relaxes to the level without a puff present. This allows for an objective and quantitative determination of the lifetime of that particular puff. Moreover, the generation of the disturbance is clearly sensed by the pressure measurement devices. After determining the lifetimes of the individual puffs quantitatively, the characteristic lifetime were extracted. It is shown that the proper scaling for the turbulent flow state is that of a repeller. Note however, that at higher Reynolds numbers the localized turbulent structures are able to split and a completely different model may be needed to properly describe the transition to turbulence.

After determining the life times of puffs, the question emerged about what is happening in more detail inside the puff. What mechanism is responsible for the puff to exist for long times and then suddenly ceases to exist? What forces act on a puff, such that it remains localized? What happens when the puff splits and why does it split instead of growing slightly? In order to find answers to these questions a direct numerical simulation was initiated. As initial condition for the simulation a puff was used that was measured using stereoscopic particle image velocimetry (see van Doorne and Westerweel (2007) for an overview of this measurement method). Another motivation for the simulation was the observation of small scale structures in the experiments, which had not been described in previous numerical simulations (van Doorne and Westerweel 2009). By using a high resolution numerical simulation, the small scale structures could be resolved.

The numerical simulations allowed for the determination of different characteristics of the puffs. The mean convection velocity of the puffs turned out to be in excellent agreement with experimental observations. However, the instantaneous velocity of the puff is not constant. Moreover, it is shown that the instantaneous velocity of the puff is correlated with the total amount of energy excluding the energy contained in the axial motion of the fluid in the pipe. The trend of the correlation can be predicted by obtaining the energy flux over a control volume that contains the transition front. The control volume is convecting with the transition front. As the velocity of the

transition front decreases, the amount of energy that becomes available from the laminar velocity profile increases. The additional energy has to be dissipated to maintain an energy equilibrium. This can be done, either by increasing the turbulence intensity, or by increasing the amount of fluid that is turbulent. At low Reynolds numbers, i.e. when puff splitting is not present, the first scenario is observed. The fluctuation level increases as the velocity of the puff decreases and visa versa. At higher Reynolds numbers, in this case at $Re = 2300$, puff splitting is observed. The velocity of the newly generated structure is higher than that of the mother puff, and indeed the observed velocity fluctuation level is also lower compared to the mother structure. This confirms the relation between internal energy level of a puff and its velocity.

The direct numerical simulation was also used to follow the small structures first identified by van Doorne and Westerweel (2009) over time. It turns out that the structures move with a higher velocity than the puff itself and thus travel *through* the puff. Although van Doorne and Westerweel (2009) related the small scale structures to hairpin vortices, this could not be confirmed by the results from the present simulation. The small-scale structures seem to be created by large scale vortical structures that are oriented normal to the pipe axis and extend over almost over the entire diameter of the pipe.

Although it has been shown that there exists a strong relation between the velocity of a puff and its total energy content, the reason for the puff to remain localized has not been revealed. Furthermore, in literature different driving mechanisms for the puff are proposed and it would be worthwhile to assess the relevance of the structures travelling through the puff to the driving process, both numerically and experimentally.

Samenvatting

Gelokaliseerde turbulentie in pijpstromingen In veel industriële faciliteiten bestaat het hoofdproces uit een aantal verbonden pijpen waardoor procesvloeistoffen stromen. De pijpen worden gebruikt om vloeistoffen te transporteren, om verschillende vloeistoffen te mengen of om vloeistoffen te verhitten. De efficiëntie van deze processen hangt sterk af van de stromingstoestand in de pijp. Om een bepaalde hoeveelheid vloeistof te transporteren kost minder energie wanneer de stroming in de pijp laminair is vergeleken met wanneer het turbulent is. Aan de andere kant, warmte overdracht is weer veel efficiënter voor een turbulente stroming.

De oorzaken naar de omslag naar turbulentie in pijpstroming is een van de laatste onbeantwoorde vragen in de stromingsleer. Sinds de eerste experimenten van Reynolds (1883) is veel onderzoek gewijd aan het beantwoorden van deze vraag. Theoretische beschouwing van de bewegingsvergelijkingen heeft geleid tot de overtuiging dat het laminaire snelheidsprofiel lineair stabiel is. Meseguer and Trefethen (2003) hebben bewezen dat deze beweringen juist zijn voor Reynolds getallen tot $Re = 10^7$. Desalniettemin treedt de omslag naar turbulentie in de meeste praktische situaties al op rond $Re \approx 2000$. Echter, wanneer de experimentele faciliteiten met veel zorg ontworpen worden kan transitie uitgesteld worden tot zeer hoge Reynolds getallen ($Re = O(10^5)$, Draad (1996)). Hieruit kan worden geconcludeerd dat een verstoring met een eindige amplitude nodig is om de omslag naar turbulentie te initiëren en dat de stroming gevoeliger wordt voor verstoringen naarmate het Reynolds getal verhoogd wordt. Wanneer een goed ontworpen faciliteit wordt gebruikt, een faciliteit waarin natuurlijke transitie niet optreed voor Reynolds getallen lager dan $O(10^4)$, kan deze worden gebruikt voor het onderzoek naar transitie naar turbulentie. Onder ander Darbyshire and Mullin (1995) en Hof et al. (2003) hebben een dergelijke faciliteit gebruikt om de minimale amplitude te bepalen die nodig is om de transitie naar turbulentie te initiëren. Deze amplitude neemt af met toenemend Reynolds getal. Afhankelijk van het Reynolds getal blijft de gecreëerde turbulentie beperkt tot een klein gebied (gelokaliseerde turbulentei), breekt op in meerdere gelokaliseerde stukken of blijft continu groeien.

Dit proefschrift richt zich op het regime waar een grote gelokaliseerde verstoring wordt aangebracht voor een korte tijd. Zon verstoring resulteert in een gelokaliseerd gebied met turbulentie. Een gelokaliseerd gebied waarvan de lengte constant blijft staat bekend als een puff. Bij lage Reynoldsgetallen zijn puffs in staat over een korte afstand te overleven. Wanneer het Reynoldsgetal wordt verhoogd neemt de karakteristieke levensduur van puffs toe. De schaling van de levensduur met het Reynoldsgetal geeft aan of de turbulente toestand kan worden beschouwt als een repeller of een attractor. Wanneer de turbulente toestand een attractor zou zijn, is de stroming

niet in staat om op natuurlijke wijze terug te keren naar de laminaire toestand. Echter wanneer de turbulente toestand een repeller zou zijn, zal de stroming uiteindelijk altijd terugkeren naar de laminaire toestand. Dit verschil heeft enorme gevolgen voor de mogelijkheden om turbulente pijpstroming te beïnvloeden. Wanneer de turbulente stromingstoestand een repeller is, kan een kleine aanpassing van het stromingsveld ervoor zorgen dat de turbulente stromingstoestand op een traject kan worden gebracht richting de laminaire stromingstoestand. Dus de mogelijkheden voor een efficiënte manier om de stroming te beinvloeden zijn vele malen groter wanneer de turbulente toestand een repeller is dan wanneer de turbulente toestand een attractor is.

Om de juiste schaling van de transitie naar de turbulente toestand te bepalen zijn een groot aantal experimenten gedaan. In het de eerste experimentele campagne, werd op een aantal verschillende afstanden van het verstoringspunt bepaald of de stroming turbulent of laminair was. De statistieken die op deze manier zijn verkregen zijn gebruikt om de juiste schaling te bepalen. Echter, een van de grootste beperkingen van de methoden die tot dusver gebruikt zijn is dat het onbekend is of de verstoring daadwerkelijk toegepast was. Bovendien was de stromingstoestand bepaald door middel van visuele observatie door de experimentator. Hierdoor kunnen de resultaten beinvloed zijn door de verwachtingen van de experimentatoren. Om deze onzekerheden weg te nemen is een andere methode gebruikt om de statistieken van de levensduur te bepalen. Durkvalmetingen zijn gebruikt om te bepalen of een puff aanwezig was. De aanwezigheid van een puff zorgt voor een kleine toename in de gemeten drukval zolang de puff zich bevindt in de sectie waarover de drukval gemeten wordt. Wanneer een puff vervalt zal deze extra bijdrage verdwijnen. Dit fenomeen kan gebruikt worden om op een objectieve en kwantitatieve manier de levensduur van elke individuele puff te meten. Bovendien kan met behulp van de druksensoren bepaald worden of de verstoring daadwerkelijk toegepast is. Na het bepalen van de levensduur van de individuele puffs kan de karakteristieke levensduur afgeleid worden. Hiermee is bepaald dat de juiste omschrijving van de turbulente toestand die van een repeller is. Realiseer hierbij wel dat bij hogere Reynolds getallen puffs kunnen splitsen en een volledig ander model nodig zou kunnen zijn om de transitie naar turbulentie op een juiste manier te omschrijven.

Na het bepalen van de statistieken van de levensduur kwam de vraag naar boven wat er gebeurd in een puff. Welk mechanisme is verantwoordelijk voor het gedrag van puffs, dat ze voor lange tijd kunnen bestaan en dan plotseling desintegreren? Welke krachten werken er op een puff zodat deze gelokaliseerd blijft? Wat gebeurd er wanneer een puff splitst? Waarom splits een puff en groeit deze niet langzaam uit tot een iets grotere puff? Om een antwoord te vinden op deze vragen is een directe numerieke simulatie (DNS) opgezet. Als startconditie voor de simulatie is een stereoscopische PIV (particle image velocimetry, zie van Doorne and Westerweel (2007) voor een overzicht van deze meetmethode) meting gebruikt. Een extra motivatie voor de DNS was de observatie van kleinschalige structuren in experimenten die nog niet zijn beschreven in resultaten van numerieke simulaties (van Doorne and Westerweel 2007). Door gebruik te maken van een simulatie met een hoge resolutie, was het mogelijk om deze kleine structuren te simuleren.

Met behulp van de resultaten van de simulatie konden de karakteristieken van de puffs bepaald worden. De gemiddelde translatie snelheid van een gesimuleerde puff kwam perfect overeen

met de gegevens van experimentele observaties. Echter, de instantane snelheid is niet constant. Bovendien was de instantane snelheid van de puff sterk gecorreleerd met totale hoeveelheid energie in de puff wanneer de bijdrage van de axiale snelheidscomponent hier niet in meegenomen is. De trend van de correlatie tussen beschikbare energie en instantane puff snelheid kan worden voorspeld door de energie fluxen te beschouwen over een controle volume waarin het transitie front zich bevindt. Het controle volume heeft dezelfde snelheid als het transitie front in de puff. Wanneer de snelheid van het transitie front afneemt zal de hoeveelheid beschikbare energie toenemen. Deze energie zal moeten worden afgevoerd om aan de wet van behoud van energie te voldoen. Dit kan worden gedaan door of de turbulentie graad te verhogen of door de lengte van het turbulente gedeelte te verlengen. Bij lage Reynoldsgetallen, wanneer nog geen splitsende puffs aanwezig zijn, is het eerste scenario aanwezig. De turbulentiegraad in de puff neemt toe naarmate de snelheid van de puff afneemt en visa versa. Bij hogere Reynoldsgetallen, in dit geval bij $Re = 2300$, zijn splitsende puffs geobserveerd. De snelheid van de ontstane (tweede) puff is hoger dan die van de originele puff. De turbulentiegraad van deze nieuwe puff is lager dan die van de originele puff. Hiermee is de relatie tussen de snelheid van de puff en de hoeveel interne energie bevestigd.

De DNS is ook gebruikt om de kleinschalige structuren te volgen die als eerste beschreven zijn door van Doorne and Westerweel (2009). De kleinschalige structuren bewegen sneller dan de puff zelf en reizen daarom *door* de puff. Hoewel van Doorne and Westerweel (2009) deze kleinschalige structuren identificeerden als haarspeld wervels, kon dit beeld niet bevestigd worden met de resultaten van de huidige simulatie. De kleinschalige structuren lijken het gevolg te zijn van de aanwezigheid van een grote wervel die normaal op de pijp as staat en bijna over de gehele diameter van de pijp reikt.

Ondanks dat is aangetoond dat er een sterke relatie bestaat tussen de snelheid van een puff en zijn interne energie, is de drijvende kracht achter het gelokaliseerd blijven van de puff niet ontrafelt. Verder zijn in de literatuur verschillende aandrijfmechanismen omschreven voor de puff en het zou waardevol zijn om de relevantie van de kleinschalige structuren, die zich door de puff bewegen, verder te onderzoeken, zowel door middel van numerieke simulaties als experimenten.

Chapter 1

Introduction

In our daily life we experience flows all around us. Sometimes the flows around us are beneficial: for example when the toxic fumes of cars are mixed with surrounding air thereby reducing the concentration of toxic substances. On the other hand, when we travel by bike with a strong head wind, we do not appreciate the drag caused by the flow. Most of the time we are not even aware of these phenomena and the richness that is embedded in these flows. Occasionally the flow of air is visualized by snow or leafs, thereby suddenly revealing the richness of all the flows around us.

Reynolds (1883) was the first to identify that flows can be assigned to either one of two distinctive states: laminar and turbulent flows. This classification has been used ever since. Laminar flows move in a regular and smooth fashion, while the motion for turbulent flow is chaotic and irregular. The change of flow state, i.e. the change from laminar to turbulent, is called transition to turbulence. This is the main topic of this thesis.

In our own kitchen these flow states can easily be visualized using the tap whitout the aerator. By opening the tap by a small amount, the resulting jet of water reveals the first distinctive state. As the water leaves the tap the flow is very smooth: the flow is laminar. See the left part of figure 1.1 for an example. When the flow rate is increased, the flow from the tap is turbulent. The turbulent flow causes the surface of the jet to have an irregular shape.

Depending on the particular situation, either flow state is preferred. For example, when the flow is laminar the mixing of fluids and the heat transfer are driven by diffusion processes. In the turbulent state these processes are enhanced, because of the additional convective mixing, and are much more efficient. Therefore, a turbulent flow state is preferred when one wants to obtain and maintain a homogeneous mixture. However, the drawback of a turbulent flow is that the skinfriction increases. Hence, laminar flows are preferred when transporting large quantities of fluid over large distances as in gas or oil pipelines.

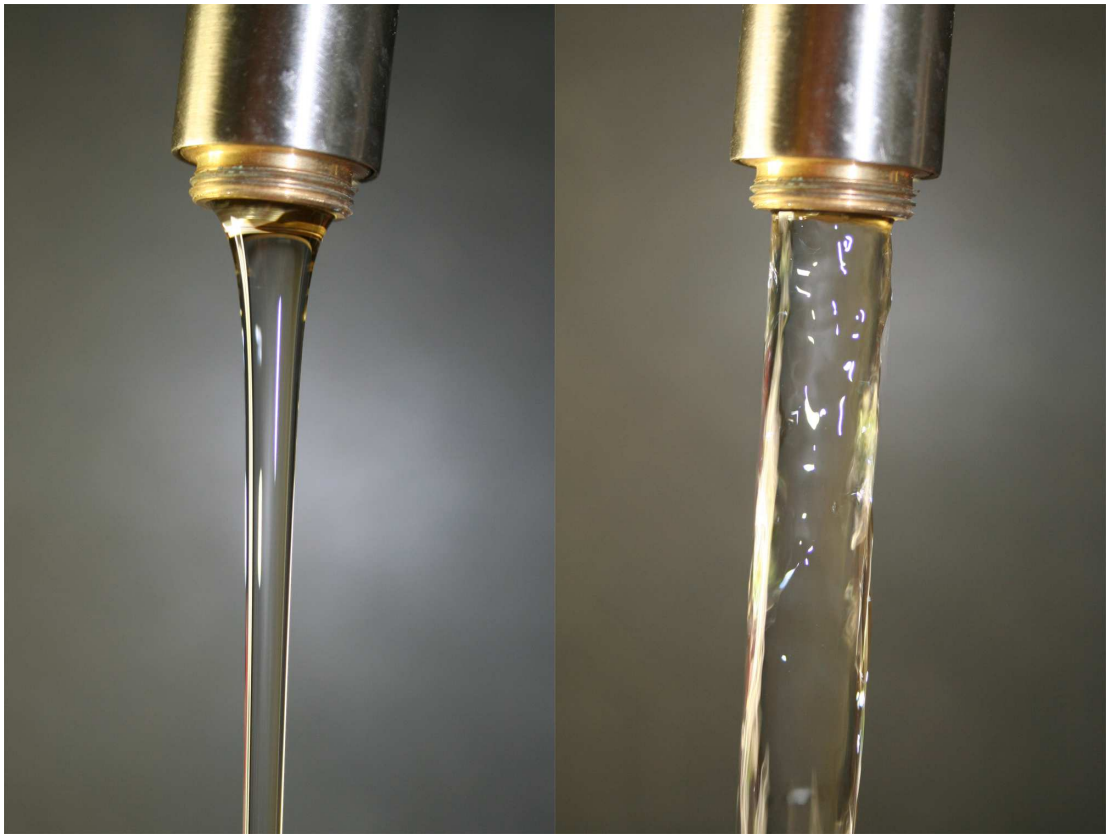

Figure 1.1: The flow of water from a tap in our kitchen: In the left part the flow shows a nice undeformed state. Here the fluid elements are all moving in parallel and this state is known as the laminar state. As the flow rate is increased, the flow becomes turbulent and irregular, random motion is observed.

1.1 Pipe flow

In figure 1.1 a free flow, i.e. the flow does not interact with a solid wall, was shown. Two distinct regimes could be identified. However, the difference between the two flows in figure 1.1 is caused by the flow *in* the tap. The first who clearly made the distinction between two separate flow regimes was Reynolds (1883) in pipe flow. His experimental setup consisted of a glass pipe in which water was flowing. The glass pipe allowed for optical access. The flow was visualized by carefully injecting dye at the centerline of the pipe. At low flow rates the dye remained a straight line at the center of the pipe. As the fluid velocity was increased, patches of mixed dye were observed. These patches were called flashes by Reynolds (1883). After further increasing the velocity, sudden transition was observed at a fixed location downstream of the entrance region. The dye downstream of the transition point was mixed over the entire diameter of the pipe. The point at which the transition occurs moved upstream with increasing flow rate. He found that the observed flow state depended on three independent variables. These could be arranged into a dimensionless number; which is nowadays known as the Reynolds number ($Re = u_{\text{bulk}}D/\nu$), where u_{bulk} is the mean or bulk velocity of the fluid, D a characteristic length scale, for a pipe this is the diameter and ν the viscosity of the fluid. In this early work it became already clear that the flow could be kept stable, i.e. laminar, for higher flow rates by minimizing the perturbations in the setup. In fact, Reynolds (1883) was able to obtain laminar flow up to $Re \approx 10^4$.

This fact has resulted in a quest to reveal the reason for the transition to a turbulent motion in a pipe. In the next sections the main topics of research are discussed in recent and not so recent years. It is categorized based on the research topic and therefore not chronological. The goal is to give a general overview of the research on the transition from laminar to turbulent flows in pipes. Although the transition process for flows of non-Newtonian liquids, which are fluids that do not show a linear relationship between the strass rate and strain rate, is important for industrial applications, only the flow of Newtonian fluids in straight pipes without swirl is considered in this thesis. For more information about the effect of non-Newtonian liquids on the transition process in pipe flow see the work of Draad (1996).

In engineering textbooks usually a *critical* Reynolds number is defined to differentiate between laminar and turbulent flow. Above this critical Reynolds number pipe flow should be considered turbulent. However, the value that should be considered as the critical Reynolds number is not consistent between textbooks and ranges typically between $Re = 2000$ and $Re = 2500$.

1.1.1 Linear stability

To determine if transition will occur for a typical flow, a classical approach in fluid mechanics is to perform a (linear) stability analysis. The response of the laminar base flow to an infinitesimal perturbation is studied. In the case of pipe flow, the base flow is found in the form of a parabolic velocity profile. This velocity profile is known as the Hagen-Poiseuille (HP) velocity profile. For the stability analysis, the HP velocity profile is substituted in the governing equations with a superimposed infinitesimal perturbation. The non-trivial solutions of the eigenvalue problem that

results after linearizing, are used for the analysis. When the amplitude of the superimposed perturbations increase over time, the flow is considered linearly unstable, consequently for linearly stable flows only decreasing amplitudes are found.

All evidence up to now on the stability analysis of the HP velocity profile, has led to the belief that pipe flow is linearly stable (Drazin and Reid 2004, Meseguer and Trefethen 2003). This means that when the fully developed laminar velocity profile in a pipe is perturbed by an infinitesimal perturbation, it will always return to the laminar flow state. Pipe flow is not unique in being considered a linearly stable shear flow. Other examples are plane Couette flow (the flow between two plates moving in opposite direction) and Taylor-Couette flow (the flow between two concentric cylinders) with only the outer cylinder rotating. However, all these flow share the common feature that in *practice* a transition to turbulence is observed, even at moderate Reynolds numbers. This contradiction between theoretical predictions and experimental observations has led to a large amount of dedicated research.

1.1.2 Developing pipe flow

As initial condition for the stability analysis of pipe flow, the fully developed parabolic velocity profile was used. However, in practice the flow entering a pipe has approximately a uniform velocity profile and has to develop before the fully developed state is reached (Durst et al. 2005). When the entrance region in the pipe is unstable, turbulence already sets in before the laminar velocity profile has been reached and this would be an explanation for pipe flow to become turbulent in practice.

The development region has been researched numerically by Tatsumi (1952a,b) and Huang and Chen (1974a,b). The results were verified experimentally by Sarpkaya (1975). They found that the entrance region is unstable to small symmetric and non-symmetric disturbances in a small region for $Re \approx 2\times10^4$.

Therefore one can conclude that the unstability of the entrance causes the transition to turbulence in pipe flow. However, the Reynolds number that was found at which the entrance flow becomes unstable is still much larger than the Reynolds number at which transition is observed in experiments. Therefore it is expected that the instability of the entrance flow is not the main reason for the transition to turbulence at low Reynolds numbers.

1.1.3 Transition of fully developed laminar pipe flow

In this section the transition to turbulence of the fully developed laminar velocity profile is considered. The research can be broadly split into two categories: transient growth of infinitesimal perturbations and the effect of finite amplitude disturbances.

In the first scenario, the governing equations in linearized form are considered. The HP velocity profile is used as a base flow. A disturbance is superimposed which can be decomposed in a

number of modes, each mode decays monotonically. However, when considering modes that are not orthogonal, the norm is able to grow when the rate of decay of these modes are different (see Gavarini (2004) for a more detailed explanation). When the norm grows to an amplitude that non-linearities become important and take over the growth in disturbance amplitude, a transition to turbulence has been realized.

An extension of the transient growth scenario was to incorporate small modifications of the base flow, Gavarini (2004) and more recent Ben-Dov and Cohen (2007). The optimal deviated base-flow profile that resulted in exponentially growing disturbances, consisted of a velocity profile with inflection points.

Although much effort has been put in the research to non-normal or transient growth of the linearized equations, Dauchot and Manneville (1997) showed in a reduced model that the linear features, especially the transient energy growth, is less important than particular non-linearities. Moreover they emphasize that one should be cautious when extrapolating results from the linear framework.

In the second approach, the effects of finite amplitude disturbances to the laminar base flow are considered. The property of linear stability for pipe flow has led to numerous experimentalists to pursue the *minimum* amplitude of a disturbance that is required to trigger a transition to turbulence. Obviously the threshold depends on the type of disturbance that was used. Here only spatially localized perturbations are considered, hence wall roughness effects or other means that influence the flow over a long distance, are not taken into account. These localized disturbances can be divided into two classes, based on the time they are active: continuous and temporal disturbances.

Obstacles that are present in the flow (Wygnanski and Champagne 1973, Durst and Unsal 2006) and time continuous flow perturbations (e.g. small section of the wall that is periodically moving (Leite 1959), periodic injection and/or retraction of fluid through a small hole or slit in the pipe wall (Draad 1996) or more sophisticated, through a porous wall (van Doorne 2004)) continuously perturb the fluid at a fixed location. The other class consists of perturbations that are applied over a short time interval and therefore create a localized disturbance in both space and time (Darbyshire and Mullin 1995, Hof et al. 2003, 2006, Peixinho and Mullin 2007, Hof et al. 2008, Kuik et al. 2010). In the transitional regime, the effects on the flow downstream depend on the class of disturbance that is applied. This is described in section 1.1.4.

To determine the mechanism that is responsible for the transition to turbulence in pipe flow, one can consider the scaling of the minimal amplitude with increasing Reynolds number. When the scaling of the disturbance amplitude ε is written as

$$\varepsilon = O(Re^{\gamma}) \tag{1.1}$$

a negative value for the exponent γ indicates an increasing sensitivity of the flow to perturbations (Waleffe 1995, Hof et al. 2003). When the exponents for different flow geometries are compared, a relative sensitivity to perturbations can be extracted. Based on numerical evidence, the amplitude scaling of Couette flow (the flow between two walls moving in opposite direction) and Poiseuille (pressure driven flow between two walls) seems to be equal to $Re^{-5/4}$ and $Re^{-7/4}$

respectively (Waleffe 1995). An exponent of $\gamma = -1$ indicates that the non-linear terms and the viscous dissipation terms of the Navier-Stokes equations are of equal magnitude (Waleffe 1995). Because different authors used different definitions, their results for pipe flow could not be compared. Therefore Trefethen et al. (2000) reformulated the results of existing data of Darbyshire and Mullin (1995) and Draad (1996) to perform a meaningful comparison. This resulted in a scaling equal to $Re^{-6/4}$ for pipe flow, which is exactly between the values that were found for Couette and Poiseuille flow.

From the experiments with a single jet-like disturbance, Hof et al. (2003) concluded that disturbance amplitude scales like Re^{-1}, indicating a balance between the non-linear and viscous dissipation terms in the Navier-Stokes equation. However, more recently Peixinho and Mullin (2007) showed that the exponent depends heavily on the perturbation that was used. Simultaneously injecting and extracting fluid appeared to be a much more efficient way to trigger the transition to turbulence. Depending on the arrangement of the injection and extraction point, the scaling ranges from $Re^{-1.3}$ to $Re^{1.5}$, which is the value resulting from the comparison by Trefethen et al. (2000).

In the search for the critical disturbance amplitude, a clear boundary is sought that separates the events that return to the laminar flow state from the events that become turbulent. However, for a single Reynolds number, there is not always a *single* threshold. To illustrate this, the experimental results of Darbyshire and Mullin (1995) are reproduced in figure 1.2. This figure shows whether or not the flow became turbulent after applying a jet-like disturbance normal to the pipe wall with an amplitude as indicated on the vertical axis. The amplitude of the disturbance is in this case defined as the ratio between the mass flux of the jet perturbing the pipe flow and the mass flux of the pipe flow itself. Figure 1.2 shows a few occasions where *increasing* the amplitude of the disturbance results in laminar flow, whereas the lower amplitude disturbance was able to trigger a transition.

This is even clearin the experimentby Draad (1996). Instead of using a localized disturbance in time, as was used by Darbyshire and Mullin (1995), Draad (1996) periodically perturbed the base flow through a slit in the pipe wall. The results for a fixed displacement volume and for different disturbance frequencies are given in the left part of figure 1.3. At first the global behavior in this experiment seems to be opposite to the results by Darbyshire and Mullin (1995): a positive slope is observed instead of a negative. Draad (1996) explained that this is the result of using a continuous disturbance, when a short localized disturbance was used; they also observed an increasing sensitivity of the base flow with increasing Reynolds number. The second important observation in figure 1.3 is that, at a single Reynolds number, multiple thresholds are present. For example at $Re = 40000$, the flow remains laminar for $V_{i,c} \lesssim 0.054$ (m/s) and turns turbulent for $0.054 \lesssim V_{i,c} \lesssim 0.056$. However when the disturbance velocity is increased beyond 0.056 the flow remains in the laminar flow state. Increasing the disturbance velocity beyond $V_{i,c} \gtrsim 0.064$ results in turbulent flow.

Similar behavior is found in a numerical simulation by Schneider, Eckhardt and Yorke (2007). A result from their simulation is reproduced in the right part of figure 1.3. Despite the fact that the disturbance amplitude can not be compared between the experiments by Draad (1996) and the

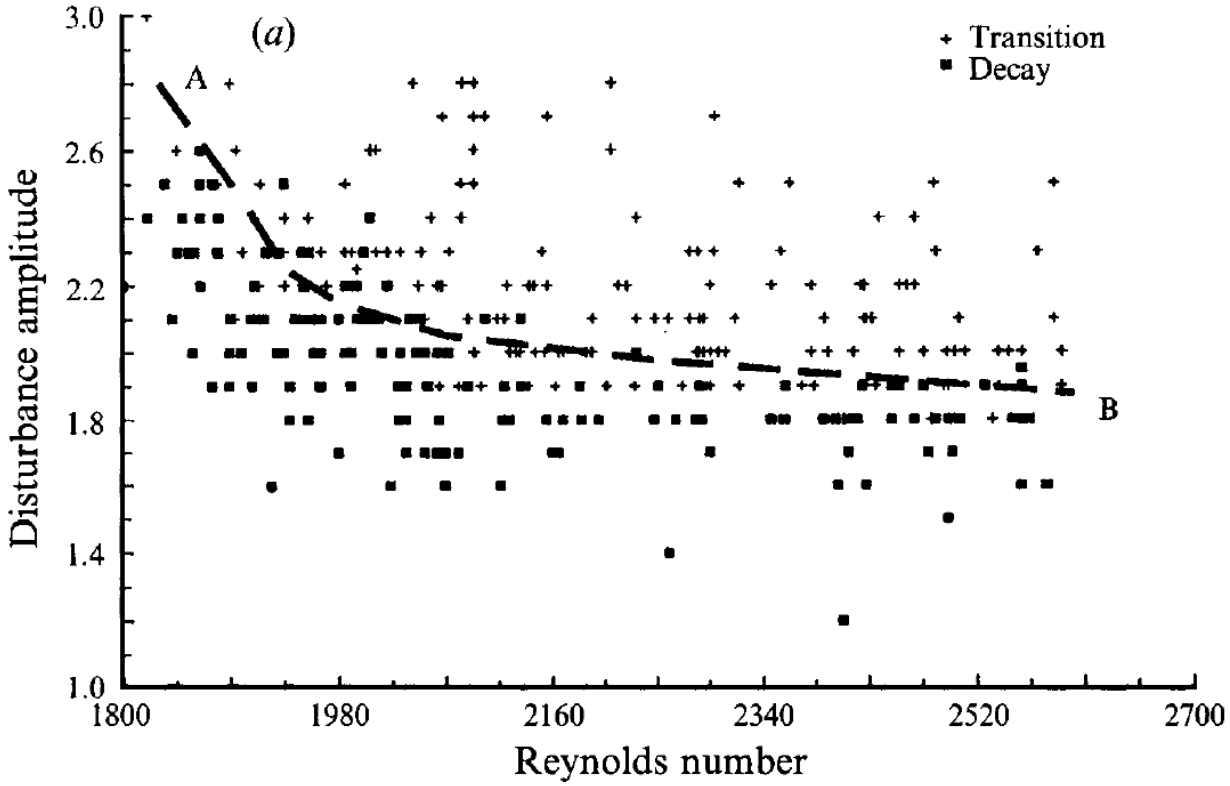

Figure 1.2: The results of the experiments by Darbyshire and Mullin (1995) to determine the critical amplitude required to trigger turbulent flow.

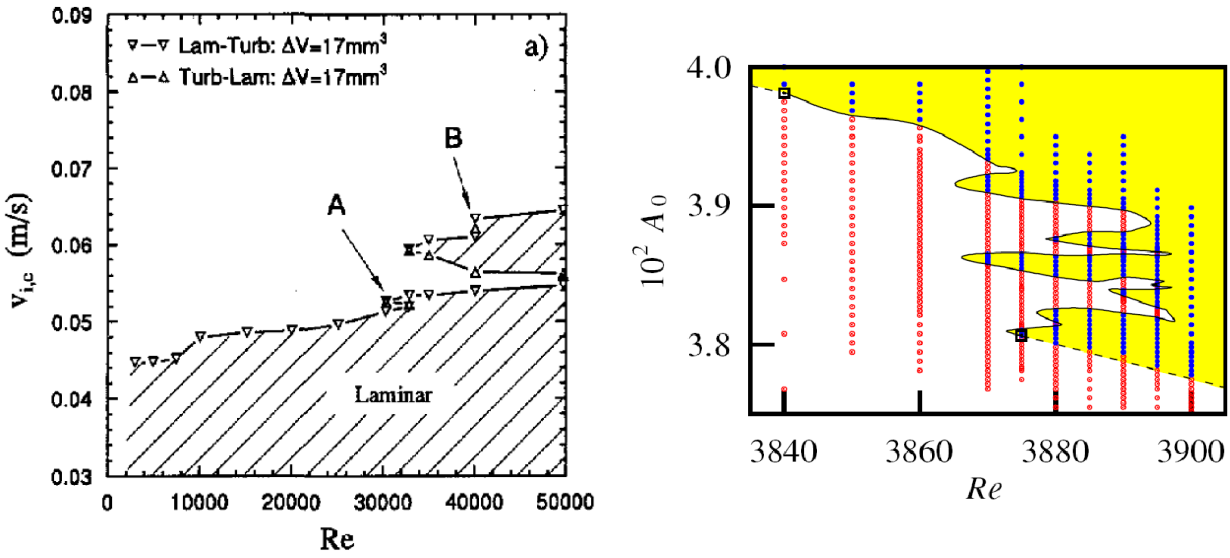

Figure 1.3: *left* experimental results by Draad (1996) on the critical amplitude to trigger turbulence. The shaded area indicated the return to laminar flow *right* similar result for numerical simulation by Schneider, Eckhardt and Yorke (2007). Be aware that here the shaded area indicates a transition to turbulence

simulations by Schneider, Eckhardt and Yorke (2007) it is remarkable that both observe multiple thresholds that trigger turbulent flow at a fixed Reynolds number.

The questions that emerge are: What resides on the boundary between laminar and turbulent flow? Can it be associated to a coherent structure? After the identification of exact solution to the Navier-Stokes equations (see for more information about this important development chapter 2) the attention of the groups that discovered the edge state was diverted to a search for the structure that separates the laminar from the turbulent flow state. Skufca et al. (2006) was the first to identify a structure separating the laminar state from the turbulent state in Couette flow and indtroduced the term *edge state*. It was called an edge state because only a minor modification in the energy contained in the structure results either in relaminarization (when the energy is decreased) or grows towards the level of turbulent flow (when the energy is increased). First Schneider, Eckhardt and Yorke (2007) and later Duguet et al. (2008) identified the edge state in a periodic pipe. The converged solution resulted in a structure that extended over the entire length of the domain. By extending the calculation domain, Mellibovsky et al. (2009) showed that the edge state was in fact a localized structure. For higher Reynolds numbers (up to 6000), Duguet et al. (2010) found that the edge state remains localized. Moreover, as could be expected by the scaling of the critical amplitude of a disturbance to trigger the turbulent flow state, the energy contained in the edge state decreases with increasing Reynolds number. This confirms that pipe flow becomes more susceptible for disturbances at higher Reynolds numbers.

1.1.4 Reynolds number effect on the type of disturbance

In the previous section it was shown that the amplitude of the disturbance is not the only factor influencing the transition to turbulence. As was shown in figures 1.2 and 1.3, the amplitude needed to trigger turbulent flow depends strongly on the Reynolds number. Peixinho and Mullin (2007) also showed that the *type* of disturbance is a third factor that influences the transition to turbulence, i.e. a particular type of disturbance can be more effective to trigger turbulence compared to others. In literature different types of disturbances are used to trigger the transition to turbulence. However, a clear description of the effect of these disturbances on the flow downstream has not been given.

In this section a disturbance either belongs to the category of continuous disturbances or to the category of disturbances localized in time. In the remainder of this section a disturbance that is applied very shortly, and is thus localized in time, is called a temporal disturbance. A continuous disturbance can either be a stationary object that is always present in the flow (Durst and Unsal 2006, Wygnanski and Champagne 1973), or a time periodic injection-extraction of fluid (Draad 1996, Eliahou et al. 1998, van Doorne 2004). The disturbance that is localized in time can either be obtained by injecting fluid through a hole in the wall again different configurations are possible, Hof et al. (2003), Peixinho and Mullin (2007), Kuik et al. (2010) or a solid object that is temporarily inserted in the flow (Durst and Unsal 2006). The effect on the flow downstream depends on the global characteristics of the disturbance, but not on the exact details of the disturbance. A schematic overview of the effects is given in figure 1.4. The color-coding represents the

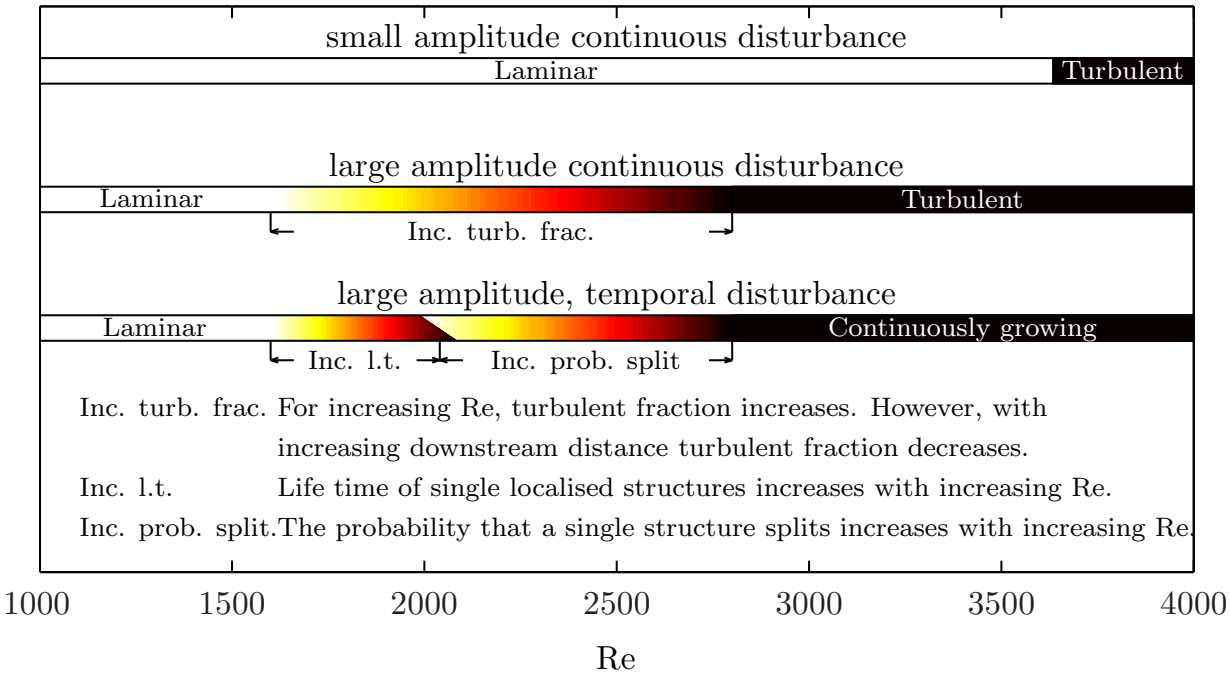

Figure 1.4: Depending on the type of disturbance, different flow patterns emerge downstream of the disturbance

flow state. In the white regions, laminar flow is obtained downstream of the applied disturbance. In the black regions the resulting flow is turbulent. In this figure three cases are considered: a small continuous disturbance present in the flow, a large continuous disturbance and a temporal disturbance with a large amplitude. In these cases the turbulence emerges in different forms, depending on the type of disturbance and the Reynolds number. Here we consider three forms together with their most distinctive properties.

In a particular Reynolds number range, the turbulent flow remains localized. This can be considered the smallest amount of turbulence that is able to sustain itself and was referred to as a flash by Reynolds (1883) and puff by Wygnanski and Champagne (1973). The latter name will be used in the remainder of this thesis to refer to this form of turbulence. Since the focus of this thesis is on puffs, section1.1.5 is dedicated to clearly define and describe the properties of puffs.

Continuously growing structures are observed in another Reynolds number regime. A localized structure that is able to grow continuously is referred to as a slug (Wygnanski and Champagne 1973). In contrast to a puff, a slug has two clearly identifiable transition fronts. The leading front has a velocity that is significantly larger than the bulk velocity while the trailing front has a velocity significantly smaller than the bulk velocity. For higher Reynolds numbers the velocity difference increases. However, the trailing transition front never advances *upstream*, i.e. it always travels in the same direction as the bulk fluid. Hence, the entire pipe will never become fully turbulent when a slug is created. The velocity statistics inside a slug are identical to the statistics for fully developed turbulent flow at the same Reynolds number.

The third form in which turbulence can appear is the fully turbulent state. This means that either

the entire pipe is turbulent or that downstream of the disturbance the flow is turbulent. The main difference between a slug and the fully developed state is that the fully developed state is present indefinitely in a pipe with finite length, whereas the slug will be convected with the flow and eventually leave the domain.

As was mentioned before, the type of turbulent flow depends on both the Reynolds number and type of disturbance. In the next paragraphs the flow that results from the two different classes of disturbances are described.

Small continuous disturbance When a small disturbance is present in the flow, the flow remains laminar up to a large Reynolds number. When the point is reached such that the disturbance is large enough to trigger turbulence, a *sudden* transition is observed. The flow downstream of the disturbance is turbulent and remains turbulent, i.e. the turbulent flow does not break up into patches with laminar and turbulent flow. For Reynolds number just below this critical value, which is unique for the disturbance, the flow remains laminar. Only a small increase in Reynolds number results in a completely different state.

In pipe flow facilities driven by a pump, the higher friction accompanied by the transition to turbulent flow causes the flow rate to decrease. Thereby the Reynolds number is also decreased and can reach a value below the critical Reynolds number. Hence the disturbance is not able to trigger turbulent flow anymore. As the part with turbulent flow is transported downstream out of the pipe, the additional friction diminishes. The flow accelerates as a result and the Reynolds number increases. When the Reynolds number passes the critical value again, turbulent flow is initiated by the disturbance. This results in a periodic transition from laminar to turbulent flow. The results of a measurement of the pressure drop and flow rate during such a cycle can be found in the work by van Doorne (2004).

Small temporal disturbance For a small temporal disturbance a similar effect is observed. When applied at low Reynolds numbers the flow remains laminar. When the disturbance is applied at a Reynolds number high enough to trigger turbulence and larger than $Re > 2800$, a slug is observed. The entire pipe will never become fully turbulent as a result of a localized temporal disturbance, because the trailing front of a slug is traveling downstream.

Large continuous disturbance As could be expected, when a large continuous disturbance is applied to the flow, the Reynolds number at which a transition to turbulence is observed decreases. However, at low ($Re \lesssim 1600$) and intermediate Reynolds numbers ($Re \lesssim 2700$) the turbulent flow cannot be sustained and part the flow breaks up into puffs. The ratio turbulent over the total flow, hereafter called the turbulent fraction, decreases with decreasing Re. The increasing turbulent fraction is visualized by the color-gradient in figure 1.4. Moreover, up to a Reynolds number of approximately 2500, the turbulent fraction decreases with downstream distance but increases with downstream distance for $Re \gtrsim 2500$ (Rotta 1956). For $Re > 2800$ the flow downstream does not show any parts that relaminarize and fully developed turbulence

is observed. This means that for a very long pipe (order of thousands of diameters), the flow returns to the laminar flow state for $Re < 2500$.

This property has been used by Hof et al. (2010) to eliminate turbulent patches. In their experiments they created a localized turbulent patch. Further downstream a continuous disturbance was present. Downstream of this continuous disturbance the flow relaminarizes, which is a property of a large continuous disturbance at these Reynolds numbers. The relaminarization process is independent of flow condition before the continuous disturbance and therefore it seems to eliminate puffs that were created upstream.

Large temporal disturbance When a large temporal disturbance is used to create turbulent flow, the effect on the flow downstream features unique characteristics. At Reynolds numbers $Re \lesssim 2040$, the temporal disturbance results in a single puff. The characteristic time or distance over which the puff is able to survive increases super-exponentially with Reynolds number. An overview of the findings up to now in this Reynolds number range is given in chapter 2. Furthermore, one goal in this thesis was to determine the proper life time scaling of puffs over a larger Reynolds number range.Detailed measurements on the life time of localized structures are presented in chapters 3 and 4.

For higher Reynolds numbers, puffs are able to split (van Doorne 2004, Nishi et al. 2008, Moxey and Barkley 2010). The higher the Reynolds number, the larger the probability that the initially single structure splits (Avila et al. 2011). Simultaneously, the probability that a puff decays vanishes rapidly in this Reynolds number range. However, although up to $Re \approx 2800$ the localized structures split, each remain localized and therefore a discrete number of puffs are present. When the Reynolds number is increased beyond $Re \approx 2800$, the structure created by a temporal disturbance grows continuously. Hence, for $Re \lesssim 2800$ puffs are observed and for $Re \gtrsim 2800$ slugs.

Avila et al. (2011) showed that the first splitting structures are observed at $Re \approx 2040$. However, Moxey and Barkley (2010) claimed, based on a numerical simulation, that the Reynolds number has to exceed $Re \simeq 2300$ before splitting structures are observed. This difference can be explained by the fact that an extreme long observation time is required before a splitting structure is observed for Reynolds numbers slightly larger than 2040. Nevertheless the difference in behavior for flows above and below $Re \simeq 2300$ is remarkable in the simulations by Moxey and Barkley (2010). Moreover, Moxey and Barkley (2010) observed a second threshold. For $Re \gtrsim 2600$ continuously growing structures were observed and since they used a period domain, fully developed turbulent pipe flow was obtained.

Recently, Barkley (2011) presented a novel one-dimensional model that captures all the observed flow states that result from a single large amplitude temporal disturbance. Although the nonlinear model is able to capture all features present in transitional pipe flow, it has not been based on the Navier-Stokes equations. A challenge for the future is to obtain such a model directly from the Navier-Stokes equations.

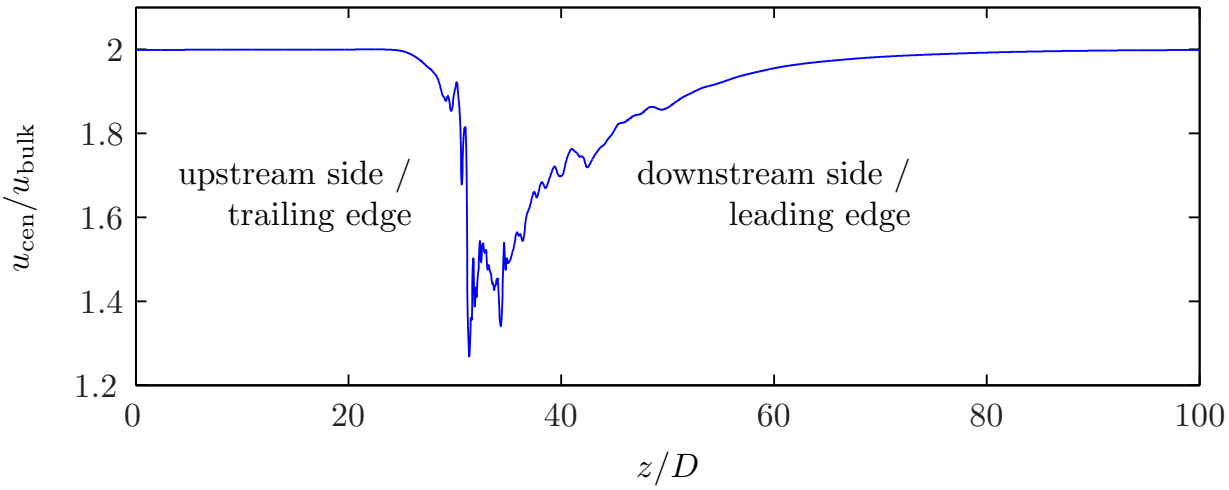

Figure 1.5: Centerline velocity in a domain with a single puff present. The flow is in positive z direction. In the figure the definition for the leading and trailing edge of the puff are given.

1.1.5 Characteristics of localized turbulent flow

This thesis focuses on *localized* turbulent structures, also known as puffs, that appear after the introduction of a localized temporal disturbance with a large amplitude. In the previous section it was shown that puffs are present for Reynolds numbers less than 2800. In this regime the length of the structure remains finite over time and does not show a continuous growth or reduction in length. The global characteristics of puffs have been described in literature based on conditionally averaged hot-wire data (Wygnanski and Champagne 1973, Wygnanski et al. 1975, Nishi et al. 2008), by using flow visualizations (Lindgren 1969, Bandyopadhyay 1986) or by exploiting the difference in axial momentum between the puff and laminar flow, which affects the outflow angle (Rotta 1956, Hof et al. 2006, 2008).

Figure 1.5 shows the classical centerline velocity distribution for a puff as obtained by the present numerical simulation. On the trailing edge of the puff, a sharp drop is present indicating a sudden transition at the transition front. Because of the clearly defined drop this has often been used to determine the location of the puff (see also section 5.5.1). On the downstream side however, a gradual increase in velocity is observed. Upstream and far downstream of the puff the centerline velocity is equal to the theoretical value for laminar flow, i.e. two times the bulk velocity. The length of the puff is ill-defined due to the gradual increase of the centerline velocity on the leading edge. In section 5.5.1 is described how the location of a puff is determined in numerical simulations. The information of the location of the puff over time is used to determine the velocity of the puff. In section 5.6.2 is shown that the velocity of the puff is strongly related to the velocity fluctuation level inside the puff.

Directly after the sharp drop in centerline velocity strong velocity fluctuations are observed. Bandyopadhyay (1986) identified a region inside the puff that they consider fully developed. Using a direct numerical simulation the average velocity fields and the velocity fluctuation fields

are obtained inside a puff and compared to fully developed turbulent pipe flow. The results are presented in section 5.5.

1.2 Outline of the thesis

When a localized temporal disturbance is applied to a fully developed laminar flow, the result is a localized turbulent structure. An overview of the research on the dynamics of these localized structures in pipe flow is presented in chapter 2. From this chapter it is clear that the scaling of the lifetimes of localized turbulent structures can give an indication of the dynamical model that describes the transition to turbulence. In chapter 3 the results are presented of a large number of experiments. The goal of these experiments was to increase the number of observations and therefore the increase the range of observed lifetimes. Although the range of life times was increased tremendously, the experiments descibed in chapter 3 did have a few shortcomings. In the experiments it was unknown if a disturbance was initiated when intended. Furthermore, it was unknown what the exact lifetime of the *individual* puffs was. The state was determined at fixed distances after the location where the disturbance was applied. Therefore new experiments were undertaken. The goal of these experiments was to quantitatively determine the life time of individual puffs. The presence of a puff was determined using pressure transducers. When a puff is present in the pipe, the pressure drop is larger when compared to laminar flow. If a puff disintegrates, the pressure drop relaxes to the level for laminar flow. By determining the moment at which the pressure drop is below a predetermined treshold, the life time of each individual puff can be determined. The results of these experiments is described in chapter 4.

A question that remained was: Are coherent structures responsible for the regeneration process? Or in a broader sence: what mechanism is required for the turbulent puff to sustain itself. In order to answer this question a large experimental campaign was undertaken. The goal was to use a pressure measurement technique, as described in chapter 4, to determine the exact location of decay. Since the location at which the velocities were measured was known with respect to the pressure measurement, this could be used to sort the measurements such that a puff could be measured *during* its decay process. Instead of using LDA to track the decay process, time resolved PIV (van Doorne and Westerweel 2009) was used to measure a quasi-instantaneous three dimensional velocity field. Unfortunately the pressure drop measurement could not be used to determine the location of decay, because of a reduced signal due to to the larger diameter of the pipe. The larger diameter of the pipe that was required for the PIV measurements.

When in the PIV measurements the contribution of in-plane velocity component to the kinetic energy was considered, distinctive localized structures were observed. The contribution of the in-plane velocity components to the kinetic energy is also known as the in-plane kinetic energy and is defined as:

$$E_{\mathrm{ip}}(z) = \frac{1}{\pi R^2} \int_0^R \int_0^{2\pi} \frac{u_r^2 + u_\theta^2}{u_{\mathrm{bulk}}^2} \, r \, dr d\theta \tag{1.2}$$

where E_{ip} is the in-plane kinetic energy, R the radius of the pipe, u_r and u_θ the radial and azimuthal velocity components respectively and u_{bulk} the bulk velocity. The bulk velocity is defined as:

$$u_{\mathrm{bulk}} = \frac{1}{\pi R^2} \int_0^R \int_0^{2\pi} u_z \, r \, dr d\theta \tag{1.3}$$

where u_z is the axial velocity component. The localized structures that were identified in the in-plane kinetic energy were similar to the structures that were found and discussed by van Doorne and Westerweel (2009). A quest to the relevance of these large amplitude structures led to a direct numerical simulation. Before the simulation was performed, it was remarkable that the structures clearly present in experiments (van Doorne and Westerweel 2009, De Lozar and Hof 2009) were never discussed before in results from numerical simulations. van Doorne and Westerweel (2009) provided an explanation for this mismatch in the form of the axial resolution used in the numerical simulations. According to van Doorne and Westerweel (2009), the small scale structures could not be resolved with the resolutions used in the numerical simulations.

This was the main reason a simulation was undertaken with a high axial resolution, such that it could resolve small scale structures. The results of this simulation is presented in chapter 5. As an initial condition for the simulation, the results of a PIV measurement were used. This ensured the presence of the large amplitude structures in the initial condition. The results form the numerical simulation allowed then for a characterization of their dynamical behavior.

Moreover, the temporal and spatial information available in the numerical simulation led to the ability to get the integral behavior of localized structures over time. The results obtained from the simulation are in very good agreement with the theoretical derived energy balance over a transition front that was already derived by Rotta (1956). Furthermore, the experiments presented in chapter 4 show that the instantaneous velocity of a turbulent structure is not constant as the structure travels down the pipe. This behavior of localized turbulent structures is confirmed by the behavior of a puff observed in the numerical simulation.

Chapter 2

Long-lived transients in transitional pipe flow[1]

The transition to turbulence in pipe flow has remained an unsolved problem in fluid mechanics. The transition from laminar pipe flow to a turbulent flow state was first investigated in detail by O. Reynolds in 1883 (Reynolds 1883), after which the Reynolds number is named, defined as $\mathrm{Re} = UD/\nu$, where U is the bulk velocity, D the pipe diameter, and ν the kinematic viscosity of the fluid. Typically, for flow rates with a Reynolds number less than 1,600 the flow is laminar, while for Reynolds numbers larger than about 2,000 the flow is strongly intermittent and laminar and turbulent flow domains co-exist (Wygnanski and Champagne 1973). These localized turbulent flow regions are called 'puffs'. However, a mathematical analysis of the laminar flow state, characterized by a parabolic velocity profile known as Hagen-Poiseuille (HP) flow, shows that it is linearly stable for all Reynolds numbers (Drazin and Reid 2004). Hence, one is not able to explain the transition to turbulence by means of an instability originating from infinitesimal disturbances, and the transition to turbulence in pipe flow remains unexplained.

A breakthrough occurred when new solutions were found for the flow through a pipe Faisst and Eckhardt (2003), Wedin and Kerswell (2004). Each of these solutions, in the form of a *traveling wave* (TW), is an exact solution of the (non-linear) equations of motion, or Navier-Stokes equations. These traveling waves (TW) are families of solutions characterized by their symmetry. Each TW solution has the character of an unstable saddle, so that one cannot create these solutions under experimental conditions. However, flow patterns that have a very strong reminiscence to these TW solutions could be identified in experimental data by Hof et al. (2004); see Figure 2.1. The TW solutions first appear for a Reynolds number of about 773 in a mirror-symmetric form. At slightly higher Re, helical and asymmetric TW's are found (Pringle and Kerswell 2007). At $\mathrm{Re} \approx 1{,}300$, those with a 2-fold and 3-fold rotational symmetry appear. All these TW solutions have a phase speed that is slightly larger than the mean flow speed; see Fig. 2.2.

[1] This chapter has been published as a chapter in a book edited by J. Dubbeldam, K. Green and D.Lenstra.

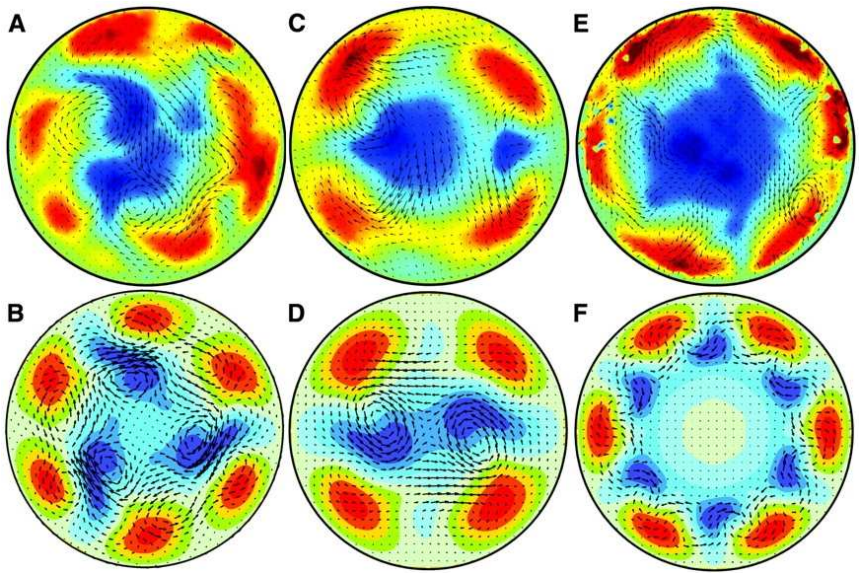

Figure 2.1: Comparison of experimental data of instationary pipe flow in a planar cross section (A-C-E) and corresponding exact traveling wave states (B-D-F). From: Hof et al. (2004).

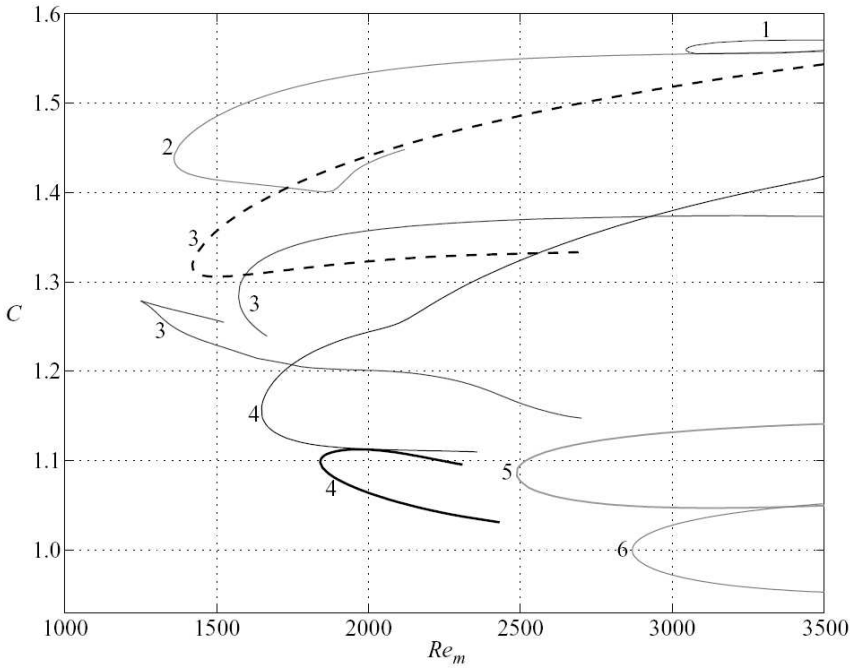

Figure 2.2: The phase speed of traveling waves (the number indicates the rotational symmetry) relative to the mean bulk velocity as a function of the Reynolds number. From: Wedin and Kerswell (2004).

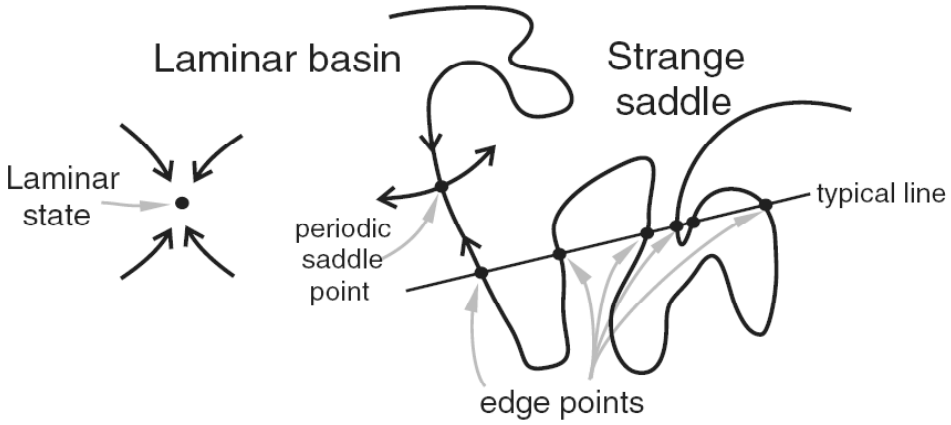

Figure 2.3: Schematic representation of phase space in pipe flow. The laminar flow state is an attractor by increasing the Reynolds number its basin of attraction reduces, if the flow is perturbed outside the basin of attraction, the flow wanders around the traveling wave solutions found by Wedin and Kerswell (2004), Faisst and Eckhardt (2003). Courtesy of: T. Schneider, Univ. Marburg.

In order to interpret the observed transition to turbulence in a pipe, we now consider the dynamical behavior of pipe flow in relation to the HP flow and TW flow solutions in terms of a representation in state space. Hagen-Poiseuille (HP) flow is then represented as a single stable node. At low Reynolds numbers all disturbances to the base flow decay back to the HP flow, which is represented in state space by a trajectory that returns to the stable node.

The TW solutions form a strange repellor. When the HP flow is disturbed sufficiently, the flow state wanders around in phase space, occasionally approaching states that are near a TW, but each time is carried away along one of the unstable directions of the unstable saddle, and eventually returns to the laminar flow state. As the Reynolds number increases, the time it takes to return to the stable HP-node increases, implying longer and longer transients with increasing Reynolds number. The time the flow state follows a complex trajectory shows large variations. This behavior is typical for a chaotic saddle (Skufca et al. 2006).

To explain a transition to sustained turbulence it is expected that at a given Reynolds number the strange repellor changes into a strange attractor so that the orbit of a disturbed HP flow no longer returns to the fixed point representing the stable base flow. In that case HP and turbulent flow coexist, and the two flow states are separated by a boundary that defines the basin of attraction for the laminar and turbulent flow states respectively (Schneider, Eckhardt and Yorke 2007, Robert et al. 2000). For small-amplitude disturbances the flow quickly returns to the laminar flow state. However, when the disturbance amplitude is large enough, the trajectory passes the boundary for the basin of attraction of the turbulent strange attractor, and thus will no longer return to the laminar base flow. This then represents a sustained turbulent flow state that explains the transition to turbulence in a pipe flow.

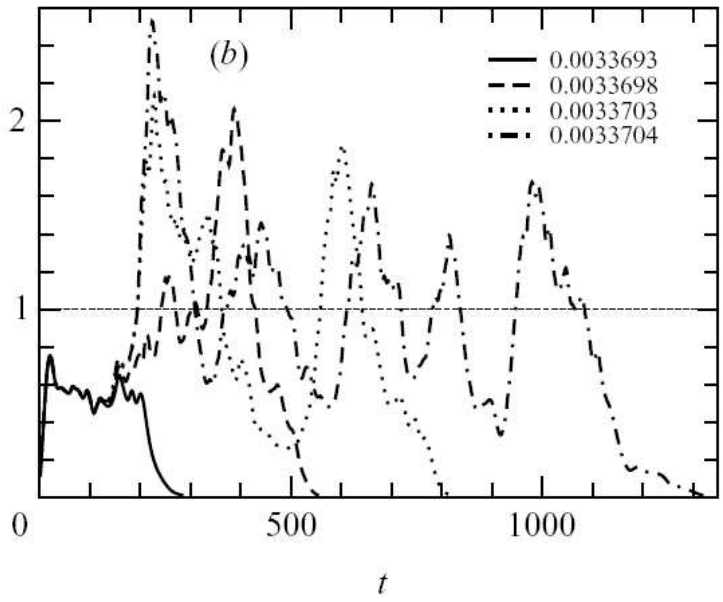

Figure 2.4: Time series of the disturbance energy for four slightly different initial conditions for a pipe flow at Re = 2,000, showing the large variation of life time. From: Faisst and Eckhardt (2004)

This transition scenario was investigated by Faisst and Eckhardt (2004) by means of a direct numerical simulation (DNS). They simulated the time evolution of localized turbulent flow (representing the turbulent portion of a puff) in a domain of 5 times the pipe diameter with periodic boundary conditions. Although only a small portion of the entire puff is simulated, the essential dynamics of the entire system is captured. Starting at low Re they determined for each realization how long it took for the flow to return to the laminar flow state. They found that there is a large variation in the time that the flow returns to the base state (see Fig. 2.4), and that the probability of decay follows an exponential distribution $P \sim \exp(-(t-t_0)/\tau)$, where τ is the characteristic life time. The probability distributions for increasing Re are shown in Fig. 2.5. This clearly shows that τ increases with Reynolds number.

By taking the time for which 50% of the disturbances had decayed, or median life time, they initially found that the life time τ diverges at a finite value of the Reynolds number, indicating a critical Reynolds number Re_c of 2250. The value of Re_c was obtained from an *extrapolation* of τ^{-1} as a function of *Re*.

Peixinho and Mullin (2006) performed an experiment in a pipe flow where they determined the life time of puffs. They generated puffs at $Re = 1900$, and then reduced to flow rate to a lower *Re*, and then determined *visually* the moment of decay. Like the numerical simulation, the probability showed an exponential decay. From these data they determined the reciprocal lifetime as a function of *Re*, and determined from an extrapolation that $Re_c = 1750 \pm 10$, where the lifetime appears to diverge. It should be noted that the uncertainty of the last 3 to 4 data

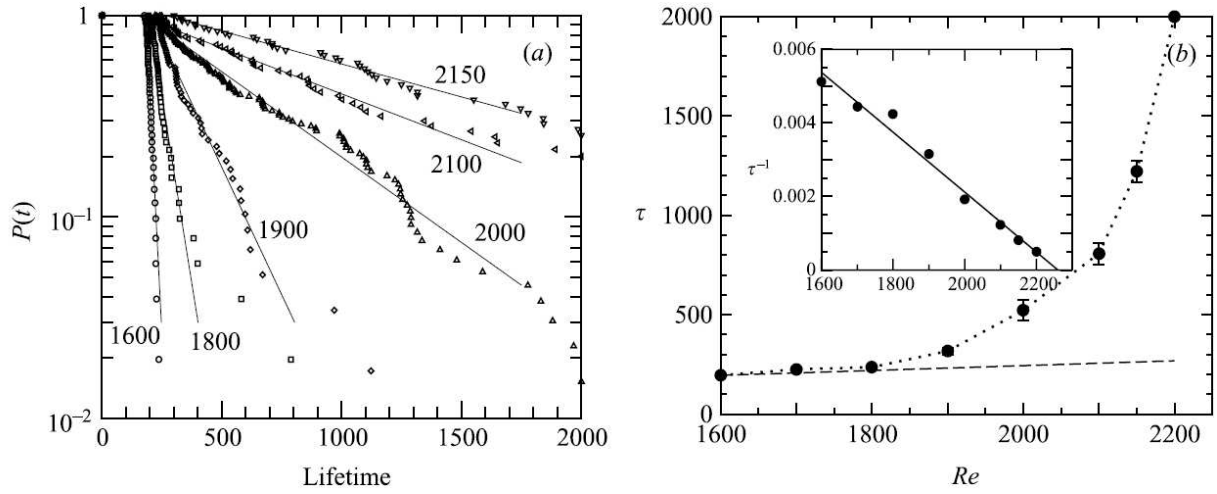

Figure 2.5: Turbulent life times as a function of Reynolds number. (left) Probability $P(t)$ for a single trajectory to still be turbulent after a time t. (right) Median τ of the turbulent lifetimes as a function of Reynolds number. The inset shows the reciprocal median lifetime vs. Re and a linear fit, corresponding to $\tau(Re) \propto (Re_c - Re)^{-1}$, with $Re_c \approx 2250$. From: Faisst and Eckhardt (2004)

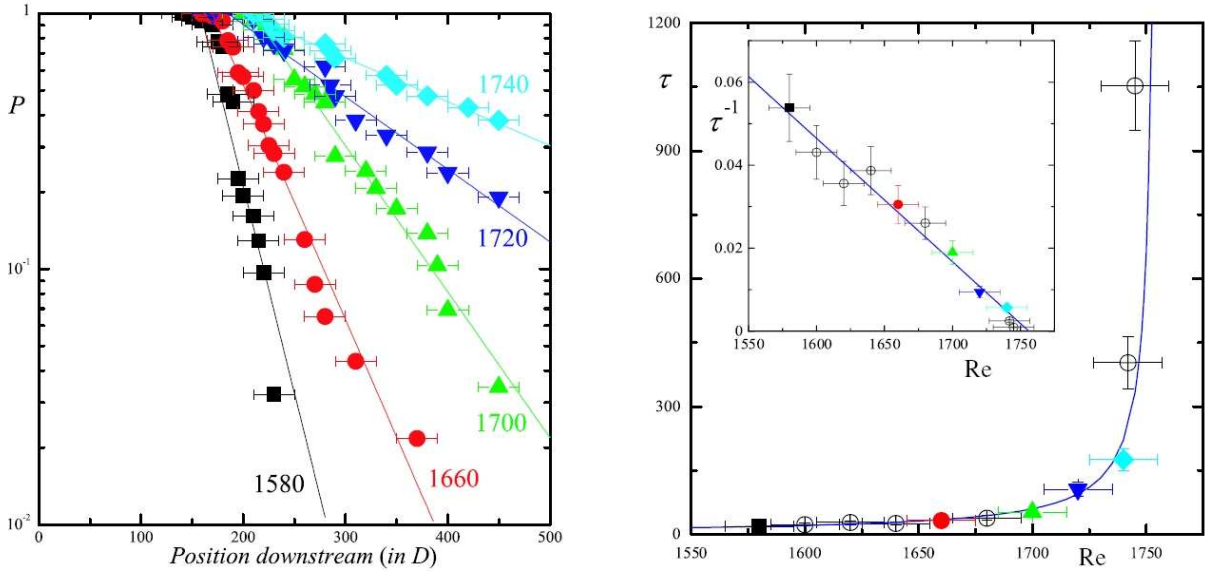

Figure 2.6: (left) Probability of observation of a puff versus downstream distance. (right) Mean decay rate as a function of Re. The inset shows the inverse life time with a linear fit indicating $Re_c \approx 1750 \pm 10$. From: Peixinho and Mullin (2006)

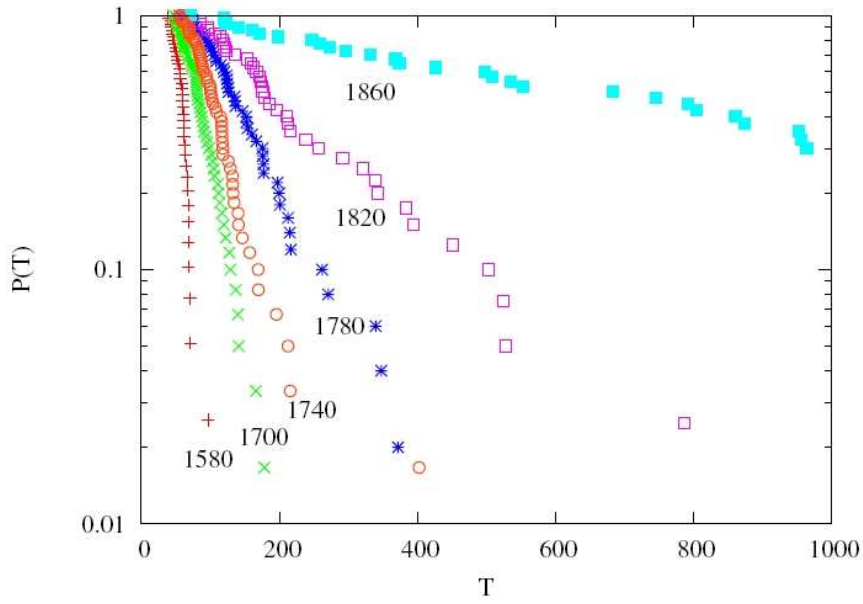

Figure 2.7: Probability $P(T)$ of the life time of a puff to exceed T. From: Willis and Kerswell (2007a)

points at the highest Re measured essentially occur at the same Re.

Willis and Kerswell (2007a) used DNS to simulate the decay of puffs in a pipe at various Reynolds numbers. The DNS was implemented with periodic boundary conditions, with a pipe length of 50 times the pipe diameter, which would be sufficiently long to contain the entire puff. The approach was very similar to the experiments performed by Peixinho and Mullin (2006): the simulation was started with a randomly selected snapshot of the velocity field of a puff in the domain at $Re = 1900$, and started at the desired Reynolds number. The probability distribution of the lifetimes was determined based on 40-60 simulations per Reynolds number. They claimed that a quantitative agreement was found between their results and the previously obtained results by Peixinho and Mullin (2006). Although they concluded to have also found a linear scaling for the characteristic life time, the critical Reynolds number was 1870, which is significantly larger than the value of 1750 found by Peixinho and Mullin (2006).

Meanwhile, another experiment was conceived by Hof et al. (2006). Rather than following disturbances in a pipe at fixed Re to determine the characteristic life time τ, one can consider a pipe with fixed length L and determine the probability that a disturbance survives: $P(t, Re; L)$. This is equivalent to considering the probability along vertical lines in the left part of Fig. 2.5 (as opposed to evaluating $P(t, Re)$ along horizontal lines). A disturbance is introduced in a pipe (after sufficient distance from the pipe inlet) and it is observed when this disturbance reaches the outlet of the pipe. When the jet emanating from the pipe dips (as a result of the lower centerline velocity in the puff) the disturbance has obviously survived for the time period required to travel a distance L along the pipe. A schematic of this experiment is shown in Fig. 2.9.

It was found from the analysis of the initial results reported by Faisst and Eckhardt (2004) that

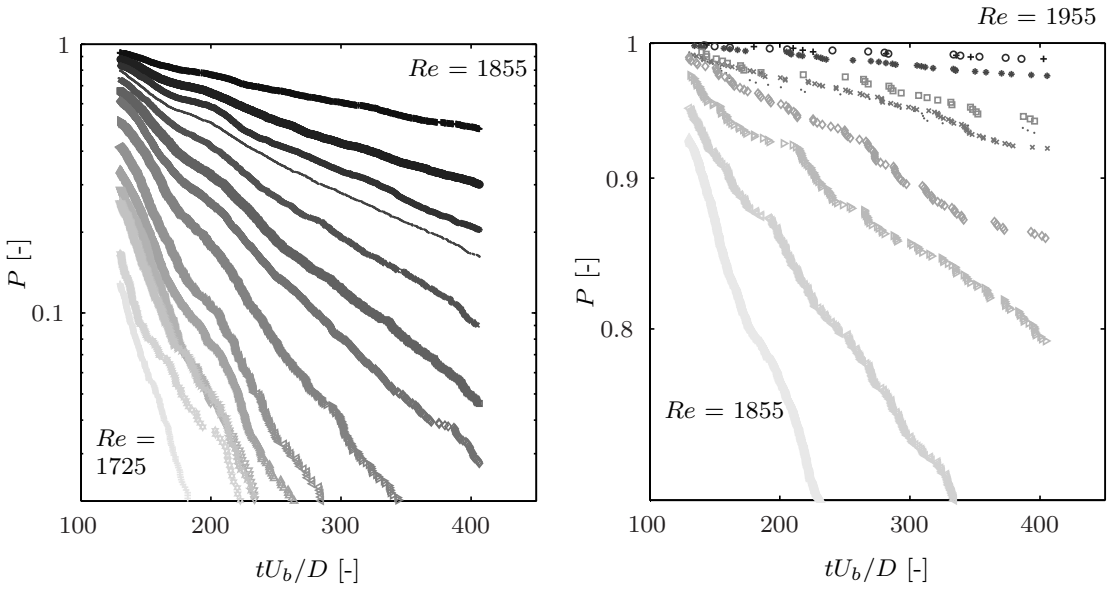

Figure 2.8: Probability P of the life time of a puff to exceed tU_b/D. From: Kuik et al. (2010)

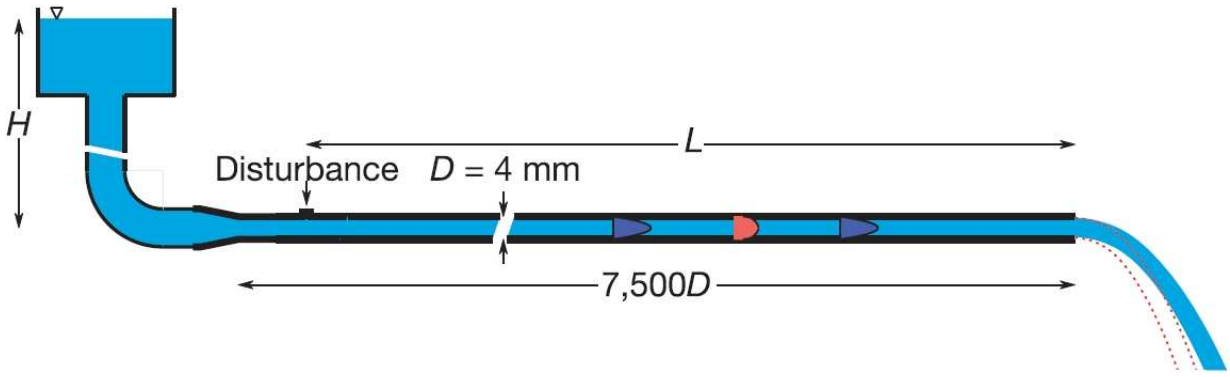

Figure 2.9: Schematic of the experiment used by Hof et al. (2006).

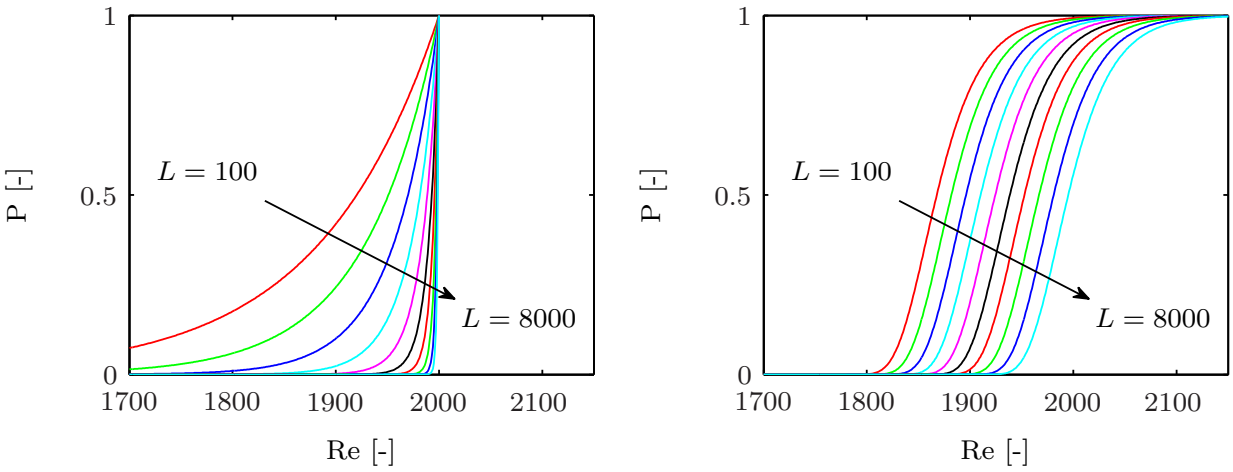

Figure 2.10: *left* probability as a function of Reynolds number if $\tau^{-1} \sim (Re_c - Re)$, with $Re_c = 2000$ *right* probability as function of Reynolds number if $\tau^{-1} \sim \exp(Re)$

the slope of the exponential distributions did not exactly correspond to the reported lifetimes that were based on the median lifetime extracted from Fig. 2.5. Further analysis conjectured that the lifetime might actually scale as $\tau^{-1} \sim \exp(Re)$ (Willis and Kerswell 2007a). This has the important consequence that the life times does not diverge at a finite critical Reynolds number, and implies an important fundamental issue in regard to understanding the transition to turbulence.

The difference between these two scaling regimes can be readily observed in $P(t, Re; L)$, as indicated in Fig. 2.10. In the case of a linear scaling of τ^{-1} with a divergence of the lifetimes at finite Re_c, the observed probabilities for fixed L have an exponential shape, all culminating at $P = 1$ for $Re = Re_c$. Whereas for the exponential scaling, the probability curves have distinct S-shapes that shift to higher Re for increasing pipe length.

Note that the curves for $P(t, Re; L)$ for low probabilities $(P < 0.3)$ look very similar. This implies that it is difficult to determine the difference between the two scaling regimes when only data is available for low Reynolds numbers and short pipes or observation times. This is a serious complication for numerical investigations, as not only the required integration time increases with Reynolds numbers, but also the computational cost.

The linear scaling leads to an interesting thought experiment as the probability approaches a step function when $L \to \infty$. Consider a very long pipe driven by a constant pressure with the Reynolds number of the flow just below Re_c. Then each disturbance introduced at the beginning of the pipe decays and for all disturbances the flow at the pipe outlet remains undisturbed. (The very long pipe length implies that the flow rate as determined by the pressure drop is not affected by introducing the disturbance.) Then a second, identical pipe is placed next to the first one. However, it is made slightly shorter, so that the flow rate increases just above the critical Reynolds number. When the same disturbance is now introduced to both pipes, all disturbances in the second pipe will survive. Provided that the pipe are long enough, the difference in the two pipe

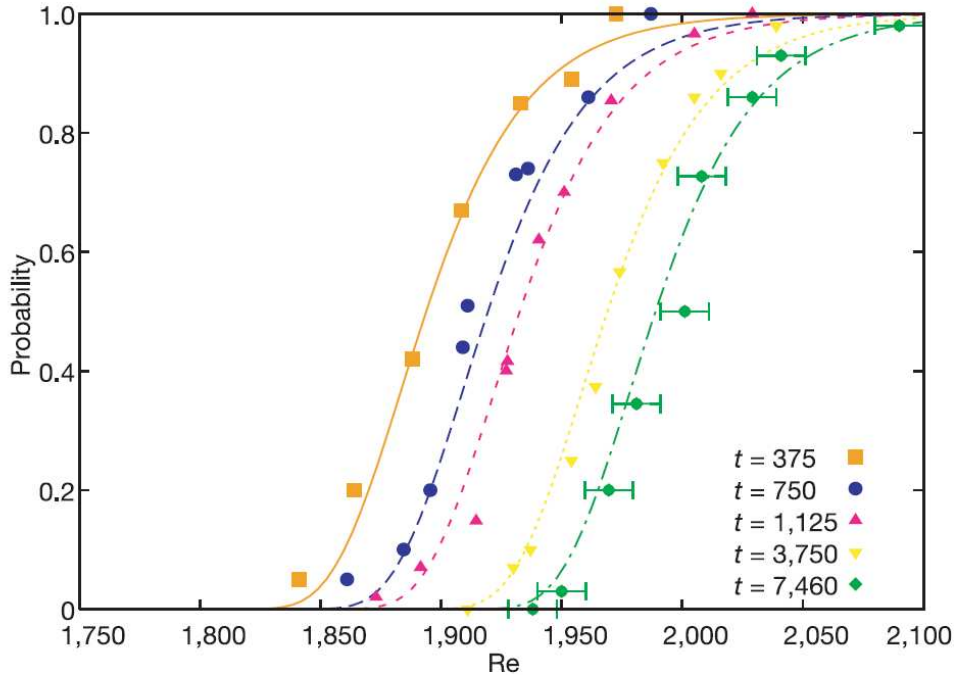

Figure 2.11: Probability distribution obtained by Hof et al. (2006) showing clearly the S-shaped curves

lengths can be made arbitrarily small, so that the two pipes appear to be identical, yet their behavior in terms of the disturbances at the pipe exits are completely different.

In the case of the exponential scaling of the lifetime the two (almost identical) pipes behave almost identically, with the slightly longer pipe having a slightly lower fraction of puffs surviving all the way to the pipe exit.

In order to make a distinction between the two scaling regimes, it is necessary to perform the measurements in very long pipes, preferably exceeding 1000-2000 pipe diameters in length. First a 4 mm diameter pipe with a length of 11 m (L/D = 2,750) was constructed in Delft, and later a 4 mm diameter pipe with a total length of 30 meters (i.e., L/D = 7,500) was constructed in Manchester. The results of the measurements by Hof et al. (2006) in both pipes are shown in Fig. 2.11. Note that the probability curves have a distinct S-shape, which already indicates qualitatively that the lifetime of the disturbances does not diverge at finite Re. Further analysis indicated that the data indeed show an exponential scaling of the lifetime as a function of Re over the range of Reynolds numbers investigated.

Further experiments were conducted to extend the range of lifetimes that could be measured and to determine the location of decay quantitatively. Rather than considering the median lifetime, the rate of decay was determined. Thus it was possible to determine τ for pipe lengths that were shorter than $U\tau$ (where U is the mean flow velocity) and it was possible to determine the decay rate over a very large range between 1 and 10^8. The results over the very large range in escape rates were reported by Hof et al. (2008). Later these results were confirmed by a quantitative

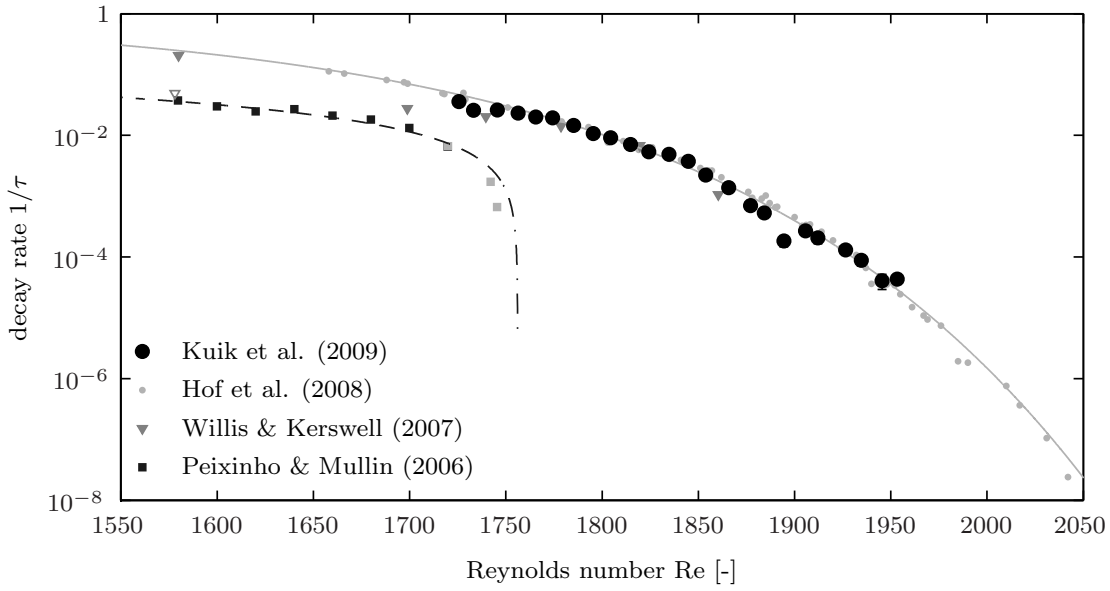

Figure 2.12: The life time of decay rate for $P(t)$ as a function of Reynolds number. After: Kuik et al. (2010)

measurement of the lifetime as reported by Kuik et al. (2010). The results for the life time (viz., decay rate or escape rate) as a function of Re are reproduced in Fig. 2.12, together with the previous experimental and numerical results. It appears that the scaling is not exponential, but rather super-exponential, i.e. the life time τ is given by Hof et al. (2008)

$$\tau^{-1} = (U/D)\exp[-(Re/c)^n] \tag{2.1}$$

with c = 1549 and $n = 9.95$, where n is related to the rate at which the laminar basin of attraction shrinks with increasing Reynolds number (Tél and Lai 2008). The data fits quite well with the experimental and numerical data obtained by others, except for very low Reynolds numbers and for Reynolds numbers where the observation is limited by the actual pipe length. The super-exponential scaling also appears in so-called spatio-temporal chaotic systems, where transients increase super-exponentially with the size of the system (Tél and Lai 2008).

The conclusion of the experiments is that the lifetimes of localized disturbances rapidly increases with Re. The scaling of the lifetime with Re as measured in the experiments suggests that the divergence of the lifetime does not occur at a finite critical Reynolds number[2]. This suggest that, for the Reynolds numbers investigated, no evidence is found for the existence of a strange attractor[3]. If the scaling found in the experiment holds for larger Re than those investigated,

[2]The work of Borrero-Echeverry et al. (2010) shows that a similar type of scaling is found for the life time of a turbulent patch in Taylor-Couette flow. Thereby showing that this type of behavior can be considered more general as a feature of linear stable shear flows and not a feature unique to pipe flow.

[3]In a numerical simulation by Avila et al. (2010) exactly the same type of scaling is found for puffs in a pipe. The results show a remarkable *quantitative* agreement between the data obtained from the simulation and the results from experiments.

then it would imply that the turbulent flow state should be considered as a transient, albeit an extremely long-living one (Lathrop 2006). For example, to extend the observation time for the data shown in Fig. 2.12 that are valid for water flowing through a D = 1 cm pipe to a Reynolds number of 2,200 would imply observation times exceeding the lifetime of the universe. Evidently, to extrapolate the experimental results to any value of the Reynolds number beyond those investigated experimentally should be taken with great caution. The problem arises that the predicted lifetimes for higher Reynolds number become simply impractically large. Next to that, at higher Reynolds numbers the localized nature of the turbulence is lost. From Reynolds number higher than approximately 2350, turbulent puffs can split and for Re larger than about 2700 can form 'slugs' (Wygnanski and Champagne 1973, Nishi et al. 2008) . This behaviour cannot be explained by the current dynamical systems point of view on the transition to turbulence. Another remaining question is what the relation is between the exact periodic solutions that were found numerically (TW's) and the turbulent puff.

Chapter 3

Repeller or Attractor? Selecting the Dynamical Model for the Onset of Turbulence in Pipe Flow[1]

The collapse of turbulence, observable in shear flows at low Reynolds numbers, raises the question if turbulence is generically of a transient nature or becomes sustained at some critical point. Recent data have led to conflicting views with the majority of studies supporting the model of turbulence turning into an attracting state. Here we present lifetime measurements of turbulence in pipe flow spanning 8 orders of magnitude in time, drastically extending all previous investigations. We show that no critical point exists in this regime and that in contrast to the prevailing view the turbulent state remains transient. To our knowledge this is the first observation of superexponential transients in turbulence, confirming a conjecture derived from low-dimensional systems.

Finding appropriate models and concepts describing fluid turbulence is one of the outstanding challenges in the physical sciences. Shear flows with a linearly stable laminar state, such as pipe, channel, duct, or Couette flow have proven to be particularly intricate in this regard Eckhardt et al. (2007). Here the laminar and the turbulent state coexist Grossmann (2000), Pomeau (1986) without a clear transition point, yet at large flow rates the laminar state becomes increasingly susceptible to perturbations. Once a disturbance is large enough the transition to turbulence occurs suddenly without any intermediate states Dauchot and Daviaud (1995), Darbyshire and Mullin (1995), Hof et al. (2003). Surprisingly, at relatively low Reynolds numbers (Re $\lesssim$ 2000) the turbulent state is not stable and after long times suddenly collapses Brosa (1989), Bottin and Chate (1998), Bottin et al. (1998), Faisst and Eckhardt (2004), Willis and Kerswell (2007a), Hof et al. (2006). This behavior is reminiscent of memoryless processes in nonlinear systems. In phase space the dynamics can be described by a complex structure giving rise to the disordered dynamics, a socalled chaotic repeller Kadanoff and Tang (1984). Underlying such a structure are

[1]The content of this chapter has been published in Physcial Review Letters (Hof et al. 2008).

unstable states and for pipe flow unstable solutions to the governing equations have been identified in the form of traveling waves Faisst and Eckhardt (2003), Wedin and Kerswell (2004). Surprisingly clear transients of such traveling waves were observed in experiments Hof et al. (2004, 2005) confirming their relevance to the turbulent dynamics. More recently traveling wave transients were also reported in numerical studies Schneider, Eckhardt and Vollmer (2007), Kerswell and Tutty (2007).

A way to probe the validity of this model is to measure the lifetime of turbulence in the transient regime. Previous experimental and numerical lifetime measurements have shown approximately exponential probability distributions Bottin and Chate (1998), Faisst and Eckhardt (2004), Willis and Kerswell (2007a), Peixinho and Mullin (2006), Lagha and Manneville (2007) which suggests that the probability for a turbulent structure to decay is independent of its age and hence that this process is memoryless as would be expected for the escape from a chaotic saddle. Here the probability for a flow to still be turbulent after a time t at a fixed Reynolds number (Re) is then given by

$$P\left(t-t_0,\mathrm{Re}\right)=exp\left[-\left(t-t_0\right)/\tau\left(\mathrm{Re}\right)\right], \tag{3.1}$$

where τ is the characteristic lifetime (τ^{-1} can be also interpreted as the escape rate) and t_0 is the initial time period required for turbulence to form after the disturbance has been applied to the laminar flow at $t=0$. The fate of the chaotic repeller is then determined by the functional form of the characteristic lifetime $\tau\left(\mathrm{Re}\right)$ and different suggestions have been made in the past. The majority of studies reported that τ^{-1} decays linearly and reaches zero at a critical Reynolds number. Here the turbulent state undergoes a boundary crisis Eckhardt et al. (2007) leading from transient to sustained turbulence. However there is no quantitative agreement for the value of such a critical point and cited values differ by more than 25%. This view has been challenged in an experimental study Hof et al. (2006) carried out in an extremely long pipe where τ^{-1} has been observed to decay exponentially. Crucially it only approaches zero and hence (unless a global bifurcation occurs at larger Re Eckhardt et al. (2007)) an infinite lifetime is only reached in the asymptotic limit $\mathrm{Re}\rightarrow\infty$. Subsequently a number of studies have questioned this finding and again entertained the occurrence of a boundary crisisWillis and Kerswell (2007a), Ben-Dov and Cohen (2007), Willis and Kerswell (2009). A clear constraint of all previous investigations is the limited range in lifetimes measured. Typically scaling laws were postulated from data covering 2 orders of magnitude. Numerical simulations are particularly problematic because in order to capture the quantitatively correct behavior computations have to be carried out in large domains, which severely restricts the number of realizations N that are manageable $\left(N<50\right)$ Willis and Kerswell (2007a). Consequently the statistics are often insufficiently resolved resulting in ambiguous probability distributions Hof et al. (2007). A further difficulty in interpreting the existing data arises from the initial formation time t_0. Most numerical measurements have been carried out at relatively low Reynolds numbers where t_0 can be larger than the actual observation time. Consequently the evaluations of lifetimes in this regime have significant uncertainties.

The experiments presented here were carried out in four pipe setups located in three different laboratories. On all four occasions the pipes were made of 1 m long precision bore glass tubes and the working fluid was water. The setups mainly differ in the diameters $\left(D\right)$ and their total

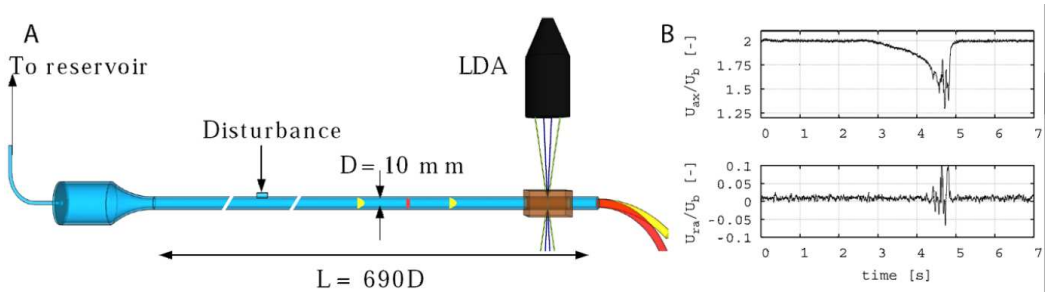

Figure 3.1: (a) Sketch of the general pipe setup. Four different pipes were used, two of them with a 10 mm diameter ($L/D = 690$ and 600) and two with a 4 mm diameter ($L/D = 2000$ and 3600). Pipes were gravity driven and turbulence could be induced by injection and withdrawal of fluid through small holes in the pipe wall at various downstream positions. Turbulence was detected by monitoring the outflow angle and by LDA velocity measurements. (b) LDA velocity trace obtained at the center line of the $D = 10$ mm ($L/D = 690$) pipe during the passage of a turbulent event. The trace shows the well-known Wygnanski and Champagne (1973) signature of a turbulent puff for the axial velocity (top) and the radial velocity (bottom).

length (L). For two pipes 4 mm (± 0.01) bore tubes were used and their lengths were $L/D = 2000$ and 3600; the other two had a diameter of $D = 10$ mm ± 0.01 and a length of $L/D = 690$ and 600. As in our previous study Hof et al. (2006) the flow was driven by a constant pressure head. To avoid fluctuations during transition caused by the differences in drag between the turbulent and the laminar motion, a large constant resistance to the flow was added to the supply line between the constant head reservoir and the flow conditioning section at the pipe entrance. This ensured that the flow rate remained constant to between 0.1% and 0.01% depending on the setup, even when transition occurred. The main improvement over the earlier study by Hof et al. (2006) was the implementation of an accurate temperature control allowing measurements to be carried out at constant temperatures (± 0.05K) for several days and hence avoiding Reynolds number changes caused by the temperature dependence of the viscosity.

In order to achieve laminar flows at Reynolds numbers in excess of 2000 the pipe sections need to be very accurately aligned and special care has to be taken at the pipe inlet to avoid turbulence being induced (see figure 3.1). In three of the pipes laminar flow could be achieved up to Re $\geq$ 3000. Detailed tests have shown that at the natural transition point turbulence is always triggered at the pipe inlet and not inside the pipe itself. For these three pipes the inlet consisted of a straight convergence reducing the diameter from 12.5 to 4 mm. In the $L/D = 690$ pipe a more sophisticated inlet was used employing several meshes and a smooth convergence . This resulted in a much higher natural transition point of Re $= 10^4$.

The experimental procedure then was as follows: First a perturbation was applied at a fixed position upstream. The perturbation amplitude was chosen large enough to trigger the transition to turbulence and the duration of the perturbations was set to between 10 and $20D/U$. The perturbed segment then develops into a so-called turbulent puff, which in this Reynolds number regime has a fixed length and travels downstream at approximately the mean velocity U Wygnanski and Champagne (1973). To determine if this turbulent puff had survived its journey to the end of the pipe or if the flow had relaminarized, the outflow angle at the pipe exit was monitored. Since for

a given Reynolds number the turbulent flow has a lower center line velocity than the laminar one, it exits the pipe at a steeper angle (with respect to the pipe axis) Hof et al. (2006), Rotta (1956). In the 10 mm pipes velocities were measured with laser Doppler anenometry (LDA) in addition to monitoring the outflow angle. These velocity measurements made it possible to determine the formation period t_0 more accurately. In the case of the single jet perturbation the value of t_0 was $t_0 = 70 \pm 5$. In order to establish if the type of perturbation used had an influence on the lifetime of the resulting turbulent flow, measurements were carried out at various amplitudes and different perturbation types. For the majority of measurements shown here a single jet was injected for a duration of $10D/U$ through a small (0.5 mm) hole in the wall. In additional studies De Lozar and Hof (2009) different types of perturbations were tested including a simultaneous injection and withdrawal of fluid through two small holes and triggering of turbulence at larger flow rates followed by a sudden reduction in the Reynolds number (this perturbation is identical to the one used by Bottin and Chate (1998), Willis and Kerswell (2007a), Peixinho and Mullin (2006)). Outside the formation period t_0 no differences, neither in the observed turbulent structures nor in their statistics were observed. Indeed, this behavior is typical for chaotic systems where the exponential divergence of neighboring trajectories quickly erases the memory of the initial conditions.

The improved temperature control allowed us to base each measurement point on observations of typically $N = 500$ and occasionally even up to $N = 100000$ puffs reducing statistical errors by an order of magnitude compared to all previous studies and increasing the range of measurable lifetimes by more than 5 orders of magnitude. The probability distributions obtained in the $D = 4$ mm pipes are shown in figure 3.2 for five different distances between the perturbation and the measurement point ($x = 140, 270, 930, 1900$, and 3500) corresponding to fixed dimensionless times $t = (x/U)(D/U)$. Our data confirm that probability distributions are S shaped and not simple exponentials as would be expected if $\tau(\mathrm{Re})$ was a linear function as proposed in Refs. Bottin and Chate (1998), Faisst and Eckhardt (2004), Willis and Kerswell (2007a), Peixinho and Mullin (2006). In particular the dotted lines show the exponential distributions that follow from the proposed boundary crisis in Willis and Kerswell (2007a). Both scalings (exponential and S-shaped curves) agree well for $\mathrm{Re} < 1870$. Here differences only occur for very short pipes, where errors due to uncertainties in t_0 are very large and make a distinction of the decay rates very difficult. For $\mathrm{Re} > 1870$ our data clearly disagree with the proposed exponentially divergent curves and instead fall on the S curves resulting from the fit shown in figure 3.3.

The observed distributions however also differ from the S shape suggested by Hof et al. (2006): they are not selfsimilar but instead their maximum slope (at $P(t) = 0.5$) increases with L/D. For each of the measured probabilities $P(t)$ inverse characteristic lifetimes $\tau^{-1}(\mathrm{Re})$ can be determined using equation 3.1, and the values are plotted in figure 3.3.

In addition to the data obtained in the 4 mm pipes, the data of the 10 mm pipes is also included in the graph. All the data collapses onto a single curve which shows that equation 3.1 is the appropriate description for the observed decay of turbulence and hence confirms the model of a chaotic repeller. By resolving values of $P(t)$ up to 0.9999 we were able to determine escape rates down to $\tau^{-1} = 10^{-8}$ which is 4 orders of magnitude smaller than had been measured before. By

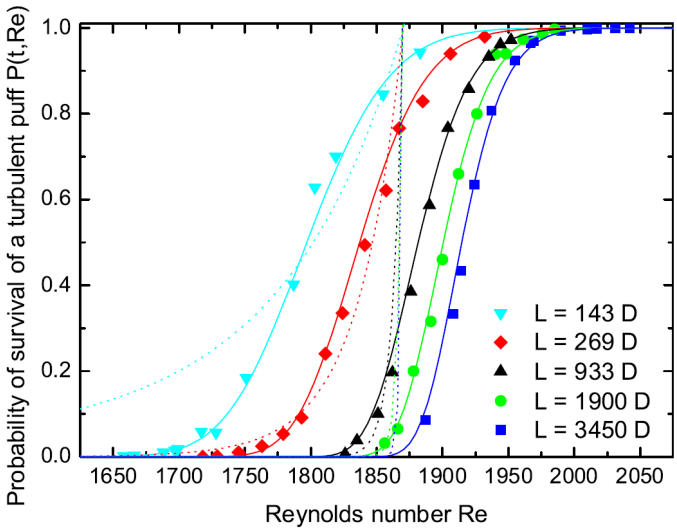

Figure 3.2: Probabilities for the flow to still be turbulent after traveling a fixed distance x. Viewed from left to right the five data sets shown correspond to the following distances: $x = 140$ (down triangles), 270 (diamonds), 930 (up triangles), 1900 (circles), 3500 (squares). The fitted curves follow directly from the superexponetial scaling shown in figure 3.3. The dotted curves show the scaling that would be expected for the critical behavior suggested by Willis and Kerswell (2007a).

resolving very small probabilities in a $L/D = 140$ pipe it was possible to determine decay rates down to $Re = 1670$ while keeping errors due to t_0 at a minimum. In principle lifetimes at even lower Re can be obtained in even shorter pipes, yet as discussed above, the uncertainty in the initial formation time t_0 is considerable when compared to the total observation time, severely restricting measurements in this regime. In addition the numerical data by Willis and Kerswell (2007a) (open squares) are plotted together with the linear fit proposed in that study. Note that the data point at $Re = 1580$ of Willis and Kerswell (2007a) has been refitted as suggested in Hof et al. (2007). The numerical data is in excellent agreement with our measurements (taking the relatively large uncertainties due to t_0 at small Re into account). However the data of our experiments clearly does not follow the linear fit [dashed curve in figure 3.3(a)] proposed in their study. Turbulent puffs are still found to decay well beyond the critical point of $\mathrm{Re}_c = 1870$ postulated by Willis and Kerswell (2007a). The exponential scaling suggested by Hof et al. (2006), shown by the solid black line, gives a reasonable fit only over 2 orders of magnitude in τ^{-1}, but fails over the far larger range measured in the present study. Over these 2 orders of magnitude also the shape of the probability distributions of the present study are indistinguishable to the ones by Hof et al. (2006). Outside this overlap region the S curves in the present study are observed to become steeper with Re. Such a Re dependence had not been seen in the earlier study Hof et al. (2006). Note that the solid black line in figure 3.3 was shifted by $\Delta\mathrm{Re} = -48$ with respect to the one shown in Eckhardt et al. (2007). This shift of the data corresponds to a 2.5% difference in the absolute value of Re. In particular the uncertainty of the pipe diameter in Hof et al. (2006) with $(\pm 1.5\%)$ was comparatively large; furthermore in the present study greater care was taken to measure the absolute value of the temperature allowing to determine the viscosity values more accurately.

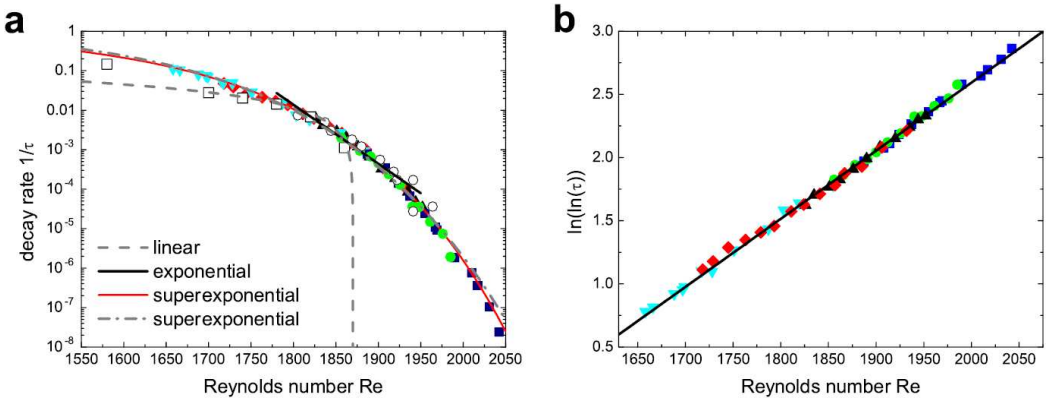

Figure 3.3: Decay rates plotted on a log linear scale. Circles represent data obtained in the $D = 10$ mm pipes while the full symbols were measured in the $D = 4$ mm pipe. The dashed line and the open squares are a reproduction of the data points and the linear fit given by Willis and Kerswell (2007a). The black line has the same slope as the exponential scaling observed by Hof et al. (2006). The light solid curve assumes a superexponential dependence of the decay rate on Re. The dash-dotted line shows an alternative superexponential fit (see text for details). (b) Data on a log-log linear scale. The data could be fitted by a straight line over the entire regime. This two parameter fit was then used to plot the five curves in figure 3.2 as well as the light solid curve in figure 3.3(a).

The robustness of the scaling behavior was tested by applying a periodic modulation to the flow rate. At a frequency of up to 2 Hz and an amplitude of $\Delta\mathrm{Re} = \pm 10$ the shape of the S curves remained unchanged within experimental errors. Equally small intentional misalignments of the pipe segments did not show any noticeable influence on the distribution shape. S-shaped probability distributions have also been observed in plane Couette Hof et al. (2006), Schmiegel (1999) flow suggesting that this scaling behavior applies to a variety of shear flows.

In figure 3.3(b) the present data are shown on a double log linear scale. On this scale a straight line can be fitted to the data suggesting lifetimes scale superexponentially with Re: $\tau^{-1} = \exp\left[-\exp\left(c_1\mathrm{Re} + c_2\right)\right]$, with $c_1 = 0.0057$ and $c_2 = -8.7$. As shown in figure 3.3 this two parameter fit captures the observed escape rate dependence over 8 orders of magnitude. Equally the S-shaped curves plotted in figure 3.2 directly follow from this straight line fit without any additional fitting parameters. While the data allows to rule out functional forms which are subexponential, it should be noted that adequate fits can also be obtained by other superexponential functions.

For instance, $\tau^{-1} = \exp\left[-\left(\mathrm{Re}/c\right)^n\right]$, with $c = 1549$ and $n = 9.95$ [dash-dotted line in figure 3.3(a)]. Here the magnitude of the exponent n is related to the rate at which the basin of attraction of the laminar state shrinks as Re increases Tél and Lai (2008). Discriminating between the different superexponential scalings would require measurements over a substantially larger Reynolds number range. However, due to the rapid increase in lifetimes the parameter space observable in experiments is rapidly approaching its limit. In order to measure the escape rate at $\mathrm{Re} = 2100$ would require an estimated time of 46 yr in our setup, and at $\mathrm{Re} = 2200$ with 10^{12} yr the experimentation time would have to surpass the age of the Universe. Previously long lived transients whose lifetime scales superexponentially with system size, so-called Type-II supertransient Tél

and Lai (2008), had only been observed in low-dimensional dynamical systems.

In conclusion, by increasing the range of measured lifetimes by 6 orders of magnitude and significantly reducing statistical errors the decay rate of turbulence has been measured far more accurately than previously possible. The observation of a critical point reported in many recent studies is not supported. The superexponential behavior found here identifies turbulence in pipe flow as a type-II supertransient Tél and Lai (2008), Crutchfield and Kaneko (1988), which had been conjectured as a potential description of turbulence two decades ago Crutchfield and Kaneko (1988). This scaling shows that at least in the intermittent regime, the correct dynamical model of turbulence in linearly stable shear flows is that of a strange repeller.

The authors would like to thank B. Eckhardt, J. Vollmer, T. M. Schneider, C. Poelma, and R. Delfos for helpful discussions. This resarch was supported by the EPSRC (Grant No. EP/F017413/1), the Max Planck Society, and FOM (Foundation for Fundamental Research of Matter).

Chapter 4

Quantitative measurement of the lifetime of localized turbulence in pipe flow[1]

Transition to turbulence in a pipe is characterized by the increase of the characteristic lifetimes of localized turbulent spots ('puffs') with increasing Reynolds number (Re). Previous experiments are based on visualization or indirect measurements of the lifetime probability. Here we report quantitative direct measurements of the lifetimes based on accurate pressure measurements combined with laser-Doppler anemometry. The characteristic lifetime is determined directly from the lifetime probability. It is shown that the characteristic lifetime does not diverge at finite Re, and follows an exponential scaling for the observed range $1725 \leqslant Re \leqslant 1955$. *Over this small Re range the lifetime increases over four orders of magnitude. The results show that the puff velocity is not constant, and the rapid disintegration of puffs occurs within 20-70 pipe diameters.*

4.1 Introduction

The transition to turbulence in pipe flow can be characterized by the lifetimes of localized turbulent spots, or 'puffs.' These puffs co-exist with the laminar flow state, and travel downstream with a velocity of around the bulk velocity (Lindgren 1969, Wygnanski and Champagne 1973). Faisst and Eckhardt (2004) used a direct numerical simulation (DNS) to investigate the lifetime of the turbulent flow state in a short periodic pipe. They found that the probability $P(t;Re)$ of survival at a given Reynolds number (Re) decays exponentially with time, reminiscent of a memoryless process, i.e.

$$P(t;Re) = \exp[-(t-t_0)/\tau(Re)], \tag{4.1}$$

where t_0 represents a formation time of the disturbance, and $\tau(Re)$ the characteristic lifetime of the disturbances. Faisst and Eckhardt (2004) obtained $\tau(Re)$ from the median lifetime of the disturbances, which appeared to scale as $\tau^{-1} \propto (Re_c - Re)$, where Re_c is a *critical Reynolds*

[1]This chapter has been published in the Journal of Fluid Mechanics (Kuik et al. 2010)

number at which the lifetime diverges. Earlier, new solutions of the Navier-Stokes equations for pipe flow, in the form of *traveling waves*, were identified (Faisst and Eckhardt 2003, Wedin and Kerswell 2004, Hof et al. 2004). These solutions were thought to form a *strange saddle* in phase space, so that a disturbance of the base flow, i.e. Hagen-Poiseuille flow that is represented as a stable node, leads to a transient for which the duration increases proportional to the Reynolds number. A divergence of the duration of the transient, or lifetime of the disturbance, that occurs at *finite* Reynolds number implies a transition from a strange saddle to a strange attractor in phase space (Eckhardt et al. 2007). The strange attractor would implicate turbulence as a sustained flow state.

Faisst and Eckhardt (2004) found $Re_c \cong 2250$, which agrees with empirical data. However, re-examination of the data, where $\tau(Re)$ was evaluated directly from the slope of $P(t;Re)$ in a semi-log plot, showed that $\tau(Re)$ scales exponentially, i.e. $\tau^{-1} \propto \exp(-Re)$, so that the lifetime does not diverge at a finite critical Reynolds number (Hof et al. 2006). To examine in which way the lifetime diverges with *Re* requires long observations times of several hundred or even thousands of integral time scales.

Peixinho and Mullin (2006) carried out an experiment to determine $P(t;Re)$ by observing the decay of a puff in a constant mass flux pipe. First a puff was generated at *Re*=1900, and when it had survived 100 pipe diameters the Reynolds number was reduced, and the decay of the puff was observed. The turbulent motion in the puff was visualized with small platelets, and the moment of decay was determined visually. The results confirmed the exponential probability in (4.1), and it was found that τ^{-1} scales linearly with $Re_c \cong 1750 \pm 10$. Willis and Kerswell (2007a) represented the experiment in a DNS. They also found an exponential distribution for $P(t;Re)$ and a linear scaling of τ^{-1}, although the observation times where rather short, with $Re_c \cong 1870$. However, re-evaluation of their data showed that the same results would be reconcilable with an exponential scaling of τ^{-1} (Hof et al. 2007, Willis and Kerswell 2007b). Recent data (Hof et al. 2008) showed that the lifetime scales *super-exponentially*, i.e. $\tau^{-1} \propto \exp[-(Re/c)^n]$ with n=9 and c=1549, over eight orders of magnitude in τ.

The measurements of $\tau(Re)$ by Hof et al. (2006, 2008) are based on the probability $P(Re;L)$ that a puff survives a given pipe length L as a function of Reynolds number. This probability has a characteristic S-shape in the case of an exponential scaling of $\tau(Re)$. However, this *implicitly* assumes that $P(t;Re)$ has the form given in (4.1). Also, this experiment does not allow to constantly monitor the formation of the puff after the injection, the motion of the puff along the pipe, and its sudden decay. Especially at high Reynolds number, where only a very small fraction of puffs decays before reaching the pipe exit, it is difficult to make a distinction between puffs that decay in the pipe and a possible misfiring of the disturbance mechanism or disturbances that failed to generate a puff. Furthermore, this approach requires an estimate of the mean puff velocity, in order to convert the distance L into a lifetime.

In this paper we report results of quantitative lifetime measurements that are based on accurate pressure measurements. This makes it possible to directly determine $P(t;Re)$, rather than relying on an implicit assumption that the lifetime probability follows (4.1). Since we measure over a pipe section that excludes the injection it is possible to determine $\tau(Re)$ irrespective of the puff

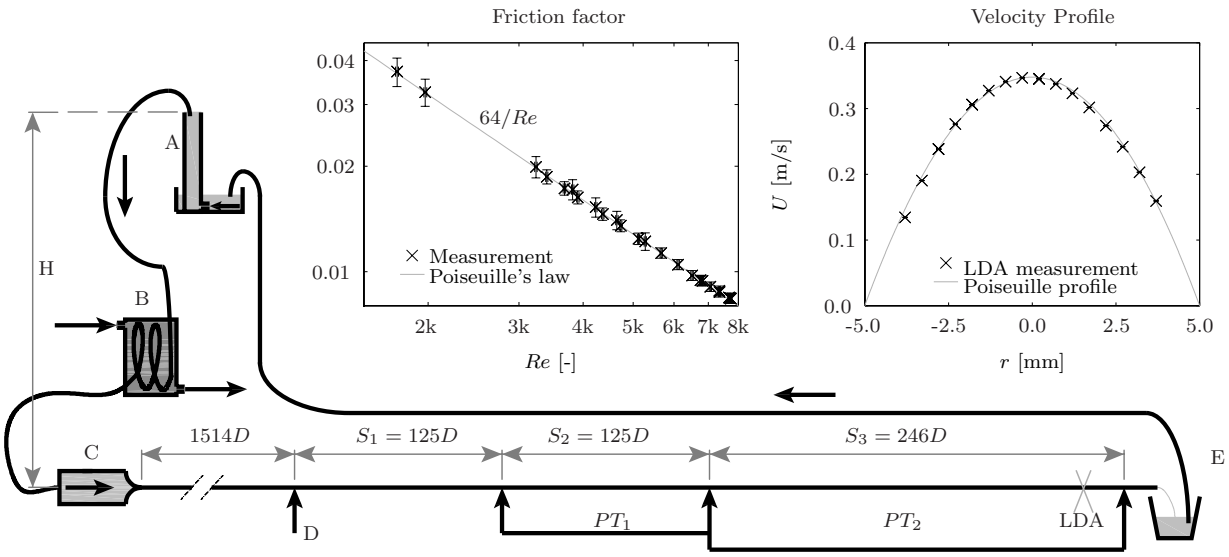

Figure 4.1: Schematic of the experimental setup. A: overflow reservoir to maintain constant pressure head (H); B: heat exchanger; C: flow conditioner containing several meshes with reducing grid size and a smooth 1:100 area contraction; D: flow disturbance; E: pipe exit with second reservoir from which fluid is pumped back into reservoir (A); $PT_{1,2}$: pipe sections over which the pressure drop is measured by a pressure transducer. *S*: indicates a pipe section; LDA: location of velocity measurement by LDA. *Inset, left*: Measured friction factor ($\times$) as a function of Reynolds number together with Poiseuille's friction law (—); error bars represent an estimate of the total experimental error. *Inset, right*: Velocity profile measured with LDA ($\times$) together with a calculated velocity profile based on the mass flow rate (—).

formation. The inlet length for laminar pipe flow at Re=2×10^3 is $\sim$120D, so that any applied disturbances that failed to generate a puff are expected to have decayed before the first pressure tap at L/D=125 (see section 4.2). Apart from being able to directly measure the lifetime t that individual puffs travel along the pipe, it is possible to determine the decay time during which the puff disintegrates. It is thus possible to validate the assumption of sudden puff decay that underlies the expression for $P(t;Re)$ in (4.1).

4.2 Experimental setup and method

The flow facility used for the measurements is similar to the setup used by Hof et al. (2006, 2008). Figure 4.1 shows a schematic overview of the setup. The main difference is that in the current setup special care is taken to reduce pressure fluctuations. The 20-meter long pipe is made of 16 glass tubes, each 120-130D in length, with an inner diameter of $D = 10 \pm 0.01$ mm. The pipe sections are joined by PMMA connectors with the same inner diameter, that contain 0.5 mm holes which could either be used for sensing the pressure or to introduce the flow disturbance. The water flow is driven by the constant pressure head generated by the height difference between the free surface of the overflowing reservoir (A) and the outflow of the pipe (E). At regular intervals the fluid from reservoir E is pumped back into the base from which the overflowing

reservoir is fed. The flow rate of the system can be adjusted manually by changing the total pressure head between 3.0 and 3.5 meters (corresponding to 30–35$\times 10^3$ Pa).

To reduce pressure fluctuations in the pipe, the amount of overflowing fluid has been minimized. Furthermore, the fluid was introduced from the bottom and guided through a set of flow straighteners to remove any remaining fluctuations caused by the pump and the introduction of the fluid into the reservoir. From the top reservoir, the fluid flows through a feeding line consisting of two segments: one 10-meter long copper tubing segment and one 15-meter long flexible tubing segment.

The 20-m pipe section is thermally insulated from the environment. To control the temperature of the working fluid, temperature-controlled water is forced around the copper segment (B), creating a heat exchanger by which the daily temperature variation is maintained to within $\pm 0.3\ ^\circ$C. To determine the exact Reynolds number at which each measurement is taken, the temperature of the water is continuously monitored at the pipe exit (E) using a calibrated mercury thermometer. Using a digital camera, the temperature reading could be determined with a precision of $3.4\times 10^{-3}\ ^\circ$C.

The main pressure drop occurs between sections A and C, where the tube has a smaller diameter (6 mm) than in the straight pipe. In this section the flow remains turbulent, and the total pressure loss is much larger than in the 10-mm diameter pipe. Introduction of a turbulent disturbance in the pipe (D) lowers the flow rate by the additional friction of the local turbulent flow. However, one can easily verify that the flow rate changes by less than 0.01% for the current configuration, because of the large pressure drop over the feeding line. Therefore this setup can be considered to effectively operate with a constant mass flux condition. In a numerical investigation Willis and Kerswell (2009) showed that the lifetime statistics for puffs (for sufficiently long computational domains) did not change for either constant pressure drop or constant mass flux conditions. Therefore it is valid to compare the present results with those found in experiments and numerical simulations under constant mass flux conditions.

To validate that the pipe is internally smooth, the friction factor was determined by measuring simultaneously the pressure drop and the flow rate. The pressure difference was measured by an inverted U-tube manometer between pressure taps at 625D and 1514D from the pipe inlet, covering almost 890D. The first pressure tap was far enough from the entrance to avoid effects due to the development of the flow, even at high Reynolds numbers (the entrance length for Re=8000 is approximately 500D). The flow rate was determined by measuring the weight of the fluid that exits the pipe over at least 200 seconds. The result for the measured friction factor F as a function of Re is shown in figure 4.1, in comparison to Poiseuille's law (F=64/Re). A laminar flow state could be sustained for $Re > 9\times 10^3$, before natural transition occurred. Since experiments are carried out only for $Re < 2000$, it is not expected to observe spontaneous generation of turbulence. Using laser-Doppler anemometry (LDA), a velocity profile was measured at 2000D from the pipe entrance for Re=1750. Figure 4.1 shows the measured velocity profile in comparison to a parabolic Poiseuille profile based on the measured flow rate. In the lifetime experiments, the centerline velocity was measured by LDA at the same location to validate that the flow disturbance has the typical characteristics of a puff. This is more reliable than observing the jet angle at

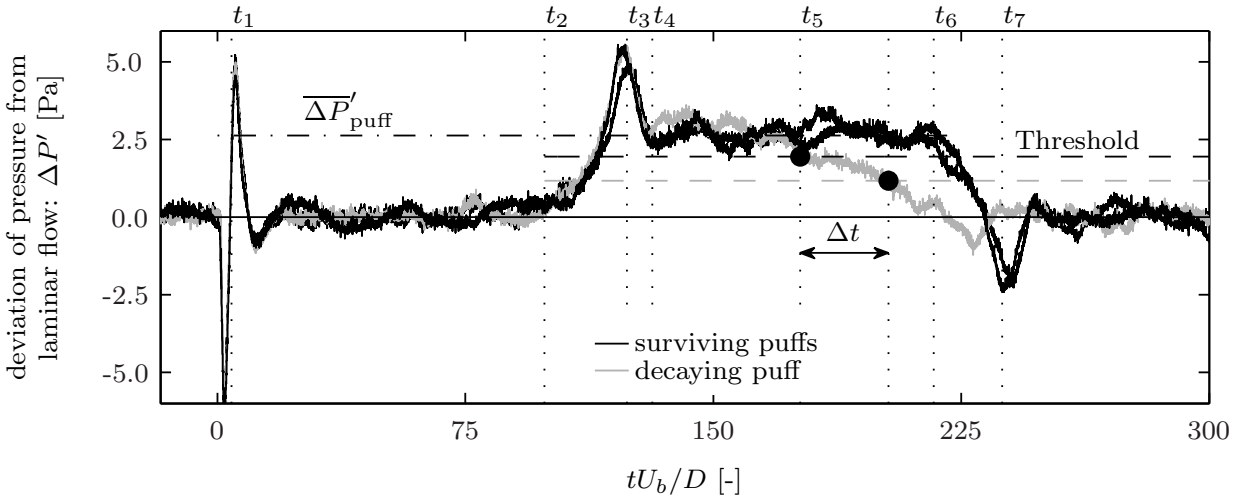

Figure 4.2: Three instantaneous time series of pressure data at $Re = 1822$, measured by PT_1 showing two surviving and one decaying puff. The dashed black line is the threshold level (T_1) used to determine the location of decay, the second (dashed grey line) threshold (T_2) is used to determine the puff disintegration time. See text for details.

the pipe exit (Rotta 1956, Hof et al. 2006). After each measurement series, the Reynolds number is determined based on the measured mass flow rate and measured temperature, and could be determined with an estimated total uncertainty of ± 4 (i.e., 0.2% at *Re*=2000).

In a lifetime experiment, the fully developed laminar flow is shortly perturbed to create a localized flow disturbance. In the current experiment the flow is disturbed by a zero mass flux disturbance, at 1514*D* from the pipe entrance. The non-dimensional amplitude of the disturbance was equal to 0.1, based on the ratio of disturbance mass flux and pipe-flow mass flux. The amplitude is above the critical amplitude to create a puff (Darbyshire and Mullin 1995, Hof et al. 2003). The flow is perturbed during 0.0625 s (1.1-1.2D/U_b), which is much shorter than the disturbance time of 10-20D/U_b used in previous experiments (Hof et al. 2006, 2008, De Lozar and Hof 2009). Previously, Mullin and Peixinho (2006) found that the critical Reynolds number is reduced by increasing the disturbance amplitude. The amplitude was chosen in correspondence to the lowest critical Reynolds number reported by Mullin and Peixinho (2006). However, De Lozar and Hof (2009) already showed that the type of disturbance did not change the lifetime scaling.

In the present experiment the lifetime of a puff is determined using two differential pressure sensors (Validyne DP45). One pressure transducer (PT_1) measures the pressure drop between taps at 125*D* and 250*D* (S_2) from the disturbance, and the second (PT_2) between 250*D* and 496*D* (S_3). Both pressure transducers were calibrated using a micro-manometer (Betz) and have a full range of 150 Pa with an accuracy better than 0.75 Pa. In the remainder of this section only the results from the first pressure sensor (PT_1) are shown, but an identical analysis applies to each time series measured for PT_2. The extension to much larger domains by adding more pressure sensors is trivial.

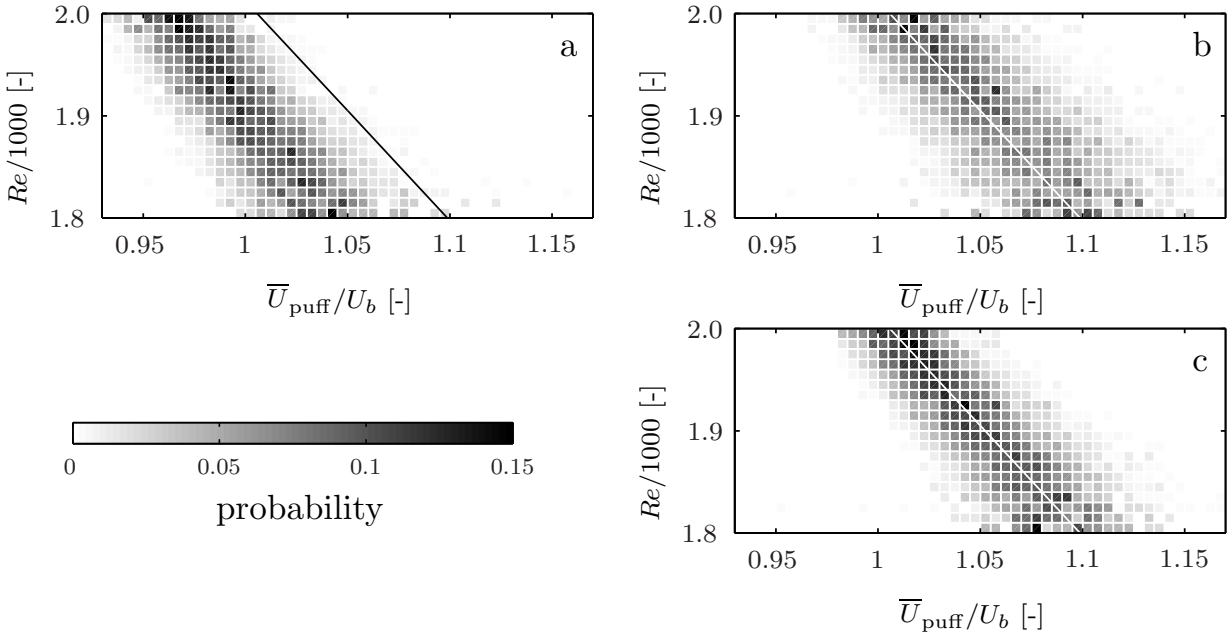

Figure 4.3: Probability density functions of relative average puff velocity as a function of *Re*; *(a)* in section S_1; *(b)* in section S_2; *(c)* in section S_3. The inclined straight line is a least square fit to the velocity distribution in section S_2 and is given in the other plots for comparison.

Figure 4.2 shows three signals recorded by PT_1; for clarity the pressure drop due to laminar flow ($\Delta P \sim 64$ Pa) has been subtracted. The recording starts just before the disturbance is applied at t_1, where the signal shows a single oscillation with a large amplitude. The oscillation ensures that the disturbance was applied. The short-duration pressure oscillation does not induce any significant acceleration or deceleration of the fluid mass in the pipe. The amplitude of the oscillation would be much larger when generated by a non-zero mass flux injection, i.e. when the injected mass is not simultaneously removed.

After the flow has been disturbed, the disturbance forms into a puff and is convected downstream. Since the puff is now present in section S_1, the pressure drop measured by PT_1 is only due to laminar flow, hence the additional pressure drop $\Delta P' = 0$. At t_2 the puff begins to enter section S_2, indicated by the increase in $\Delta P'$, which reaches a maximum at t_3. Then it falls to approximately half the maximum value, which is indicative of an adverse pressure gradient at the transition side of the puff. Rotta (1956) derived that the theoretical upper limit of the pressure *increase* due to the transition from a laminar velocity profile to a uniform velocity profile is equal to $\frac{1}{3}\rho U_b^2$. This would imply a pressure rise of almost 10 Pa. This is not observed in the present data, because the mean velocity profile inside the puff is not uniform. Nevertheless, the predicted adverse pressure gradient is clearly visible.

Figure 4.2 shows the pressure time series (black lines) for two arbitrary puffs. Both time series show the same characteristics, with a constant additional pressure drop between t_4 and t_6, indicating that the entire puff is inside section S_2. When the puff leaves this section, the same characteristics in pressure are observed as when the puff enters the domain. Due to the presence

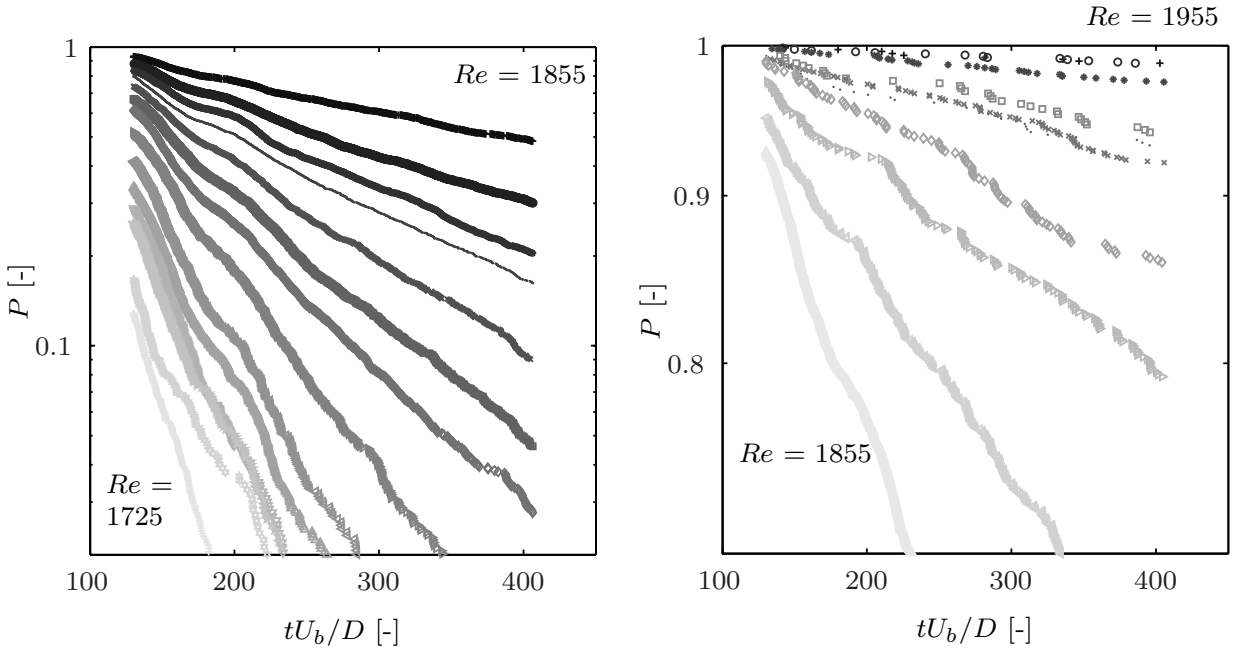

Figure 4.4: Semi-log plots of the probability $P(t;Re)$ that a puff survives a time $t\ U_b/D$, where U_b is the bulk velocity and D the pipe diameter, for Re between 1725 ± 5 and 1955 ± 5, in increments of 10. The data for Re=1855 appears in both graphs for reference. The slope of each curve determines $\tau(Re)$ defined in (4.1), which increases with Re.

of only the transition front inside section S_2, a sub-laminar pressure drop ($\Delta P' < 0$) is observed around t_7. Hence, both puffs survived while passing section S_2. For the time series represented in light grey the behavior up to t_5 is the same as previously described. However, for $t > t_5$ the sub-laminar pressure difference is not observed, from which it can be concluded that the puff decayed within section S_2.

This allows for the determination of the lifetime of each individual puff by observing the time at which $\Delta P'$ drops below a certain threshold. The threshold value should be chosen below the additional pressure due to the presence of a puff, but should be higher than the noise amplitude of the signal in the absence of a puff. After some preliminary investigation a single threshold value of 1.95 Pa was chosen for all Reynolds numbers (indicated in figure 4.2). The mean value for $\Delta P'$ between t_4 and t_6 ($\overline{\Delta P'}_{\text{puff}}$) was determined for all puffs that survive beyond the downstream pressure tap. A minimum value of $\overline{\Delta P'}_{\text{puff}}$ = 2 Pa was found. The pressure signal noise fluctuation is estimated at 0.37 Pa for laminar flow, which is less than one-fifth of the selected threshold. The individual lifetimes that were found depended on the selected threshold value, although the result for the scaling of $\tau(Re)$ did not change significantly for threshold values between 1.2 and 2.7 Pa.

In figure 4.2 it is clearly visible that the sub-laminar pressure peak in t_7 does not occur at $t\ U_b/D = 250$, which would be expected when the puff travels with the bulk velocity. This indicates that the puff is not traveling at the bulk velocity, but slightly faster. Given the dis-

tance between the pressure taps and the time difference between the occurrence of the pressure peaks, the average velocity of the puff can be determined. Only puffs that survive beyond the last pressure tap (at $496D$ after the injection point) are taken into account. Since hardly any puff survived beyond $496D$ for $Re < 1800$, only the measured mean velocities for $1800 < Re < 2000$ are determined.

Figure 4.3 shows the probability density function of the mean puff velocity in sections S_1, S_2 and S_3. If puffs would move at a constant mean velocity through the pipe, these figures would be identical. Comparing the graphs in figure 4.3 shows that the puff first accelerates as it moves downstream, while the velocity PDF in sections S_2 and S_3 appear to be identical.

Clearly, the puff velocity at given Re is not fixed. An open question is whether each puff travels at its own constant velocity (for fixed Re), or that the puff velocity is variable as it travels along the pipe. An indication of the validity of the second statement is the correlation coefficient of the puff velocity in sections S_2 and S_3, which turns out to be between 0.49 and 0.51. This implies that the puff velocity is variable.

Note that in earlier measurements (Hof et al. 2006, 2008), in which the survival probability was determined for a fixed pipe length L, the characteristic non-dimensional lifetime was determined as $\tau = L/U_{\text{puff}}$, where U_{puff} is the mean puff velocity determined from the time difference between the moment of injection and the moment the puff reaches the pipe exit at a distance L. Since the puff velocity is not uniquely defined, we prefer to non-dimensionalize the directly measured lifetime with D/U_b.

4.3 Results

To determine the characteristic lifetime τ, first the lifetime of each individual puff was determined. Then the measurements were sorted according to their Reynolds number (given by the temperature reading at the pipe exit) and binned with a width of ± 5 for Re=1725,1735,1745,...,1955. The total number of measurements for each Re is between 500 and 3500. The number of puffs that decayed before arriving at the first pressure tap were removed from the data. Next, $P(t;Re)$ is found as the number of surviving puffs over the total number of data, where it drops by one count for each measured lifetime, until the lifetime exceeds the domain covered by the pressure transducers.

In figure 4.4 the resulting probability distributions are plotted. Each point in this figure represents the measured lifetime of an individual puff. The results for $P(t;Re)$ are clearly exponential (i.e. data follow straight lines in a semi-log plot). This is in agreement with the results for $P(t;Re)$ found by Peixinho and Mullin (2006) and Willis and Kerswell (2007a). However, here we observe that even for Re above the critical Reynolds numbers of 1750 and 1870 identified by Peixinho and Mullin (2006) and Willis and Kerswell (2007a) respectively, numerous puffs decay. Moreover, decaying structures are observed for $Re > 1900$, which is the Reynolds number at which the disturbances were initiated in the experiments by Peixinho and Mullin (2006).

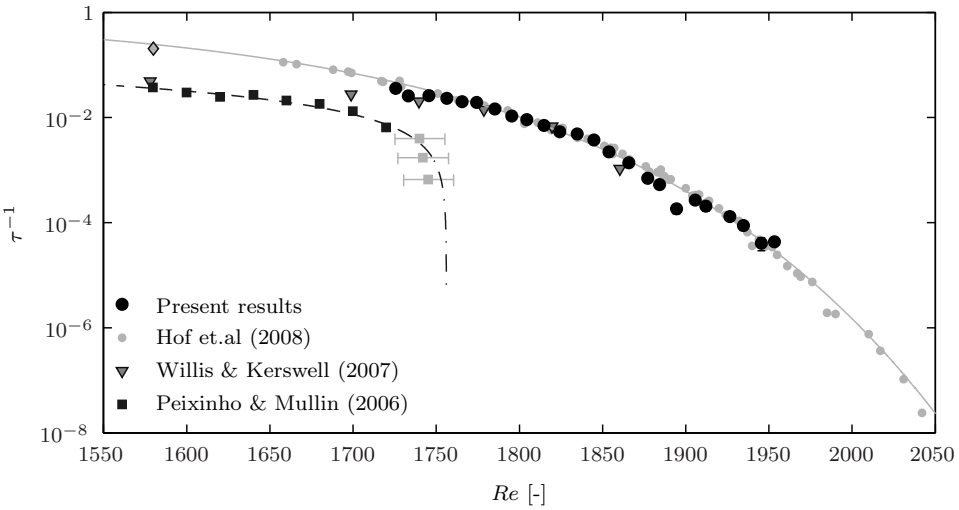

Figure 4.5: The inverse of the characteristic lifetime τ^{-1} as function of Reynolds (*Re*) number. Data from Peixinho and Mullin (2006) and Hof et al. (2008) are included, together with their linear and super-exponential scaling respectively. The data points of Peixinho and Mullin (2006) for $Re \geq 1740$ are plotted in light grey since they are, considering the error estimates, measured at the same Reynolds number. The data of Willis and Kerswell (2007a) is shown, in which the data point at *Re*=1580 is reinterpreted (Hof et al. 2007, Willis and Kerswell 2007b)(Hof et al. 2007, (◇), original (▼))

.

In previous investigations the characteristic lifetime $\tau(Re)$ was obtained by determining the median or half lifetime, i.e. the lifetime for which the survival probability equals 0.5 (Faisst and Eckhardt 2004, Peixinho and Mullin 2006, Willis and Kerswell 2007a, 2009). This approach depends heavily on the initial formation time, indicated as t_0 in (4.1), which is the time needed for the disturbance to develop into a puff. Instead, the characteristic lifetime (together with the formation time t_0) can also be determined by fitting the expression in (4.1) to the probability distributions in figure 4.4. This has the advantage that τ can be determined for lifetimes that are shorter than the characteristic lifetime, which avoids the use of a pipe with extremely large values of L/D (Hof et al. 2008).

In figure 4.5 the lifetimes are given based on a least square fit to the probability distribution in figure 4.4. To estimate the confidence interval a bootstrapping method was used. By extracting 100,000 new data sets of the same length as the initial data set from the data given in figure 4.4, the median and standard deviation of the best fitting slopes was calculated, resulting in error bars smaller than the symbols used in figure 4.5. In the same figure also the data of Peixinho and Mullin (2006), Willis and Kerswell (2007a) and Hof et al. (2008), together with their proposed best fits, are given. Despite the different methods used to determine the lifetimes, the best agreement is found with the data of Hof et al. (2008).

In addition to the measurement of the characteristic lifetime and mean convection velocity of the puffs, we used the pressure measurements to determine the disintegration time ($2\,\Delta t$) of the puffs, which is the time needed to become fully laminar after decay sets in. It is determined from

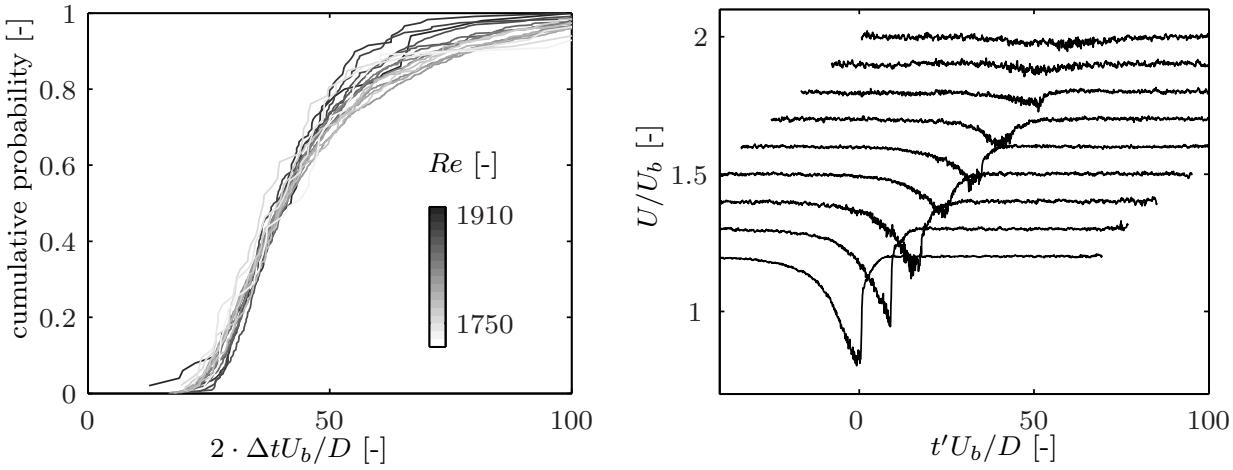

Figure 4.6: *Left* Cumulative probability distribution of the time needed between initiation and complete decay of a puff; *Right* Evolution of the conditionally-averaged centerline velocity of a decaying puff for nine consecutive times relative to the onset of decay (t_5 in figure 4.2).

the time between passing a threshold T_1 and a second threshold T_2, and non-dimensionalized by D/U_b; see figure 4.2. Cumulative probability distributions for the disintegration time were computed for decaying puffs at *Re*=1750, 1760, 1770 ... 1910, and are plotted in figure 4.6. No obvious trend with *Re* is observed, so that the disintegration process seems to be universal over this *Re* range. It is clear from figure 4.6 that it takes at least 20*D* for a puff to decay, which is approximately the length of a puff (Wygnanski and Champagne 1973). About 80% of the puffs need less than 60*D* to disintegrate completely.

To visualize the disintegration itself, the conditionally averaged centerline velocity measured by LDA was used. The pressure measurements are used to determine the location of disintegration with respect to the location of the LDA measurement point. In figure 4.6 the velocity time series for nine consecutive disintegration times are shown for *Re*= 1850$\pm$5. The top line shows the averaged velocity profile for a puff that started to decay 70*D* upstream of the LDA measurement point. The velocity profiles for the puffs that decay closer to the velocity measurement point are plotted with a vertical offset for clarity. The bottom velocity trace shows the result when a puff has survived up to the point where the velocity is measured and reveals the classical centerline velocity time series observed for a puff.

4.4 Conclusions

In this paper we present results of direct quantitative measurements for the lifetime of individual localized turbulent structures, or 'puffs', in pipe flow. The mean shape of the puff during decay could be reconstructed from conditionally-averaged LDA measurements. Pressure measurements can be used to directly determine the lifetime of each individual puff, where the measurement is based on a predefined threshold for the pressure increase when a puff is present in

a given pipe section, rather than a visual inspection of a flow visualization. By combining all measurements, the lifetime probability distribution $P(t;Re)$ is obtained, which shows an exponential decay given in (4.1), which is characteristic for a memoryless process. By using a fit to the probability function $P(t;Re)$ the characteristic lifetime $\tau(Re)$ could be determined from the slope of the distribution in a semi-log plot. The present results depend neither on the initial formation time t_0, nor on the inclusion of applied disturbances that may fail to develop into a puff. This avoids possible complications of previous investigations of the characteristic lifetime. In addition, we obtained direct measurements of the lifetime probability, rather than observing the probability $P(Re;L)$ that puffs survive a given pipe length L as function of Re, which implicitly assumed an exponential decay for $P(t;Re)$.

The present data confirm that the scaling of the lifetime with Re is super-exponential, as proposed by Hof et al. (2008). This confirms that the lifetime does not diverge at a finite critical Reynolds number Re_c within the observed Reynolds number range of $1725 \leqslant Re \leqslant 1955$, which is well above previously reported values for Re_c. For Re=1950 there is a significant fraction of puffs that decay before reaching the end of the measurement domain, with an estimated characteristic lifetime of $25 \times 10^3\ D/U_b$; see figure 4.5. This implies that no indication is found for a transition in phase space of the strange saddle into a strange attractor, which would imply a sustained turbulent flow state. Therefore each puff should be considered as a transient flow state. At much higher Reynolds numbers, puffs may split or grow in length to form into 'slugs' (Wygnanski and Champagne 1973, Nishi et al. 2008). This behavior cannot be explained by the current dynamical systems point of view, and a completely different mechanism may describe the transition to turbulence.

In addition, the measurements show that puffs do not move at a constant mean speed through the pipe, which is in contrast with previous observations. Furthermore, the puffs show a rapid decay, which underlies the memoryless process represented by (4.1), that occurs within 20-70 pipe diameters.

Acknowledgements

The authors would like to thank Bruno Eckhardt, Marc Avila, Björn Hof and René Delfos for the useful discussions on the work presented here. This work is part of the research program of the Foundation for Fundamental Research on Matter (FOM), which is financially supported by the Netherlands Organisation for Scientific Research (NWO).

Chapter 5

Simulation of localized turbulent pipe flow

5.1 Introduction

In the previous chapters, the global behavior of localized turbulence in a pipe, or puffs, is described for Reynolds numbers up to $Re = 2000$. This chapter provides a more detailed description of a puff. The first approach was to use stereoscopic PIV measurements to get more details on the behavior of the internal structures of the puff. The PIV measurements gave the velocity field in a planar cross section as a function of time. By applying a kind of Taylor hypothesis, the quasi-instantaneous 3D flow structure are reconstructed (van Doorne and Westerweel 2007). However, this does not provide any information on the temporal evolution of these structures. Therefore, the planar PIV experiments were not sufficient to get an image of the dynamics within the puff, and another approach was taken.

Van Doorne and Westerweel (2009) found, from a few experimental observations, strong and localized structures in the form of narrow ($0.09D$) peaks in the ”in-plane kinetic energy” (see equation 1.2), that were associated with regions with a high degree of symmetry in the vicinity of hairpin like coherent structures. However, in simulations on transitional pipe flow (Willis and Kerswell 2007a, 2008, Avila et al. 2010, Moxey and Barkley 2010, Duguet et al. 2010) these structures were never reported. Van Doorne and Westerweel (2009) concluded that in existing numerical simulations the axial resolution may have been not sufficient to resolve these small-scale features. This was the major motivation to perform a numerical simulation in a long domain with a very high axial resolution. Furthermore, the behavior and physical relevance of these structures was unclear. De Lozar and Hof (2009) showed two uncorrelated experimental realizations of the in-plane kinetic energy. In their results (see figure 7 in De Lozar and Hof (2009)), similar small-scale structures are observed. Note that the location of these structures with respect to the puff is different for each realization. This led to the belief that these structures would show some dynamics of their own. Van Doorne and Westerweel (2009) associated the observed structures to hairpin-like vortices.

In this chapter the results of this simulation are discussed, starting with a description of the nu-

merical procedure in section 5.2. As an initial condition for the direct numerical simulation, the results from a single PIV measurement were used. The description of the numerical procedure is followed by a description of the effect of simulating transitional pipe flow at different resolutions in section 5.3. As a validation of the numerical code, fully developed turbulent pipe flow is simulated and compared to existing numerical and experimental data. These results are presented in section 5.4. Wygnanski and Champagne (1973) and Bandyopadhyay (1986) described different parts of the puff and found a region which is comparable to fully developed turbulent pipe flow. In order to validate this, a puff at $Re = 1900$ is compared to fully developed turbulent pipe flow simulated at $Re = 5300$ in section 5.5. The localized nature of puffs introduces unique scales for length and velocity: the ones of the global structure. In section 5.6 the properties and global behavior of individual puffs at different Reynolds number, are described. It is shown that in the current simulation the small scale structures, first described by van Doorne and Westerweel (2009), are present. Since the current DNS allows for the tracking of these structures over time, the associated structure can be revealed. The structures are visualized by showing large scale vortical motion using the Q-criterion (Jeong and Hussain 1995). Furthermore, section 5.7 contains a discussion about the dynamics of these structures. Finally, concluding remarks can be found in section 5.8.

5.2 Numerical Procedure

The goal of the current direct simulation is to simulate localized turbulent pipe flow in a periodic domain. The localized nature of the flow results in structures that have a length of the order of 25 pipe diameters (Wygnanski and Champagne 1973, Wygnanski et al. 1975, van Doorne and Westerweel 2009, De Lozar and Hof 2009). To prevent the puff from interacting with itself, a minimum domain length of $50D$ is required. Here domain lengths of $50D$ and $100D$ are used. Table 5.1 shows an overview for the domain lengths used by a number of authors for their simulation of transitional pipe flow.

For the DNS of pipe flow a code has been used that was based on the code used by Ptasinski (2002). However, instead of using cartesian coordinates, the Navier-Stokes equations are represented in cylindrical coordinates. The simulation is done with a pseudospectral method in the circumferential and axial direction. In the radial direction a standard 2^{nd} order staggered finite difference method is used. The Fourier expansion of the velocity field can be written as

$$u(r,\theta,z,t) = \sum_{N_z}\sum_{N_\theta} \hat{u}_{jk}(r,t) e^{-ij\theta} e^{-ikz} \tag{5.1}$$

where r is the radial coordinate, θ the azimuthal coordinate, and z the axial coordinate. At the centerline $(r = 0)$ the velocity is not a function of θ anymore, i.e. there is only a single Fourier mode in the circumferential direction. To account for this, the number of Fourier modes in the expansion is reduced as the centerline is approached. This reduction in the number of Fourier modes also avoids problems with small time steps due to an excessively small grid spacing at the

centerline. The pressure correction method (Ptasinski et al. 2003) is used to ensure conservation of mass. The equations are advanced in time with a second order Adams-Bashforth method.

For the initial condition of the simulations of localized turbulent pipe flow, a quasi instantaneous velocity field from a PIV measurement was used. The flow was measured by a high speed stereoscopic PIV setup, similar to the setup used by van Doorne (2004). Taylor's hypothesis of 'frozen turbulence' was used to convert the time sequence obtained from the experiment to a velocity distribution that could be used as an initial condition for the DNS. The measured bulk velocity (equation 5.2) was used as convective velocity. The bulk velocity was determined by integrating the axial velocity component over the entire cross section of the pipe:

$$u_{\text{bulk}} = \frac{1}{\pi R^2} \int_0^R \int_0^{2\pi} u_z \, r \, dr d\theta \tag{5.2}$$

The flow was simulated for $t\,u_{\text{bulk}}/D = 100$ timescales in a domain of $50D$ to allow any possible measurement errors from the initial condition to be dissipated. The resulting velocity field was used subsequently as an initial condition for the flow in longer domains.

For the simulations in a periodic pipe with a length of $100D$, the velocity field was extended from $50D$ to $100D$ by laminar flow with a parabolic velocity profile. To eliminate artificially introduced noise, the simulation was continued for another $t\,u_{\text{bulk}}/D = 100$ time scales, resulting in the initial condition for further investigations in which the Reynolds number was varied.

To modify the Reynolds number, the viscosity was adjusted while maintaining a constant volume flow rate.

In section 5.4 the results for fully developed turbulent pipe flow are presented. Fully developed turbulent pipe flow was simulated to validate the numerical code and resolutions used. As initial condition two pairs of counter rotating vortices were introduced in the pipe. The counter rotating vortices were modulated by a small amplitude axial wave, which caused an unstable interaction, resulting in rapid breakdown into fully developed turbulent pipe flow.

5.3 Resolution

For the characterization of the flow different methods can be used. It will be shown that, for the description and characterization of localized turbulent flow, the most suitable quantity to use is the so-called in-plane kinetic energy. The small-scale structures found by van Doorne and Westerweel (2009) were identified by considering only the contribution of the in-plane velocity components to the kinetic energy. The advantage of this measure is particularly present in localized turbulent flow (Moxey and Barkley 2010), because the mean velocity of the in-plane velocity components equals zero for all non-swirling pipe flows, both in the laminar and turbulent regime. Therefore, by definition velocity *fluctuations* are considered only. This avoids the definition of an ensemble mean velocity for the axial component, which is inhomogeneous both

in time and space. Also, as was found in the experiments described in chapter 4, the advection velocity of a puff is not constant.

In localized turbulent pipe flow, the homogeneity of the axial direction is lost compared to fully developed pipe flow. Consequently, when the velocity is averaged over the axial direction it depends on the length of the domain. This is caused by the fact that the length of the *turbulent* part does not change with pipe length. So by increasing the domain length a longer part with laminar flow is used in the calculation of the average velocity.

This can be avoided by considering quantities that depend on axial location only. For example the total kinetic energy:

$$E_{\text{tot}}(z) = \frac{1}{\pi R^2} \int_0^R \int_0^{2\pi} \frac{u_r^2 + u_\theta^2 + u_z^2}{u_{\text{bulk}}^2} \, r \, dr d\theta \tag{5.3}$$

Because all velocity components are considered in the *total* kinetic energy, it reaches a maximum value when the flow is laminar. For laminar flow the in-plane velocity components are zero, hence the total kinetic energy is dominated by the axial velocity component. In order to obtain a relation that equals zero for laminar flow, consider the contribution to the total kinetic energy by the in-plane velocity components only. From now on this quantity is referred to as the 'in-plane kinetic energy' and is defined as:

$$E_{\text{ip}}(z) = \frac{1}{\pi R^2} \int_0^R \int_0^{2\pi} \frac{u_r^2 + u_\theta^2}{u_{\text{bulk}}^2} \, r \, dr d\theta \tag{5.4}$$

The distribution of both quantities is given in figure 5.1. Note the difference in scales. The results shown here are from the current numerical simulation for a puff at $Re = 1900$. By using the in-plane kinetic energy, the localized nature of the puff is more clear. Also note the presence of localized peaks. These peaks were observed before in experiments (van Doorne and Westerweel 2009, De Lozar and Hof 2009), but have not been discussed in literature describing results from numerical simulations (Willis and Kerswell 2009, Duguet et al. 2010).

Van Doorne and Westerweel (2009) pointed out that the resolution used by Willis and Kerswell (2007a) may have been inadequate to resolve these small scale structures. It is however not surprising why a coarser resolution was used. Since the purpose of the simulation was to obtain life time statistics for turbulent puffs, a large number of simulations had to be done. This results in opposing requirements for the total computation time and the spatial resolution. By decreasing the spatial resolution, the computation time per run decreases. With the same amount of computation time available, this results in more runs, which in turn is beneficial for the life time statistics (Hof et al. 2006, Peixinho and Mullin 2006, Willis and Kerswell 2007a, Hof et al. 2008, Kuik et al. 2010). The risk of using a reduced resolution is that not all flow scales are resolved adequately, and as a result the proper behavior of the detailed structure of a puff is not captured.

Table 5.1 gives an overview of previous direct numerical simulations of transitional pipe flow. In this table, the first column shows the length of the domain that was used. In the second to fourth

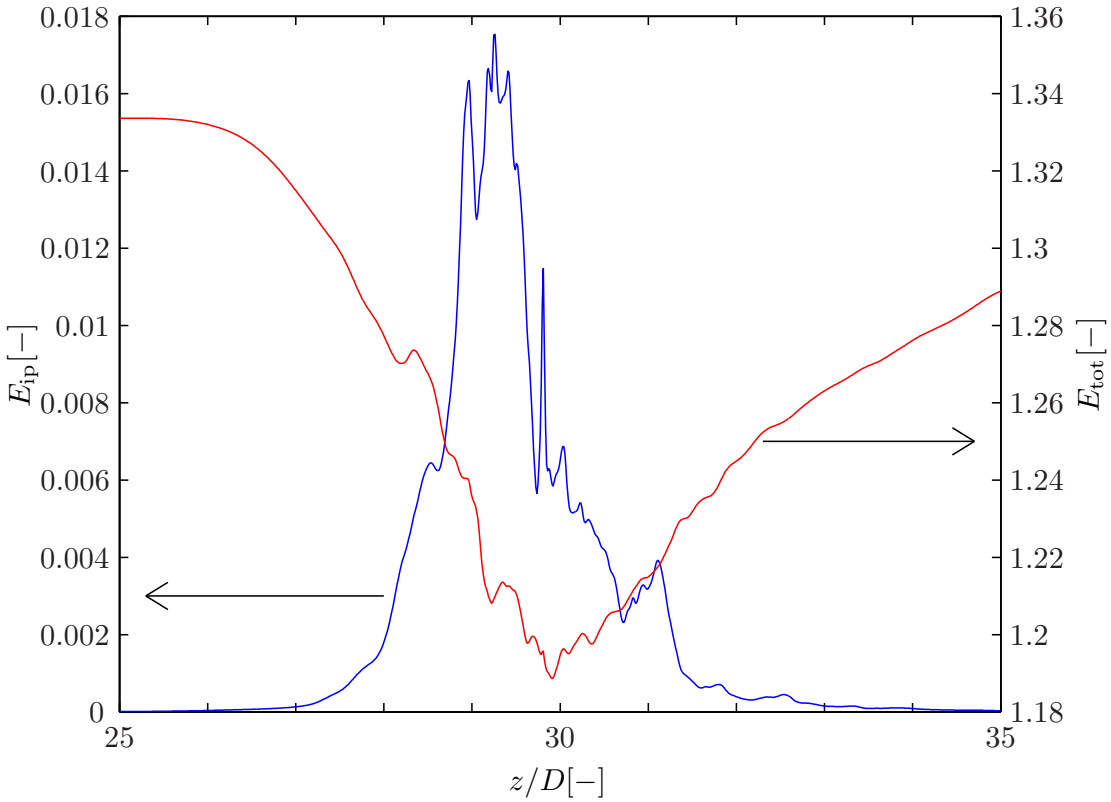

Figure 5.1: Distribution of the total kinetic energy E_{tot}, as defined in (5.3) and the contribution to the kinetic energy by the in-plane velocity components only E_{ip} (5.4)

Table 5.1: Overview of resolutions used in direct numerical simulations of transitional pipe flow.

L/D	# grid points / modes			$\frac{\Delta z}{D}$	who
	radial	azimuthal	axial		
16π	53	16	128	0.393	Shan et al. (1999)
16π	53	64	256	0.196	Shan et al. (1999)
5	50 [a]	az/17+ax/15$<$1		N.A.	Faisst and Eckhardt (2004)
5	25	32	30	0.167	Wedin and Kerswell (2004)
5	50	48	40	0.125	Wedin and Kerswell (2004)
5	50	60	60	0.083	Wedin and Kerswell (2004)
8π	33	81	321	0.078	Priymak and Miyazaki (2004)
8π	33	41	641	0.039	Priymak and Miyazaki (2004)
16π	33	41	641	0.078	Priymak and Miyazaki (2004)
16π	40	$\pm$ 24	$\pm$ 384	0.130	Willis and Kerswell (2007a, 2008)
8π	100	21	170	0.148	Shimizu and Kida (2008)
8π	80	31	511	0.049	Shimizu and Kida (2009)
50	25 [b]	33	193	0.259	Mellibovsky et al. (2009)
50	40	$\pm$ 24	$\pm$ 384	0.130	Avila et al. (2010)
50	50	$\pm$ 32	$\pm$ 510	0.098	Avila et al. (2010)[c]
8π	unstructured grid		512	0.049	Moxey and Barkley (2010)
40π	unstructured grid		2048	0.061	Moxey and Barkley (2010)
33.51	40	24	256	0.131	Duguet et al. (2010)[d]
33.51	60	48	384	0.087	Duguet et al. (2010)[e]
	Present paper				description
50	64	64	2048	0.024	Original resolution (OR)
50	64	64	4096	0.012	Increased resolution case (2 OR)
50	64	64	1024	0.049	decreased resolution case (OR/2)
50	64	64	512	0.098	lowest resolution case(OR/4)
100	64	64	4096	0.024	extra long domain case
100	64	128	4096	0.024	fully developed turbulence

[a] legendre polynomials
[b] Petrov-Galerkin in all directions
[c] High resolution reference case
[d] used for $Re \lesssim 4500$
[e] used for $4500 \lesssim Re \leq 6000$

column the number of gridpoints or the number of Fourier modes are given that were used in radial, azimuthal and axial direction. In the fifth column the axial resolution is given. This was determined by dividing the length of the domain by the number of grid points in axial direction. When the number of Fourier modes were given instead of the number of grid points, this number of Fourier modes were used. Thereby N Fourier modes give N independent grid points in space. The table shows that over the last decade both the resolution and the length of the domain, in which the simulations are done, have increased. Yet, the requirements of a domain of at least $50D$ long *and* a resolution to resolve structures smaller than $0.09D$ in axial direction are not met by any of the listed simulations. In the next section the effects of under-resolving localized turbulent pipe flow are discussed.

5.3.1 Does the axial resolution matter?

In this section the results are discussed for simulations that were done at different spatial resolutions. The main question that is addressed here is: What is the effect of the resolution used in a direct numerical simulation on the dynamics of a puff. For the current investigation, four different resolutions are used. The results in the remainder of this chapter are computed using a simulation with a resolution that is referred to as 'original resolution' (OR). The choice for this particular resolution in axial direction was based on the requirement that the small scale flow structures, with a length of about $0.095D$ observed by van Doorne and Westerweel (2009), could be resolved. The radial and azimuthal resolutions were based on the resolutions previously used for the investigation of localized turbulent pipe flow. The resolution in all directions was chosen such that the number of grid points was an integer power of 2. In section 5.4 it is shown that this resolution is sufficient to capture the flow statistics in fully developed turbulent pipe flow at a Reynolds number of $Re = 5300$. Therefore, this resolution is considered sufficient to resolve also the flow structures for localized turbulence that occurs at lower Reynolds numbers. In this section only the influence of modifying the *axial* resolution is considered. Table 5.1 gives an overview of the spatial resolutions used in other studies. In the same table the resolutions used for the present investigation are also listed.

For validation purposes one simulation is performed at a resolution of two times the original resolution (2OR). To show the effect of under-resolving the axial flow features, two simulations are done at coarser resolutions. One simulation was at half the original resolution (1/2 OR) and one at one quarter of the original resolution (1/4 OR); see also table 5.1.

The initial condition was the same for all resolution cases. The velocity field was a randomly chosen field from a simulation of a localized turbulent structure at $Re = 1900$ in a $50D$ long domain. Before the resolution was modified, this flow field was allowed to develop over several hundred time scales at the original resolution. Two options were considered for the modification of the resolution. The resolution could be modified either in real space (by linear interpolation and subsampling) or in Fourier space. In the latter method, the velocity field is first mapped to Fourier space. In Fourier space the number of modes is reduced/increased to the available number of modes at the new resolution. When the resolution is increased, the energy in the

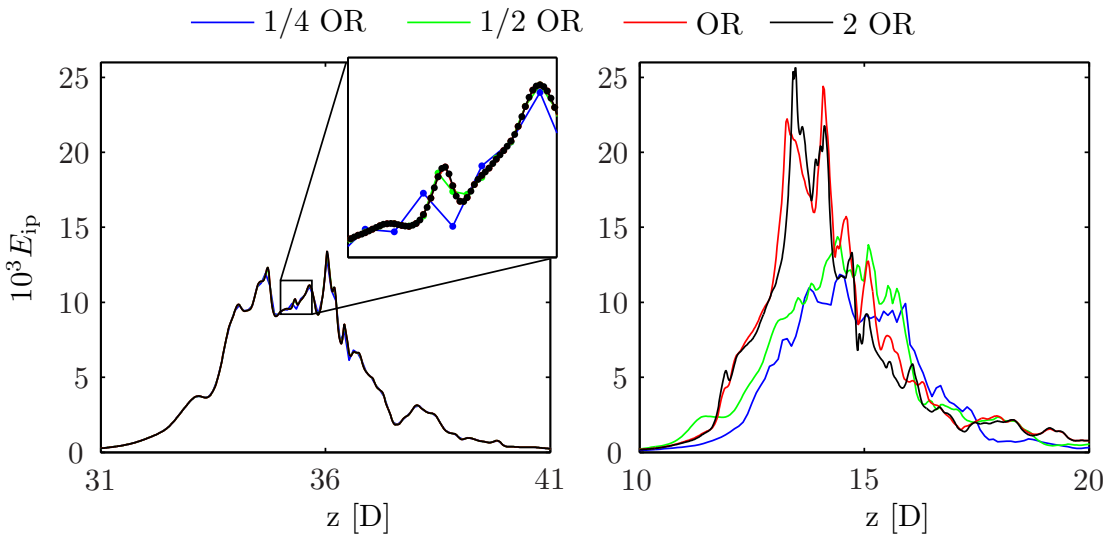

(a) initial condition ($t = 0$)

(b) at $t\,u_{bulk}/D = 28$

Figure 5.2: Distribution of in-plane kinetic energy: (*left*) initial condition, (*inset*) a part of the curve is enlarged to highlight differences in the initial condition; (*right*) after continuation over $t\,u_{bulk}/D = 28$, for four different spatial resolutions. Flow is from left to right. The values indicating the axial location shows smaller values in the right part, because of passing the periodic boundary.

newly available modes was put to zero. By decreasing the resolution, the energy in the modes that could not be presented on the new grid were discarded before mapping the result back to real space.

The left part of figure 5.2 shows the effect of modifying the resolution on the in-plane kinetic energy distribution. In this figure the in-plane kinetic energy distribution for the initial condition is shown. As could be expected, changing the resolution did not effect the large scale features of the distribution. However, when the distribution is considered in detail (see inset of figure 5.2) small differences can already be observed. Due to these small differences, it is not expected that the in-plane kinetic energy distributions will show *identical* behavior as the simulation is continued at different resolutions. This is because of the non-linear nature of the Navier-Stokes equations. However, when all energy containing modes are resolved at all resolutions, the difference is expected to remain small over a longer time.

In the right part of figure 5.2, the in-plane kinetic energy distribution is given after the simulation was continued for 28 timescales. It seems that the solutions have divided into two classes: one with an overall higher amplitude and one with a broader lower amplitude distribution. The two simulations with a high amplitude coincide with the two simulations done at the highest resolutions (i.e. the OR and 2OR simulations). This distribution also seems to be more skewed, i.e. have a higher amplitude at the upstream part. Next to that, the lower resolution cases have moved slightly farther than the other two, indicating that the resolution also has an effect on the global behavior of the puff (see also section 5.6.2 on the relation between the velocity of a puff and the total in-plane kinetic energy).

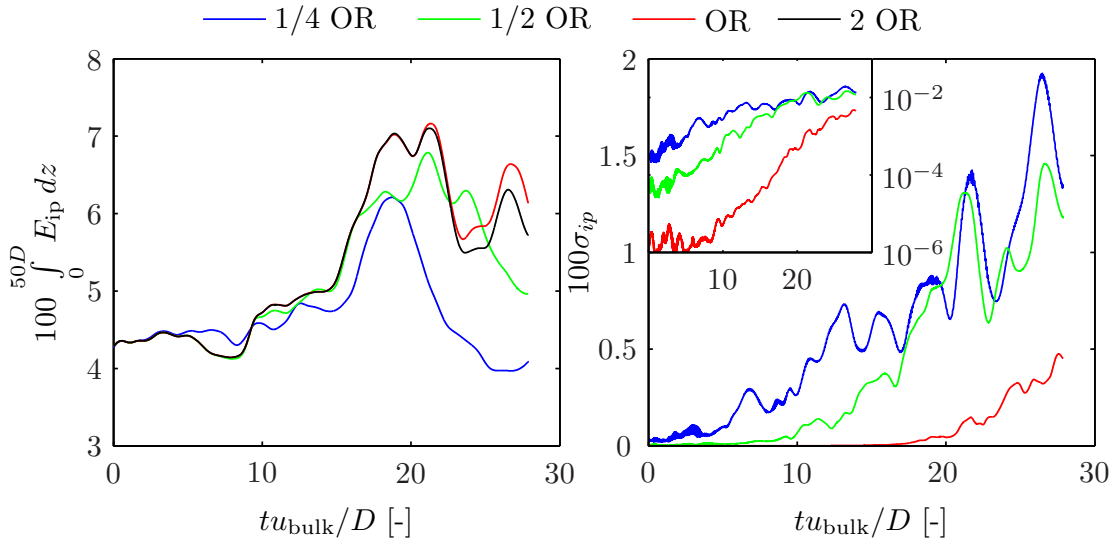

Figure 5.3: *left* Development of the total in-plane kinetic energy over time. *right* Standard deviation of the in-plane kinetic energy with respect to the 2 OR case. *inset* Standard deviation on a logarithmic scale.

To get an estimate of the mutual deviation, the in-plane kinetic energy is integrated over the whole domain. The total in-plane kinetic energy is initially the same for all resolution cases, which could already be concluded from the initial in-plane kinetic energy distribution given in figure 5.2. This results in the common origin that is shown in the left part of figure 5.3. As time progresses, the solutions start to diverge. The lower the resolution at which the simulation is performed, the sooner it deviates from the higher resolution cases and results eventually in a larger deviation.

To highlight the difference between the four cases, the standard deviation of the in-plane kinetic energy distribution with respect to the highest resolution case is shown over time in the right part of figure 5.3. It is clear that the lowest resolution simulation starts to deviate almost instantly and is soon followed by the simulation at half the original resolution. For more than ten timescales the in-plane kinetic energy distribution is the same for the two simulations at the highest resolution. The non-identical initial condition causes the results from the two simulations at the highest resolution to diverge too. However, before the deviation starts to become noticeable, the puff has travelled already more than twice its own length (see also section 5.6.1).

To assess whether the observed spikes in the in-plane kinetic energy distribution are indeed not properly resolved in the lower resolution cases, the second derivative of the in-plane kinetic energy distribution is determined. In figure 5.4 the probability distribution of this second derivative is presented. To determine this probability distribution the in-plane kinetic energy data over 28 time scales is used. The instantaneous second derivative distribution is averaged over time. Therefore this figure shows the overall behavior and it is clear that the simulation at the original resolution is able to resolve all scales. Even if the resolution is increased the probability distribution does not change, whereas for the two cases with reduced resolution, the strongest gradients could not be resolved anymore.

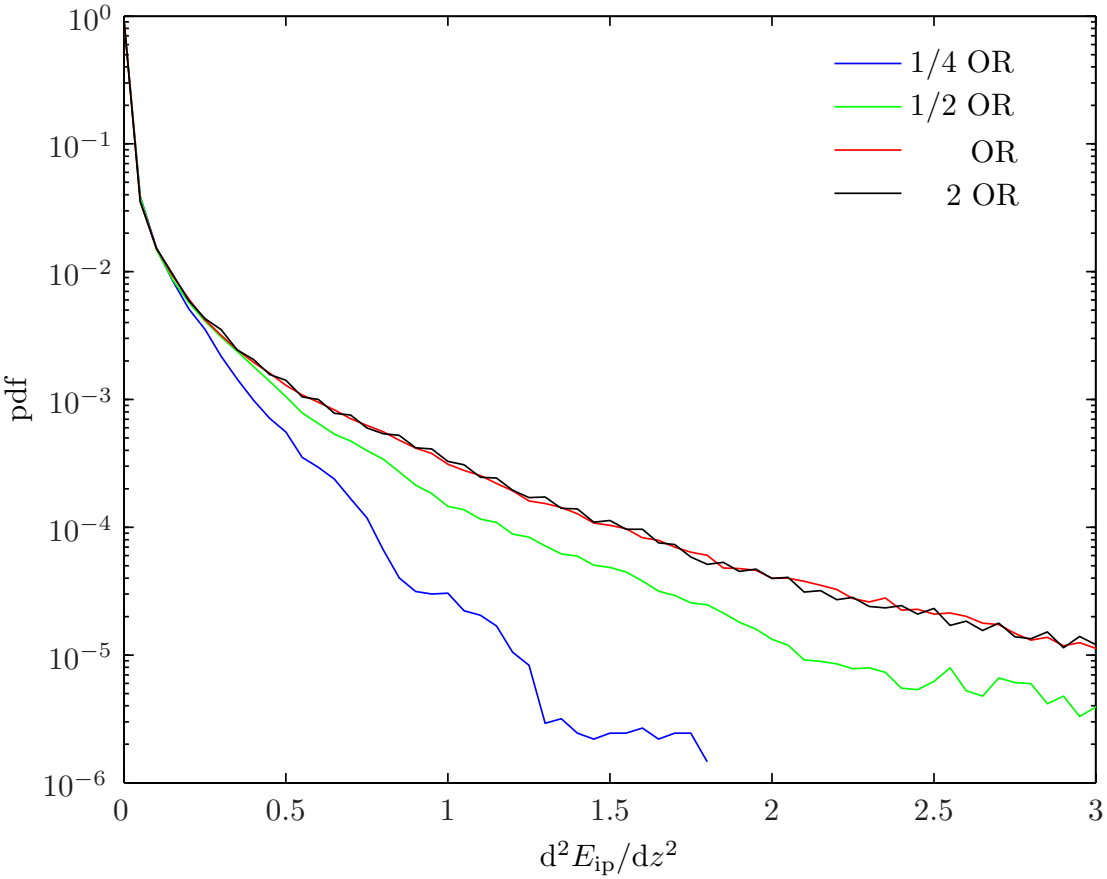

Figure 5.4: Probability distribution of the second derivative of the in-plane kinetic energy distribution for four different resolutions. This shows clearly that the simulations at the lower resolutions (i.e. 1/2 OR and 1/4 OR) are not able to resolve all small scale features of the distribution.

In order to exclude the possibility that the phenomena observed here were only valid for this particular initial condition, the analysis was repeated with a different initial flow field. Even with a completely different initial condition the same behavior was observed. These results are not included in this thesis. These observations show that a simulation which is not able to properly resolve the flow structures in axial direction will give different behavior for the internal structure of the puff, irrespective of initial condition. Therefore we conclude that it is very important to resolve the small scale features observed in experiments properly in a numerical simulation. This requires a higher resolution in axial direction than commonly used for investigating localized turbulent pipe flow.

5.4 Fully developed turbulent pipe flow

Although this investigation was focused on simulating localized turbulent pipe flow, fully developed pipe flow was simulated to validate the numerical procedure used for the current investigation. In the current simulation, the number of cores that can be employed for parallel computing was limited by the resolution in azimuthal direction. By doubling the resolution in azimuthal direction, the number of cores that can be employed is also doubled, which is done in the calculation of the fully turbulent pipe flow. For the calculation a long domain of $100D$ is used with the same axial resolution as is used for the flow at lower Reynolds numbers, resulting in a resolution of $(N_r, N_\theta, N_z) = (64, 128, 4096)$. The results are compared to data at $Re = 5300$, obtained by a finite volume method (Eggels et al. 1994), experimental PIV data by Westerweel et al. (1996), experimental LDA data by denToonder and Nieuwstadt (1997) and more recent numerical work by Wu and Moin (2008).

For the initial condition, two pairs of counter rotating vortices with a small amplitude axial wave is used. The axial wave causes an unstable interaction of the vortices and quickly results in fully developed turbulent pipe flow. The agreement of the mean velocity profiles (not shown in a figure) are excellent between the current simulation and the simulation of Eggels et al. (1994) and the experimental results of Westerweel et al. (1996) and denToonder and Nieuwstadt (1997).

In figure 5.5 the velocity fluctuations as a function of the radial location are presented, together with the results of Eggels et al. (1994), Wu and Moin (2008), Westerweel et al. (1996) and denToonder and Nieuwstadt (1997). The results obtained by the present simulations show a small deviation with respect to the data of Eggels et al. (1994), Westerweel et al. (1996) and denToonder and Nieuwstadt (1997). However, they agree excellent with a more recent simulation at a high resolution by Wu and Moin (2008). These agreements show that the code used for the present simulations is able to capture the flow statistics accurately at a Reynolds number, that is higher than the number used in the remainder of this chapter. The steep gradients present over the radial direction poses a strong restriction on the required radial discretization (Eggels et al. 1994). Since the resulting statistics were in good agreement with the results of Wu and Moin (2008), the in-plane resolution is also considered sufficient for the lower Reynolds number cases.

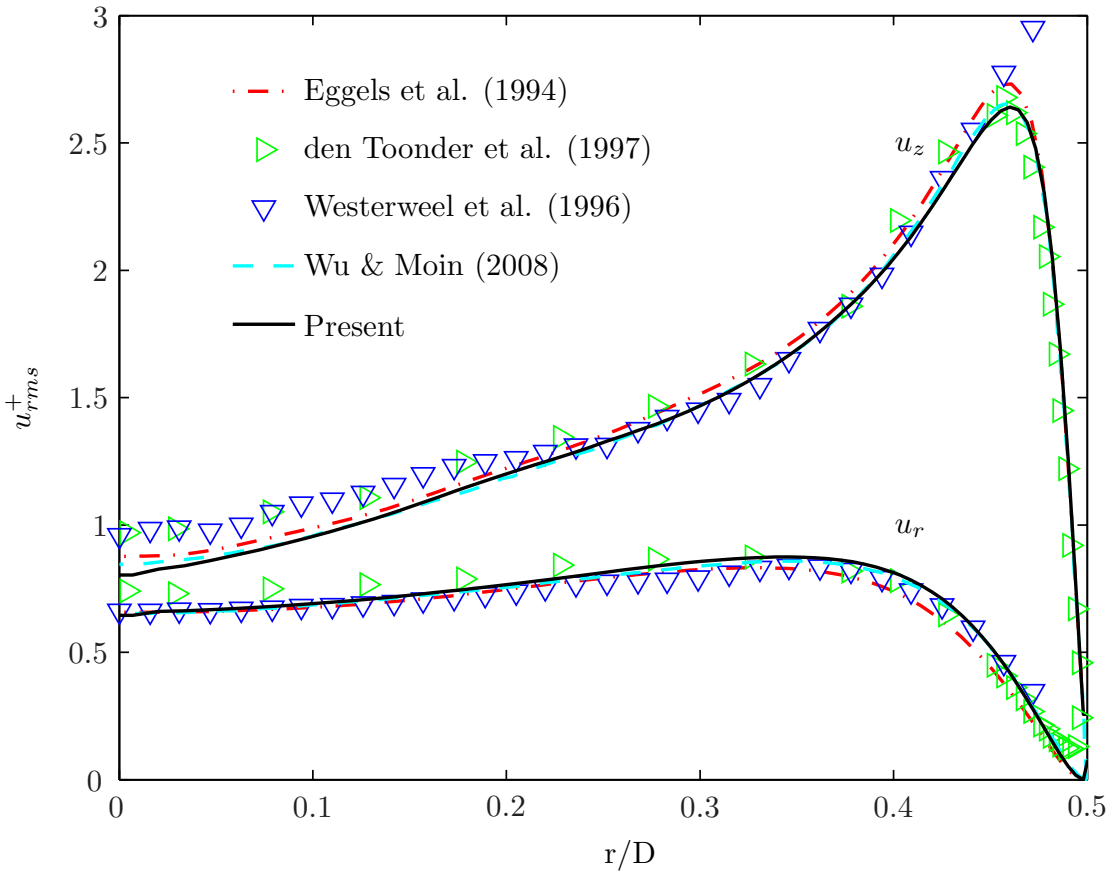

Figure 5.5: Profiles for the axial (u_z) and radial (u_r) velocity fluctuations as simulated by Eggels et al. (1994) and Wu and Moin (2008), measured by Westerweel et al. (1996) and denToonder and Nieuwstadt (1997) and the present simulations.

5.5 Comparison of fully developed pipe flow $(Re = 5300)$ and localized turbulent pipe flow $(Re = 1900)$

In this section fully developed turbulent flow is compared to the flow at a Reynolds number at which localized turbulent structures are observed. In localized turbulent pipe flow, the flow over a length of about $5D$ can be considered to consist of fully developed turbulent flow (Wygnanski et al. 1975, Bandyopadhyay 1986). However, to the knowledge of the author, no quantitative comparison has ever been attempted to validate this claim.

Moxey and Barkley (2010) found in their simulations two critical Reynolds numbers: $Re \simeq 2300$ and $Re \simeq 2600$. Below $Re \simeq 2300$ a single disturbance convects downstream and remains localized. Between $Re \simeq 2300$ and $Re \simeq 2600$, a single disturbance might split into multiple *localized* structures. Above $Re \simeq 2600$, the localized nature of the structures is lost and, since they used a periodic domain, fully developed turbulent pipe flow is obtained. The localized turbulent flow is therefore simulated at $Re = 1900$ and the statistics are compared to fully developed turbulent flow at $Re = 5300$.

In figure 5.6 the in-plane kinetic energy distribution for both fully developed turbulent pipe flow and for a puff are given. By considering only this in-plane contribution the localized nature of turbulent flow at $Re = 1900$ becomes immediately clear. The contribution is not only confined in space, its amplitude is significantly higher compared to fully developed flow. The maximum amplitude observed in figure 5.6 are in excellent agreement (difference $< 5\%$) with the values reported by van Doorne and Westerweel (2009) for a puff measured at $Re = 2000$. When compared to older experimental data by Wygnanski et al. (1975) for a turbulent puff at $Re = 2200$, a good agreement is found. They report that in the interior of a puff the turbulent intensity is about four times higher compared to fully developed turbulent pipe flow. In the present study a factor of up to three times is observed for peak to peak difference in in-plane kinetic energy for the puff in comparison to fully developed turbulent pipe flow.

In the next section the mean velocity profile and the turbulent statistics are compared between fully developed turbulent pipe flow and a turbulent puff.

5.5.1 Comparison of velocity statistics

Determining statistics for fully developed pipe flow is almost trivial compared to the case with localized turbulent flow. Since in the axial direction only about $30D$ of the domain is filled with turbulence, the velocity statistics become dependent on the length of the domain. When only a single disturbance is present in the domain, the length of the part that is turbulent does not change as the length of the pipe is increased (provided the length of the pipe is sufficiently long). Therefore it is important to know what part of the domain belongs to the puff before determining the flow statistics. Moreover, since the turbulent puff consists of different regions (Bandyopadhyay 1986), it is essential to align the turbulent regions properly. This is discussed in the next paragraphs.

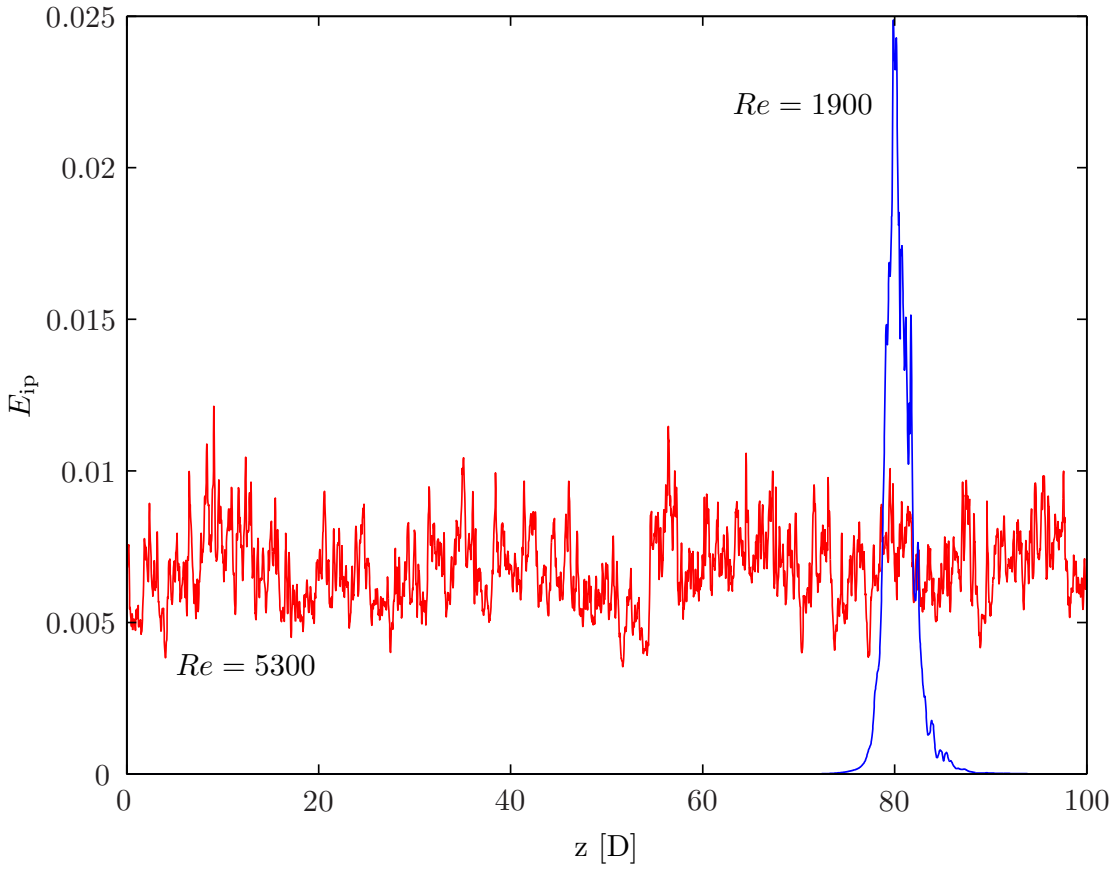

Figure 5.6: The kinetic energy of the in-plane velocity components for fully developed turbulent pipe flow ($Re = 5300$) and localized turbulence occuring the form of a puff ($Re = 1900$)

To properly determine the mean velocity, a convective frame of reference has to be employed, and therefore knowledge of the current location of the puff is needed. When the location of the puff is known, the instantaneous velocity fields can be aligned to get the average flow field. Furthermore, tracking the location of the puff allows for the extraction of the velocity of the puff. See section 5.6.1 for more information about the velocity characteristics of puffs.

The location of the puff can be determined in a number of ways. Willis and Kerswell (2007a) used the sudden decrease present in the centerline velocity to track the puff. They needed smoothing of the velocity profile in order to avoid jumps in the location of the puff caused by vortex shedding at the trailing edge of the puff. Wygnanski and Champagne (1973) first acknowledged this problem and used a threshold on $\log du_z'/dt + \log du_r'/dt$ to determine the laminar-turbulent interface. Eckhardt and Schneider (2008) used the center (first order moment) of the in-plane kinetic energy distribution to determine the location of a puff. This resulted in accurate information on the location and smooth translational velocity information, without the need to smooth the data. The distribution of in-plane kinetic energy was also used by Moxey and Barkley (2010) to visualize the location of puffs and their behavior over time. They showed that individual puffs could be identified and tracked over time. Even the splitting of puffs could be clearly observed.

Based on these experiences the first moment of the in-plane kinetic energy distribution was used as the measure of the location of a puff, which was then used to align the puffs. In the numerical simulation, however, a periodic boundary is present in axial direction. When the puff extends over this boundary the first moment of the in-plane kinetic energy distribution can not be determined in a proper way. Therefore the location of the puff is determined by using the following procedure:

1. determine the maximum intensity of the in-plane kinetic energy
2. rearrange the data such that the maximum is located midway the pipe section
3. determine the first moment of the in-plane kinetic energy distribution
4. rearrange the data such that the first moment of in-plane kinetic energy distribution is in the center of the pipe

In the remaining part of this chapter we refer to the first moment of the in-plane kinetic energy distribution as the 'center' of the puff. The rearranged data can then be used to determine the average velocity distribution in a puff. Note however that the average and the fluctuations of the velocity are influenced by the possible variations in length of the puff (see section 5.6.3 for a more detailed discussion on the length properties of puffs). The average velocity distribution of a puff has not been compensated for the variations in length. It is expected that this does not have a major influence on the results presented here.

Figure 5.7 gives an overview for the velocity profiles in a turbulent puff. Be aware that the pipe wall is located at the bottom in every subfigure, as indicated in parts *a* and *b*. The major conclusion to be drawn from this figure is that the puff does not have a region with the same

statistics as for fully developed turbulent flow as was originally proposed by Bandyopadhyay (1986).

In the top part of figure 5.7 (*a* and *b*) contour plots are given for the average velocity distribution in a puff. The difference in axial velocity with respect to the laminar flow is given in *a*, and the radial velocity distribution is given in *b*. The flow is from left to right in these figures and red indicates a velocity higher than the laminar velocity and blue is a region with a lower velocity. When the information in these figures is combined, the image of a toroidal vortex emerges. This was already found by Wygnanski et al. (1975) using conditionally averaged velocity fields of hotwire data. Fluid that enters the puff is on average first transported from the center towards the wall and after the transition front has passed, transported back to recover the laminar velocity profile. However, as was already shown by Bandyopadhyay (1986), the toroidal vortex is only an artifact of the averaging procedure and does not occur in the instantaneous flow field of a puff. This was also confirmed by the measurement of van Doorne and Westerweel (2009).

As was stated above, the average velocity distribution was calculated by rearranging the velocity data such that the center of the in-plane kinetic energy was centered in the pipe, i.e. at $z/D = 0$ in figure 5.7. The location at which the flow towards the wall (red in figure 5.7*b*) changes into a flow away from the wall, is at the same location. Hence, the center of the apparent toroidal vortex coincides with the center of in-plane kinetic energy. In figures 5.7 *c* to *h* mean velocity and velocity fluctuation level profiles are given for three different locations in the puff. The locations at which these profiles are taken are indicated by three green lines in figure 5.7 *a*, indicated by *I*, *II* and *III*.

In figures 5.7 *c* to *e* the mean velocity profile is shown for the puff by a red line. As a reference, the mean velocity profile for fully developed turbulent pipe flow at $Re = 5300$ (blue dashed) and the parabolic Hagen-Poiseuille profile (green dash-dot) are given.

Figure 5.7 *c* shows the velocity profile at the trailing edge of the puff (indicated by *I* in part *a*, two diameters upstream of the center in in-plane kinetic energy), where the strongest inflection point is present. This is consistent with the work of Hof et al. (2010), who also identified an inflection point at the trailing edge of the puff. For the determination of the strongest inflection point, the same method has been used as can be found in the supplementary material of the paper by Hof et al. (2010). They claim that the transition to turbulence is caused by this inflection point in the velocity profile. The presence of an inflection point feeds the regeneration process of the puff. They concluded, by considering the vorticity transport term, that vorticity is transported upstream at the upstream side and downstream at the downstream side of the point where the inflection is maximal. This leads to the conclusion that the vorticity had to be *produced* by the inflection point, and the inflection point is a vorticity source. However, the inflection point shown in figure 5.7 *b* is the result of the averaging procedure, but obviously inflection points are also present in the instantaneous velocity profiles of turbulent flow. Moreover, an inflection point is a *necessary* condition for flow instability but it is not a *sufficient* condition to get an unstable flow (Drazin and Reid 2004).

The question remains what the order of causality is: Does the inflection point *cause* an unstable velocity distribution, which *results* in a transition to turbulence or is the inflection point a *result*

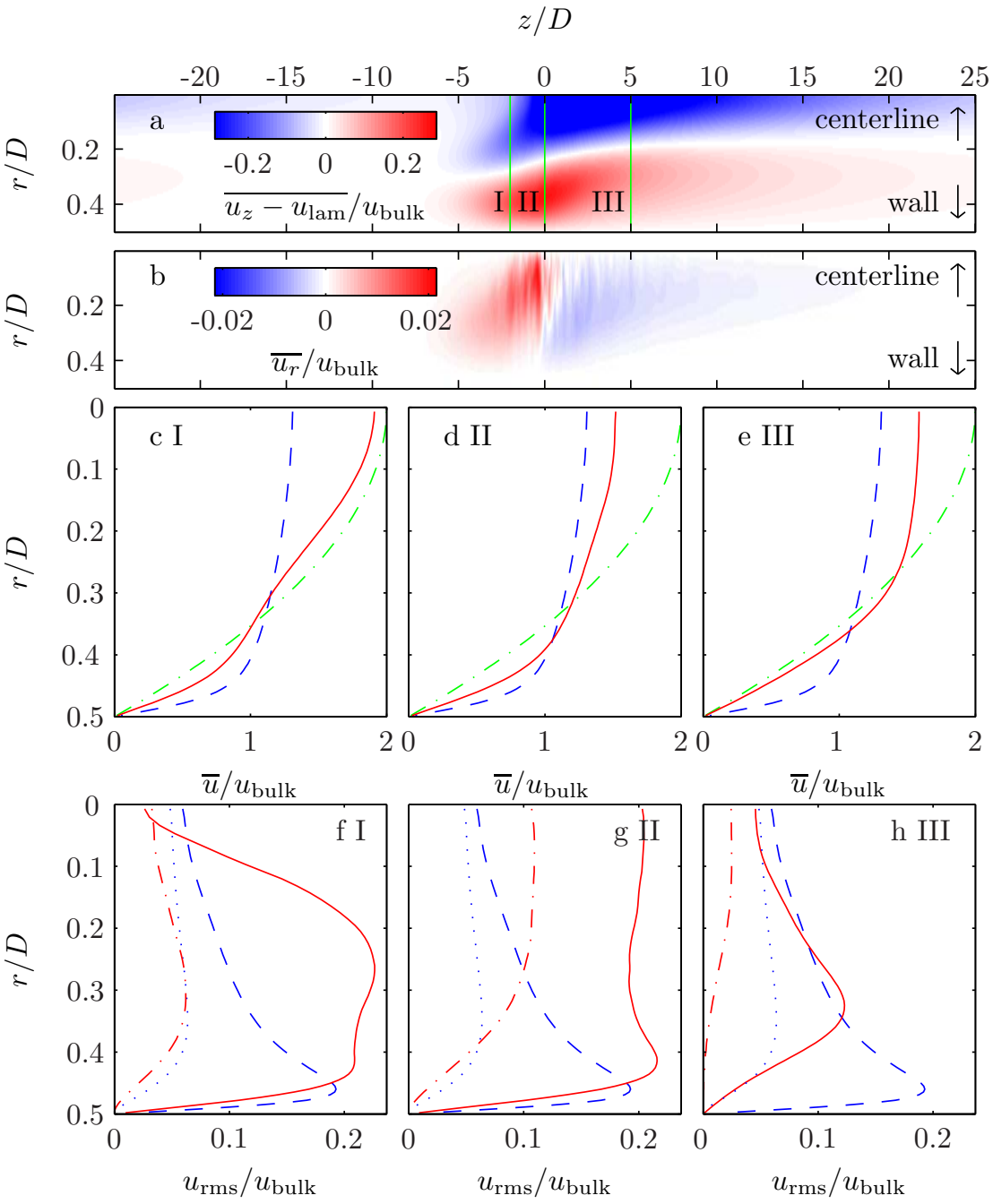

Figure 5.7: (*a*) Mean axial velocity distribution with respect to the laminar flow, the flow is in positive *z* direction. (*b*) the same for radial velocity component. (*c-h*) velocity profiles for laminar (green), fully developed turbulent flow (blue) and the puff (red) at locations *I*, *II* and *III* as indicated in *a*. (*c-e*) mean velocity profiles for a puff (red, continuous), fully developed turbulent pipe flow (blue,dashed) and laminar flow (green, dash-dot) (*f-h*) radial distribution for the velocity fluctuations for the axial velocity component of a puff (red, continuous), the radial component (red, dashed-dot). As a reference the velocity fluctuations for fully developed flow is given in axial (blue, dashed) and radial (blue, dotted) component.

of the transition to turbulence? Unfortunately all these mechanisms are coupled, and a clear order of events can not be extracted. Hof et al. (2010) already gave an explanation for the case when one assumes the inflection point to be the source of the transition process. Another approach, in which the vortical structures are the source for the transition to turbulence, can be as follows:

Since it is a self sustained mechanism, one can start at any point in the cycle. For the explanation of the scenario, the processes that are continuously present and are happening in parallel are presented here as if they happen sequentially. Assume as initial condition a small patch of turbulent fluid, that is spanning the entire diameter and is order $1D$ long. Consider a convective reference frame with the same velocity as the puff, which is approximately equal to the bulk velocity (see also section 5.6.1). Due to the velocity profile, the perturbed fluid in the center of the pipe will leave the domain on the downstream side of the control volume, whereas perturbed fluid close to the wall will leave on the upstream side.The perturbations leaving the domain on the upstream side interact with the incoming laminar velocity profile and provide a finite amplitude disturbance needed for the laminar velocity profile to become unstable. The breakdown of the laminar velocity profile into turbulence provides then the energy to drive the velocity fluctuations. Hence, with these renewed velocity fluctuations, the process is back at its initial condition and the process can continue. Note that in this scenario, the inflection point in the velocity profile is the effect of the vorticity distribution and transport process.

The average velocity profile in the center of in-plane kinetic energy ($z = 0$), which was used to align the puff to obain the average velocity distribution, is given in figure 5.7*d*. The velocity profile is closest to that of the fully developed turbulent flow, compared to the velocity profiles adjacent to this location. This region corresponds to the region identified by Bandyopadhyay (1986) as the fully developed turbulent region. Indeed the average velocity profile assumes a shape close to the velocity profile for fully developed turbulent pipe flow, but is actually never reached. Moreover, according to Bandyopadhyay (1986) this region extends over five pipe diameters, but appears to be much shorter here. When the velocity profile is observed $5D$ downstream of the puff alignment location (figure 5.7*e*), the flow is already redeveloping into laminar flow. The fluid in the core region is accelerated and decelerated near the wall, see figure 5.7 *e*. Hence, the region in which nearly fully developed flow is observed, based on the average velocity profiles, is limited to a small region close to the center of the in-plane kinetic energy.

The velocity fluctuations at each location are given in figure 5.7*f*-*h*. The mean velocity fluctuation level for a puff for the axial velocity component are given by continuous lines. The dashed-dotted lines represent the profiles for the mean velocity fluctuation level in radial direction. As a reference, the mean velocity fluctuation level for fully developed turbulent flow in the axial direction (dashed) and the radial direction (dotted) are given. Obviously, for fully developed turbulent pipe flow the profiles do not change with axial location, and therefore these distributions are the same in all three figures. In these figures the mean velocity fluctuation level is *not* normalized by the friction velocity ($u^* = \sqrt{\tau_w/\rho}$, $\tau_w = \nu\partial\overline{u}/\partial y$) as is common for fully developed turbulent pipe flow, but by the bulk velocity instead. The reason for this is that the friction velocity depends on the location within the puff, and is small compared to the friction velocity for turbulent flow. Especially in the relaminarization region of the puff ($z/D > 5$ in fig-

ure 5.7), where the velocity gradient at the wall gets close to the gradient for laminar flow; When the data is normalized by the local friction velocity this would result in a very large value for the mean fluctuation level in the puff, and therefore the mean velocity fluctuation level with respect to the bulk velocity is given in figures 5.7*f* -*h*.

At the location in axial direction where the inflection point has the highest value (location *I*), the velocity fluctuations at the centerline of the puff are very small, as can be seen in figure 5.7*f*. Although the fluctuation level at the centerline of the pipe is small, the average velocity is already significantly lower compared to the theoretical value for laminar flow (see figure 5.7*c*). Closer to the wall, the amplitude of the fluctuation level and the region over which a higher level is observed is significantly larger than for fully developed turbulent pipe flow.

In the central region of the in-plane kinetic energy distribution (figure 5.7*g*), the fluctuation level is almost homogeneous over the entire pipe diameter. When comparing the fluctuation levels at the centerline in figures 5.7 *f* and *g*, a rapid increase in downstream direction is observed. This is in agreement with the jump observed in the axial velocity component at the centerline of the pipe in the classical image of a puff: see e.g. Wygnanski and Champagne (1973), van Doorne and Westerweel (2009).

Downstream of the center in in-plane kinetic energy (i.e. for $z/D > 0$), the mixed fluid relaminarizes. The relaminarization is initiated close to the wall, as can be seen in the velocity profile in figure 5.7 *e*. The velocity fluctuation level close to the wall is strongly reduced, and the maximum of the turbulence intesity moves towards the center of the pipe (figure 5.7*h*). This corresponds to the conical region observed by Bandyopadhyay (1986).

In conclusion; figure 5.7 summarizes the general behavior of the puff. When the velocity profiles are conditionally averaged with respect to a frame of reference moving with the velocity of the puff the image of a toroidal vortex emerges. The puff consists of three regions: On the upstream side, the flow close to the wall is perturbed by disturbances that travel upstream with respect to the puff. These perturbations cause the finite amplitude disturbance needed for the laminar velocity profile to become unstable. The kinetic energy that is contained in the laminar velocity profile gets released and becomes available for fluctuations (Rotta 1956) and results in a well-mixed region that corresponds to the center of in-plane kinetic energy. In the downstream direction, the flow relaminarizes and the maximum fluctuation level shifts towards the pipe axis.

5.6 The behavior of a single puff

In this section the results are presented of puffs simulated at different Reynolds numbers. An overview of the total simulation time for each case is given in table 5.2 as a reference. The puff that was simulated at $Re = 1800$ decayed after approximately $t\,u_{\mathrm{bulk}}/D \approx 300$, and therefore this simulation was not continued beyond this.

In the previous section the interior of a puff was compared with fully developed turbulent pipe flow. It was assumed that the central region of a puff can be considered to be the same as fully

Table 5.2: Total simulation time for each Reynolds number case

Reynolds number	1800	1900	1900	2000	2100	2300
domain length $[D]$	100	50	100	100	100	50
sim. time $t\,u_{\text{bulk}}/D$	305	1350	400	400	400	850

developed turbulent pipe flow. From the analysis in section 5.5.1 it became clear that this is not valid. Next to the difference in the interior flow field, the localized nature of turbulence for a puff introduces new quantities that are unique to a puff, e.g. the propagation velocity, that are not defined for fully-developed turbulent pipe flow. The properties of the instantaneous propagation velocity of a puff are discussed in section 5.6.1. Because the puff has a finite length given its localized nature, a length of the localized domain can be defined. With that the *total* in-plane kinetic energy is also finite and is independent of the length of the domain, as long as the entire puff is taken into account. Obviously it does depend on the length of the domain, if the domain is shorter than the puff. The relation between the total in-plane kinetic energy, the length of the puff, and the velocity of the puff are discussed in sections 5.6.2 and 5.6.3.

5.6.1 Motion of an individual puff: its velocity

Due to its localized nature, the puff has a certain velocity by which it propagates along the pipe. Wygnanski et al. (1975) concluded that, based on their experimental data, the velocity of an equilibrium puff moves at approximately the bulk velocity. A few years earlier Lindgren (1969) showed that the puff velocity decreases with increasing Reynolds number (*Re*). When the *Re* range is reached where splitting puffs and eventually puffs that grow in length over time (slugs) are observed, the trailing edge velocity continues to decrease with increasing Reynolds number. The leading edge velocity branches off and increases.

Lindgren (1969) did not report on the convection velocity of structures for $Re \lesssim 2000$. Hof et al. (2005) took measurements for localized structures at lower Reynolds numbers. For their measurements at $Re = 1500$ to $Re = 1800$ a very interesting behavior is observed. In this range of Reynolds numbers, the turbulent structures have a finite lifetime (Hof et al. 2005, 2006, Peixinho and Mullin 2006, Willis and Kerswell 2007a, Hof et al. 2008, Kuik et al. 2010, Avila et al. 2010). In order to get an estimate for the variations in puff velocity, Hof et al. (2005) determined the velocity in two parts of the pipe separately. In the first $25D$ after the disturbance the average velocity was used for the *low* velocity estimate. The average velocity of the structures in the subsequent $37D$ was used to get the *high* velocity estimate. No conclusions were drawn by Hof et al. (2005) on this behavior while there are at least two possible explanations:

(i) Since the structures have a high probability of decay in the observed Reynolds number range, it is very likely that decaying structures were used for the determination of the velocity. This leads to one possible explanation: during the decay of a turbulent puff the structure accelerates (see also section 5.6.2), and therefore a higher velocity is observed in the second pipe section.

(ii) Another explanation is related to the formation of turbulent structures. In the experiments of Hof et al. (2005), the velocity of the structures was determined directly after their creation. When the disturbance is applied a puff is not instantly formed. Instead, the introduced velocity fluctuations have to be dissipated or redistributed to create a puff. This process can result in a different convection velocity of the structure (see also section 5.6.2). Therefore it is expected that the behavior of a disturbance directly after its creation is different from the behavior of a *puff* at that particular Reynolds number.

Kuik et al. (2010) observed in their experiments similar behavior for puffs as Hof et al. (2005), see chapter 4. Kuik et al. (2010) determined the velocity of a disturbance over three consecutive pipe sections (each with a length $L \approx 125D$). Over the entire Reynolds number range that was considered, it was found that the velocity in the first pipe section was lower compared to the velocity in the other two pipe sections. While the puff velocities in the following two pipe sections were similar, yet uncorrelated. This implies that the puff fluctuates in velocity during its advection through the pipe. Only structures that survived beyond this point were taken into account in the velocity determination. Therefore it is not plausible that the acceleration that was found between the puff forming in the first pipe section and the velocity in the following two sections, was caused by the decay process of the puffs. Hence, it is concluded that a disturbance that is introduced in fully developed laminar pipe flow has a lower velocity during its formation into a turbulent puff, compared to its final velocity.

How a turbulent puff is formed from a disturbance has been extensively investigated by Duguet et al. (2010). They studied the formation of a turbulent puff with an edge state as initial condition. The edge state is a state between laminar flow and the fully developed turbulent flow state. It is a structure that is localized and is able to sustained itself (Mellibovsky et al. 2009). When the amplitude is slightly increased, it develops rapidly into the turbulent state and returns directly to the laminar flow state when the amplitude is slightly decreased.

The space-time plots given by Duguet et al. (2010) show that the disturbance initially has a higher velocity and decelerates as the puff is formed. This is in contrast to the observations in experiments by Hof et al. (2005) and Kuik et al. (2010) and can be caused by the fact that in the experiments not the edge state, but a local disturbance is used to initialize the turbulent state. It is clear from all these investigations that during the formation of a turbulent puff its convection velocity is not the same as in its final state.

De Lozar and Hof (2009) also determined the velocity of puffs over a similar Reynolds number range as considered by Kuik et al. (2010). De Lozar and Hof (2009) report that the puff velocity is the same irrespective of its position in the pipe, i.e. the velocity does not change with downstream distance. This observation confirms the classical view of an equilibrium puff, which was introduced by Wygnanski et al. (1975). However, it disagrees with the findings of Kuik et al. (2010) and Hof et al. (2005). Therefore the question remains whether or not the puff moves with a constant velocity. A varying velocity would be indicative of large scale dynamical processes within the puff. Which might provide a clue for the lifetime behavior of puffs at low Reynolds numbers.

The velocity characteristics of puffs are investigated using the present direct numerical simula-

tion. The advantage of numerical simulations is that both the spatial distribution of a puff and its development over time are available. The behavior of a puff can be captured in a single space-time plot, which is given in figure 5.8. The red region in this figure represents the puff. On the horizontal axis the spatial extend of the structure is given in a reference frame that moves with the bulk velocity. The convective frame of reference is used to highlight the motion relative to the bulk velocity. In vertical direction the time evolution is shown. In this figure, the color contours show the magnitude of in-plane kinetic energy on a $\log_{10}$ scale, where red corresponds to $E_{\mathrm{ip}} = 10^{-1}$ and white to $E_{\mathrm{ip}} = 10^{-5}$ (the definition for E_{ip} is given in equation 5.4).

When the puff would have moved at the same velocity as the bulk velocity it would have appeared as a vertically aligned region in this figure. The puff shown in figure 5.8 is moving faster than the bulk fluid, i.e. there is a net transport of fluid from the leading edge to the trailing edge of the puff. The behavior shown in figure 5.8 is opposite to what was observed by Eckhardt and Schneider (2008). From a simulation at the same Reynolds number they found a convection velocity that was lower than the bulk velocity (see also figure 5.9).

Next to the mean motion, it is clear from this figure that the *instantaneous* velocity of the puff is not constant over time. In the right part of figure 5.8 the instantaneous velocity of the puff is plotted, the dashed line indicates the bulk velocity. The velocity at each time instant was determined by applying a linear fit to the location versus time data over 20 units of time. The location of the puff was determined by the method described in section 5.4. Applying a linear fit in this way results in a moving average velocity of the puff, which clearly shows the instantaneous behavior of the puff. When the data was fit over more than 20 units of time the curve in the right part of figure 5.8 would have been smoother, and less smooth if a shorter time was used. The currently selected integration time has been chosen to reveal the behavior observed in the left part of figure 5.8. Most of the time the puff moves faster than than the bulk fluid, however for a considerable time the puff is moving at a velocity which is lower than the bulk velocity. It is clear that the velocity of a puff is not constant at a constant Reynolds number. It is emphasized that the bulk velocity in the DNS is maintained constant during the entire simulation.

Shimizu and Kida (2009) also found a fluctuating velocity for the puff in their simulation. They concluded that the variations in puff velocity were caused by variations in bulk velocity. The variations in bulk velocity were present because they prescribed the pressure gradient that drives the flow instead of the mass flux. When the portion of turbulent flow fluctuates the total resistance of the flow varies, which results in a fluctuating bulk velocity. This reveals directly the major drawback of prescribing a pressure gradient in a transitional pipe flow simulation. Because of the fluctuating bulk velocity, the Reynolds number is not fixed. Therefore it is not clear from their simulations what the motion of the puff would be at a fixed Reynolds number, i.e. under constant mass flux conditions. To conclude: the results given in figure 5.8 confirm the behavior of puffs observed in the measurements by Kuik et al. (2010), but they disagree with the earlier findings of Wygnanski et al. (1975) and De Lozar and Hof (2009). They report that the velocity of a puff is constant.

The mean velocity of a puff can be determined by applying a linear fit to all the location data of a single puff over time. This was done for four simulations at different Reynolds numbers.

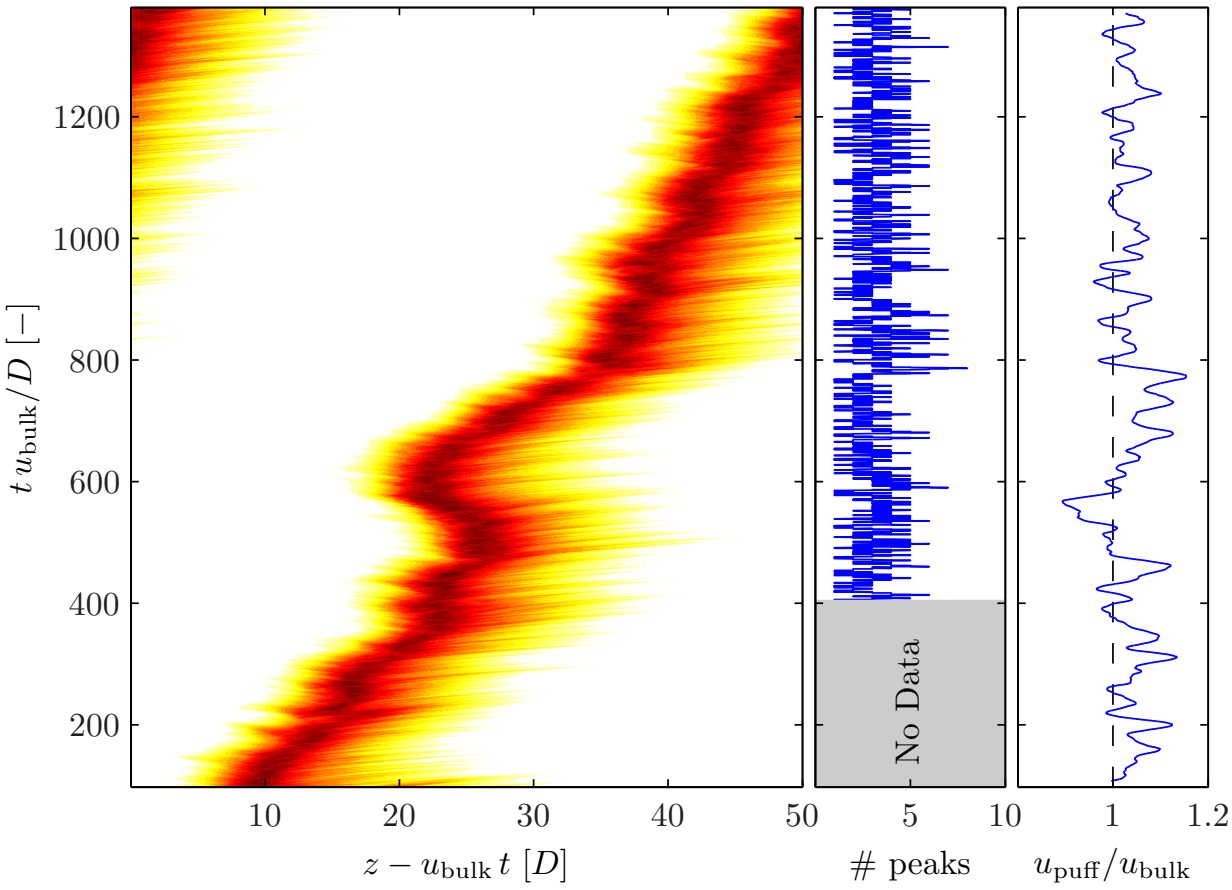

Figure 5.8: *Left*) Dynamics of a single puff at $Re = 1900$. The colors give the amplitude for in-plane kinetic energy on a $\log_{10}$ scale: red means turbulent ($E_{\mathrm{ip}} = 0.1$), white laminar ($E_{ip} = 10^{-5}$). In the horizontal direction the spatial extend is given in a convective reference frame (moving at the bulk velocity) and the time evolution is given in vertical direction upwards. *Center*) Number of peaks detected over time (see section 5.7). *Right*) Moving average velocity of the puff taken over 20 units of time: an illustration of the instantaneous behavior of the puff. The mean velocity of a puff for these data is $u_{\mathrm{puff}} = 1.04\,u_{\mathrm{bulk}}$

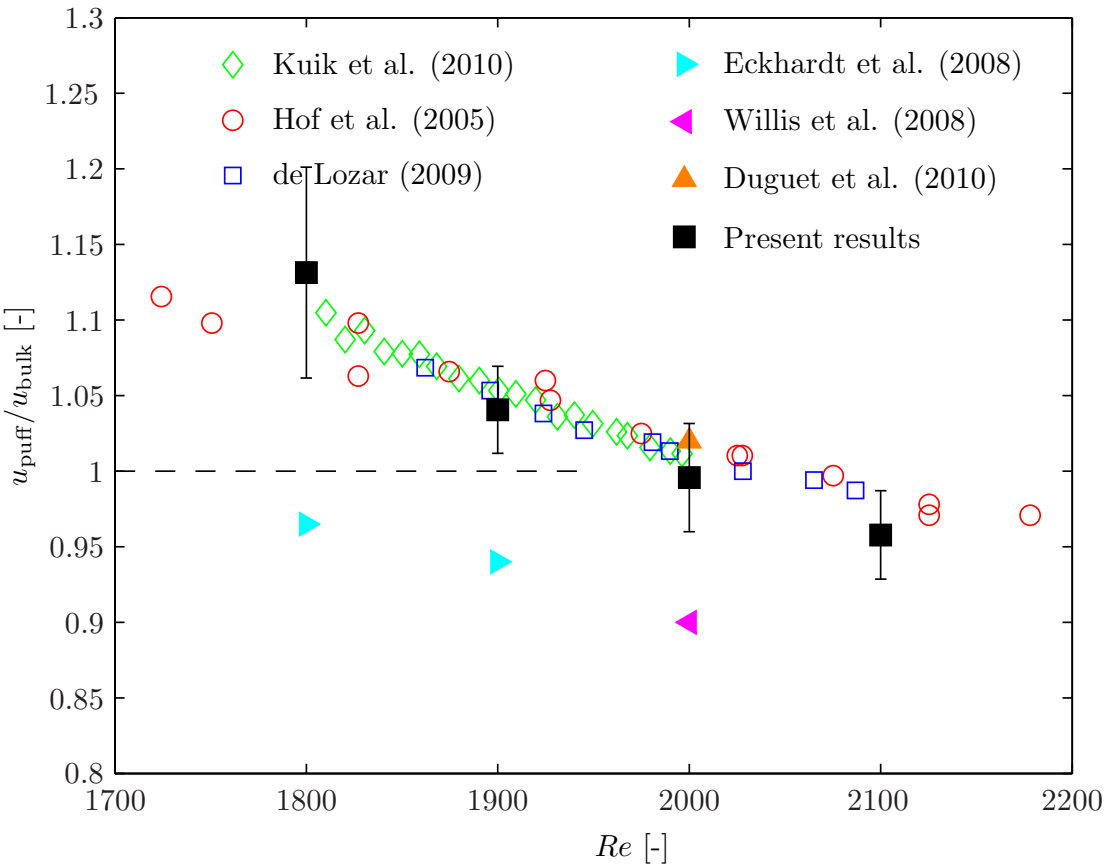

Figure 5.9: Average velocity of a puff as a function of the Reynolds number. Results obtained by experiments are given by open symbols, while filled symbols are the results from numerical simulations. The error-bars indicate the actual variation in puff velocity and is determined by taking the standard deviation of the mean instantaneous puff velocity.

The results shown in the next figures are from simulations done in a domain with a periodic length of $100D$. In section 5.2 it was already described how the Reynolds number was changed and how the simulation was initialized. From the four simulations the mean convection velocity of the puffs was extracted, and the results are shown in figure 5.9. To get an estimate for the variations in velocity, the instantaneous velocity was determine as discussed previously. The standard deviation of this instantaneous velocity with respect to the average velocity is used as an indicator for the variations in convection velocity. The error bars in figure 5.9 do *not* show the error on the mean velocity, but represent the standard deviation of the *variation* in convection velocity of a puff.

In figure 5.9 the experimental results obtained by Hof et al. (2005), De Lozar and Hof (2009) and Kuik et al. (2010) are given as a reference. The puff velocities that were found by Eckhardt and Schneider (2008) and Willis and Kerswell (2008) are significantly below the experimental data and the velocities found in the present simulations. At first it was suspected that the resolution at which these simulations were performed were not adequate to resolve the flow structures and thereby the global behavior of the puff. This has been verified by continuing the simulations given in section 5.3 in a $50D$ domain at the lowest resolution (one quarter of the resolution used for the other cases). The resulting average velocity was 1% *higher* than the velocity found at high resolution. An explanation for the higher velocity is that not all velocity scales could be resolved and that this is effectively the same as simulating at a lower Reynolds number. The additional damping due to insufficient spatial resolution can be considered as an increased viscosity. Following the trend given by the experimental data in figure 5.9, it is concluded that the velocity of the structure should be higher at this lower Reynolds number. Therefore it is concluded that the difference in resolution is not the explanation for the large difference in puff velocity.

In the work of Duguet et al. (2010) only the velocity of structures for $Re \geq 2000$ are reported. The velocity of a puff at $Re = 2000$ is approximately 3% higher in their simulations than the velocity found in the results of the present simulations. When considering the resolutions (see table 5.1) it is surprising that the simulations of Willis and Kerswell (2008) and Duguet et al. (2010) show such a large difference for the puff velocity, since the resolutions are comparable.

Another explanation for the difference in velocities found in experimental data and numerical data can be the domain size. In an experiment there is only a single puff present in a domain which is at least a few hundred diameters long. The length of the domain in a simulation is limited and has a periodic boundary, this results in the simulation of not a single puff, but an infinite train of puffs. The length of the domain used by Duguet et al. (2010) is *shorter* than the domain used by Willis and Kerswell (2008). Therefore it is expected that the interaction between the puffs is more significant in a shorter domain and that the velocity of the structure is influenced more.

To measure the amount of interaction between successive puffs, consider the centerline velocity. When the centerline velocity is able to recover to the theoretical value for laminar flow, i.e. two times the bulk velocity, the puffs can be considered independent and no interaction is present. Hence, the level to which the centerline is able to recover is a measure for the amount of interaction with itself. The domain size in the current simulation was set to $100D$ and the centerline

velocity deviates only 0.01% from the theoretical value. In the $50D$ domain the difference has already increased up to 0.6%. Because the laminar velocity profile provides the energy required for the turbulent puff to be sustained (Rotta 1956), it is essential that a fully developed laminar velocity profile is entering the puff to get the correct behavior for the puff.

In this section we showed that the mean advection velocity of a puff was correctly captured by the current simulation. Furthermore, it was shown that the instantaneous velocity of a puff is not constant. It is expected that both the domain size and the resolution at which the simulations are done influence the instantaneous behavior of the puff.

5.6.2 Total in-plane kinetic energy related to puff velocity

In the previous section it was shown that the velocity of a puff is not constant during the lifetime of the puff. An unanswered question that remains is: What is the reason for this variation in velocity? Directly related to this question is what determines the velocity of a puff.

In order to answer these questions, consider the following model of a puff that was introduced by Rotta (1956). Assume that the puff consists of a single transition front, and take a control volume around this transition front. The inflow condition is a fully developed laminar velocity profile, and on the outflow side the flow is that of a fully developed turbulent pipe flow. The transition front inside the control volume redistributes the velocity profile from laminar to turbulent. It was already shown in section 5.4 that the velocity profiles for the interior of the puff are not the same as for fully developed turbulent pipe flow, but nevertheless it is a good initial approximation for the problem at hand.

By applying a momentum balance, Rotta (1956) showed that the pressure should *increase* over the transition front. The pressure increase does not depend on the velocity of the transition front. This phenomenon has already been confirmed experimentally for the upstream part of a slug by Draad (1996) and for a puff by van Doorne (2004) and Kuik et al. (2010).

When an energy balance is considered over the same control volume, the following relation can be derived (Rotta 1956):

$$\dot{E}_u + \pi D u_{\text{bulk}} \int_{z_L}^{z_T} \tau_0 \, dz - \dot{E}_d - \dot{E}_f = 0 \tag{5.5}$$

where $\dot{E}_d$ is the energy dissipation, and $\dot{E}_f$ the energy associated with the velocity fluctuations. Both terms are always positive and can only *remove* energy from the system. The second term gives the production due to the friction at the wall and depends on the length of the puff. This contribution is always positive and for now take this contribution to be constant; see section 5.6.3 for more information about the length variations of a puff.

The remaining term $\dot{E}_u$ gives the contribution caused by the rearrangement of the mean velocity

profile by the transition front and is given by:

$$\dot{E}_u = \pi R^2 \frac{\rho}{2} u_{\text{bulk}}^3 \overbrace{\left\{ 2\int_0^1 (u_L^{\text{x}})^3 \eta \, d\eta - 2\int_0^1 (u_T^{\text{x}})^3 \eta \, d\eta \right.}^{\text{contribution by changing velocity profile}} \underbrace{\left. - \left(2 + u_{\text{puff}}^{\text{x}}\right) \left[2\int_0^1 (u_L^{\text{x}})^2 \eta \, d\eta - 2\int_0^1 (u_T^{\text{x}})^2 \eta \, d\eta \right] \right\}}_{\text{contribution by pressure drop over control volume}} \tag{5.6}$$

where $u_L^{\text{x}} = u_L/u_{\text{bulk}}$ and $u_T^{\text{x}} = u_T/u_{\text{bulk}}$ are the normalized average laminar and turbulent velocity profiles respectively and η the normalized radial coordinate: r/R. The normalized convection velocity of the puff is given by $u_{\text{puff}}^{\text{x}} = u_{\text{puff}}/u_{\text{bulk}}$. The first term, indicated by *contributionbychangingvelocitypro* gives the direct contribution to the energy due to the change of the velocity profile, from laminar to turbulent. The energy caused by the pressure difference on both sides of the control volume is indicated by *contributionbypressuredropovercontrolvolume*. This term has been rewritten into the present form by using the momentum balance over the control volume. Equation 5.6 can easily be integrated after substituting the parabolic velocity profile $(u_L/u_{\text{bulk}} = 2[1-(r/R)^2])$ and a power law relation for the turbulent velocity profile $(u_T/u_{\text{bulk}} = [1-(r/R)]^{(1/n)})$ (Schlichting 1968), where $R = D/2$ is the radius of the pipe. When a value of $n = 6$ is substituted, the integrals can easily be solved, and the equation reduces to

$$\dot{E}_u = \pi D^2 \frac{\rho}{2} u_{\text{bulk}}^3 \left(2 - 1.077 - \left(2 + u_{\text{puff}}^{\text{x}}\right)[1.333 - 1.027]\right). \tag{5.7}$$

$\dot{E}_u$ can be both positive and negative, depending on the puff velocity. It equals zero for a transition front velocity (u_{puff}) of 1.05 times the bulk velocity. From figure 5.9 it is clear that for $Re \geq 1900$ the *average* velocity of a puff drops below this value. When a puff is able to survive in this regime it means that the only energy source that is left is the friction at the wall.

However, it was shown in the right part of figure 5.8 that the instantaneous velocity of the puff shows large variations. From equation 5.7 it is clear that the amount of energy that is available for conversion into fluctuations and dissipation also fluctuates. To get an estimate of the turbulent fluctuations in a puff, the in-plane kinetic energy can be integrated over the entire domain. This quantity is independent of the size of the domain, as long as the entire puff is inside, because the length of the puff is finite. It is expected, based on equations 5.5 and 5.6, that the total in-plane kinetic energy will be highly correlated to the velocity of the puff. To illustrate this, a scatter plot with these two quantities is given in figure 5.10. In this figure the total in-plane kinetic energy is given with respect to the instantaneous puff velocity, for different Reynolds numbers. In this figure, the quantity is also shown for the $Re = 1900$ case for two different domain lengths. These two data sets show a large overlapping region. The puff traveling in the shorter domain shows a larger variation in its velocity. This difference might be either due to the limited domain length, or due to the fact that the observation time for the shorter domain case was longer.

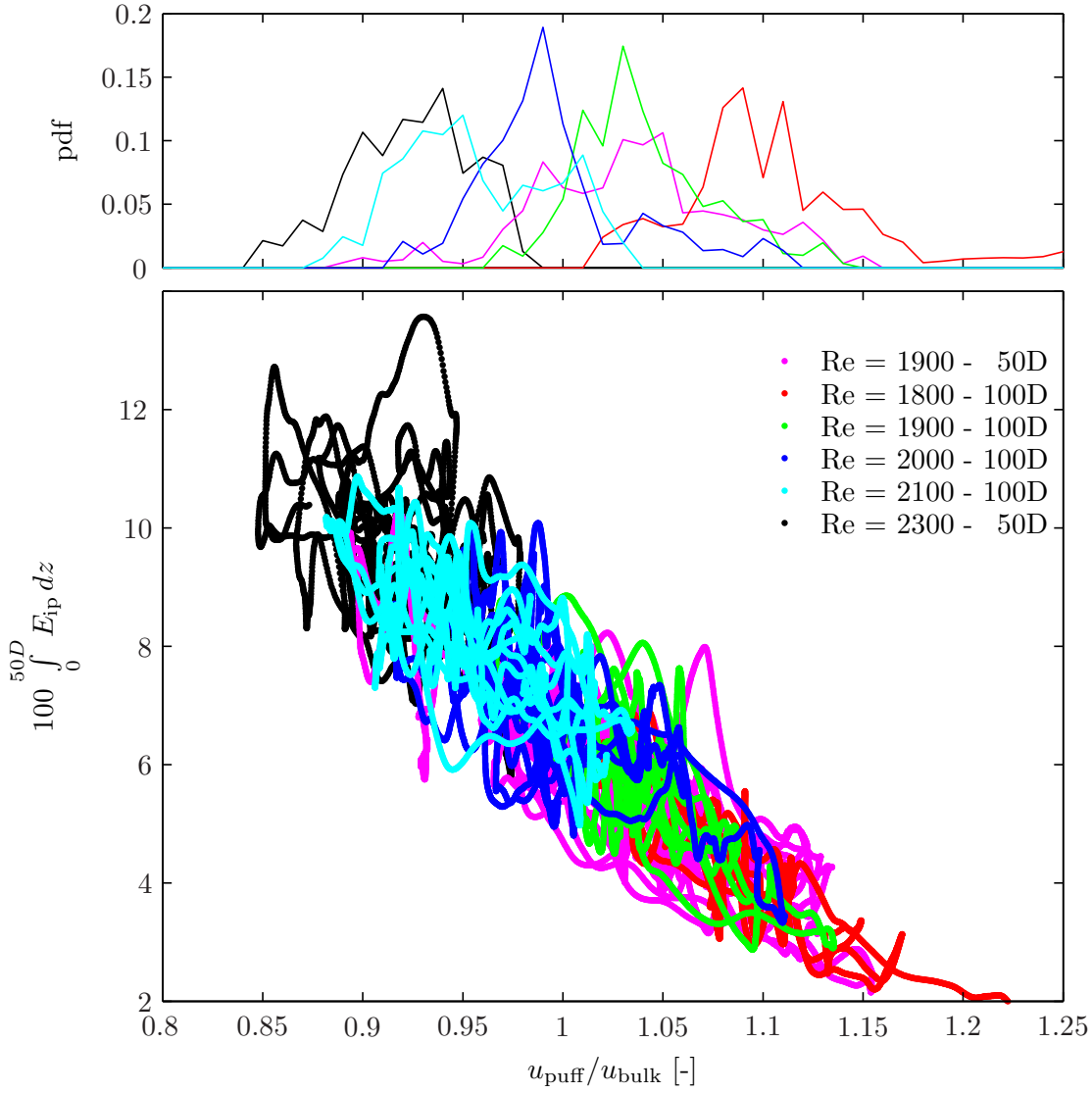

Figure 5.10: The correlation between the instantaneous velocity of a puff and the total in-plane kinetic energy. Only the data for $Re = 2300$ before the structure splits into two separate puffs are considered in this figure. It seems that the behavior of the puff is independent of Reynolds number and that the velocity is determined by the total amount of in-plane kinetic energy.

Two puffs that are represented in this figure show special behavior. The puff at $Re = 1800$ decayed during the simulation, this is visible in figure 5.10 by the red lines that disappears at the bottom right of the figure. Note however that the behavior of this decaying structure confirms the hypothesis that a decaying structure *accelerates* during its decay.

The other puff that showed special behavior was simulated at $Re = 2300$. Initially there was only one puff present in the pipe. After simulating for $t\,u_{\text{bulk}}/D \approx 500$, the structure split into two separate structures. Only the data is shown for $t\,u_{\text{bulk}}/D < 500$, thus for the time a *single* structure was present.

In figure 5.10 the same trend is observed as would be expected based on equation 5.7. The total energy content in the fluctuations *increases* for *decreasing* transition front velocity. Equation 5.7 does not contain the Reynolds number explicitly. The *average* velocity of the puff does depend on the Reynolds number, as was shown by figure 5.9. Nevertheless, when considering the total in-plane kinetic energy as function of the puff velocity for different Reynolds numbers given in figure 5.10, the weak dependence of the Reynolds number seems to be confirmed. The behavior of a puff is determined by the energy content and its associated velocity. The route of a single puff through the energy-velocity domain was followed in order to determine the causality of events, i.e. does the decrease in velocity cause the increase of energy? One would expect to observe a small latency between these events if the one is *caused* by the other. Unfortunately no clear trend was observed: in some cases the energy content increased rapidly while maintaining its velocity. On other occasions a direct coupling was found: an increasing energy was observed simultaneously with a decrease in velocity, or vice versa. This behavior was observed for all Reynolds numbers. By changing the Reynolds number only the frequency of occurrence in a certain part of the energy-velocity domain is changed. As was stated before, the puff simulated at $Re = 1800$ decayed: the flow in the entire domain became laminar. On this single observation, it seems that this decay is associated with a high puff velocity and a low in-plane kinetic energy content. For future research it is worth to investigate if a puff cannot recover once a particular puff velocity threshold is exceeded, or if there exists a total in-plane kinetic energy threshold, below which the puff cannot sustain itself anymore.

It is clear from equation 5.7, and especially figure 5.10, that the frequency of occurrence close to these thresholds reduces for increasing Reynolds number. This can be an explanation for the observed increasing lifetime for increasing Reynolds number (Hof et al. 2006, Peixinho and Mullin 2006, Willis and Kerswell 2007a, Hof et al. 2008, Kuik et al. 2010).

Here we showed that the instantaneous total in-plane kinetic energy in the puff is strongly related to the instantaneous velocity of the puff. Unfortunately, it is not possible to extract the causality of events, i.e. if a decrease in in-plane kinetic energy *causes* the puff to slow down or that the velocity of the puff itself is the driving factor. Nevertheless, a possible explanation is given for the decay process and the lifetime statistics observed in previous studies.

5.6.3 The length of a puff

The localized nature of a puff introduces a 'new' length scale unique to this type of flow: the length of the puff (see also figure 1.5). Due to the smooth interface at the downstream side of the puff it is hard to determine the exact length of a puff (Coles 1981). Therefore a large range of lengths for a puff are reported in the literature. However, many authors do not measure the length of the puff themselves, but refer to classical work (e.g. Wygnanski and Champagne 1973, Wygnanski et al. 1975). Wygnanski et al. (1975) showed that the length of a puff appears to be constant for a given Reynolds number and the length is of the order of $20D$. However, they also showed in their paper that the length of a puff decreases for $Re < 2200$ and increases with downstream distance when the Reynolds number exceeds 2300. Either the length observed at each measurement station was the same for a given Reynolds number *and* all puffs at a given Reynolds number showed the same behavior, or the length is not constant at a given Reynolds number as was stated in their conclusion.

Nishi et al. (2008) reports that the puff length ranges between $5D$ and $20D$ and states that the length of a puff depends on Reynolds number. Unfortunately they did not report on the length of puffs they observed themselves. By using a flow visualization method, Bandyopadhyay (1986) divided the puff into three regions, from which the total length can be deduced: a transitional region, a fully developed turbulent region, and a relaminarization region.

The transitional region, in which the laminar fluid is converted into turbulent motion, extends over 3 to $4D$. The second part contains fully turbulent fluid and is approximately $5D$ long. However, as was already shown in section 5.5, fully developed turbulent flow is not observed in the current investigation. Moreover, the region in which the average velocity profile is close to fully developed turbulent pipe flow is much shorter than reported by Bandyopadhyay (1986). The length of the remaining and longest part is not specified explicitly and depends strongly on what the observer considers to be part of the puff. Nevertheless, since it is the longest part, the total length of the puff has to exceed $15D$.

In a more recent experimental investigation, De Lozar and Hof (2009) only state that the disturbances they applied generated puffs of constant length. Unfortunately, it is unclear *what* the length of the structure is.

In the current simulation the length is determined by considering the in-plane kinetic energy distribution. The reasons for selecting the in-plane kinetic energy to extract the instantaneous behavior of the puff also apply here. In the previous section the first order moment of the in-plane kinetic energy distribution was used to extract the location of the puff. For an estimate of the length of the puff, the second order moment of the in-plane kinetic energy is used.

Figure 5.11 shows the correlation between the instantaneous velocity of the puff and the length of the puff. The horizontal axis gives the velocity with respect to the bulk velocity, similar to figure 5.10. The length of the puff is given on the vertical axis.

In this figure two states of a puff seem to be present. One state is a puff where the length of the puff is does not depend on either Reynolds number or the velocity of the puff and remains

limited. The second state is a puff with a maximum velocity equal to the bulk velocity. The puff has a variable length instead of a variable velocity over time. The puff is in the first state for $Re \leq 2000$, and the length seems to be bounded between $2D$ and $5D$.

As the Reynolds number is increased above 2000 the upper boundary, of $5D$, seems to be breached. If the Reynolds number is increased even more the length increases dramatically, and the second state is reached. In this state the velocity seems to be limited by the bulk velocity (value equal to one in figure 5.11).

The large magnitude reached for the puff at $Re = 2300$ is mainly caused by the method the length is determined. After observing the in-plane kinetic energy distribution at the moment the longest length was reached, it was clear that the major increase in length was caused by a relative small contribution of in-plane kinetic energy downstream of the puff. It was as if a fluid package, containing velocity fluctuations, was shed from the main puff. When the fluctuations in this package decayed, the measured length decreased again. This also explains why the dramatic increase was not observed in the total in-plane kinetic energy (figure 5.10). Only a small amplitude fluctuation was shed from the puff, which hardly contributes to the total in-plane kinetic energy.

Comparable to figure 5.10, figure 5.11 contains limited amount of data for the $Re = 2300$ case (only $t\,u_{\text{bulk}}/D < 500$). A very short time later the puff splits into two parts, where the new puff is generated downstream of the existing structure. The newly generated puff convected downstream during its formation process faster than the parent puff. During this phase, the in-plane kinetic energy contained in the puff was also lower, which is consistent with the observations in the previous section. Once it was well established, the amplitude is of the same order as the parent puff as is its velocity. By this single observation an explanation for the generation of new puffs from existing puffs is given, that is consistent with the relation between the in-plane kinetic energy and puff speed.

When the Reynolds number is increased even more, the slug regime is entered (Wygnanski and Champagne 1973). In this regime a continuously growing structure is observed. Lindgren (1969) already showed that the velocity of the rear transition front decreases with increasing Reynolds number. Based on equation 5.5 it becomes clear that the amount of energy released by the transition from laminar to turbulent also increases. Either this energy has to be dissipated, for example by creating stronger gradients and smaller structures, or by increasing the length of the structure, so the energy can be converted into more fluid with velocity fluctuations. The latter of these two options has already been observed, which led to the definition of the slug regime, i.e. continuously growing structures.

Up to now it is still unclear what drives the velocity of the transition front. However, from the current investigation the effects of the changing transition front velocity on the total energy and the length of the puff can be explained and surprisingly do not strongly depend on the Reynolds number that is considered.

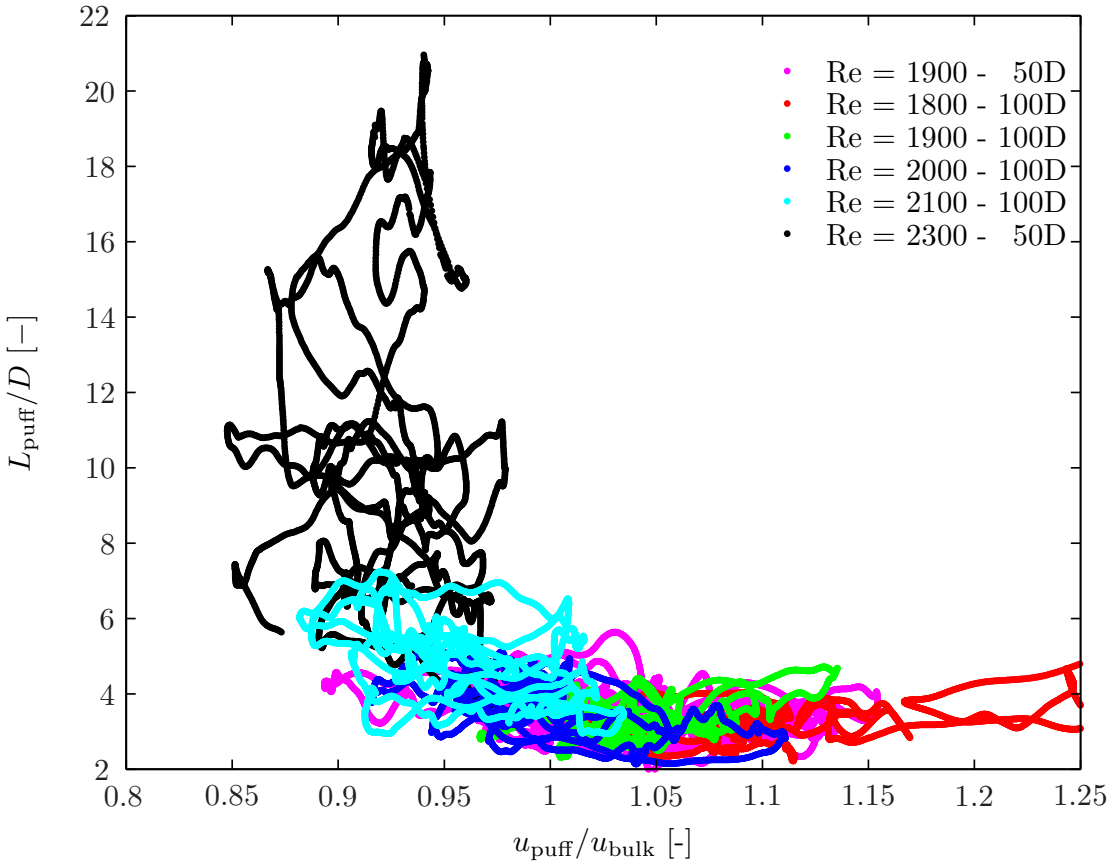

Figure 5.11: The correlation between the length of the puff and its instantaneous velocity. The length of the puff does not depend on the velocity of the puff. For $Re < 2100$ the velocity is bounded to $\approx 5D$. This boundary is breached when $Re > 2000$. Only the data for $Re = 2300$ for time $tu_{\mathrm{bulk}}/D < 500$ are taken into account, this is just before this structure splits into two puffs.

5.7 Dynamics of structures within a puff

One of the main motivations to perform a simulation at a very high resolution, was the discrepancy between small scale structures that were observed experimentally (van Doorne and Westerweel 2009) in in-plane kinetic energy and the available resolution in simulations done so far. The high energetic peaks in in-plane kinetic energy observed by van Doorne and Westerweel (2009) were reproduced in an experiment by De Lozar and Hof (2009). They showed the in-plane kinetic energy distribution for two individual realizations. The distributions revealed that the location of the high energetic peaks were at different locations. This shows that the peaks in in-plane kinetic energy are not stationary structures that travel at the same velocity as the puff. Unfortunately, De Lozar and Hof (2009) did not comment on the origin and behavior of these energetic peaks.

In this section a brief description of the characteristics of these peaks is given, starting with the identification and tracking of the high energetic peaks in in-plane kinetic energy. In section 5.7.2 their dynamical behavior is discussed. Since van Doorne and Westerweel (2009) only measured a single quasi-instantaneous puff, the dynamics of the observed peaks could not be resolved. Based on their single measurement and their comparison with flow visualizations they deduced that the high energetic peaks are caused by hairpin vortices. In the final section a single peak is followed and the underlying structure is discussed.

5.7.1 Peak identification and tracking

Before the characteristics of the peaks can be identified, a 'peak' event has to be defined. Consider the in-plane kinetic energy distribution given in figure 5.1. To extract the location of the peaks, the obvious approach would be to take the first derivative of the signal and detect the zero-crossings. However, this would result in a very high number of detected peaks, since every small wiggle in the in-plane kinetic energy distribution would be identified as a peak. In this way the significance of the peak is not accounted for. We are looking for the dominant peaks, and should disregard the smaller peaks. To account for the amplitude of the peak, the following definition and procedure is used to identify the most significant peaks only:

First, the global maximum of the in-plane kinetic energy is established. This peak is then followed over time by a nearest neighbor approach: At the next time-step all local maxima are determined by identifying the zero crossing for the derivative of the distribution. Then the peaks, i.e. zero crossings, closest to the peaks that have to be tracked are selected. Because in general the distance between peaks is much larger than their relative displacement between two consecutive time steps of the simulation, the nearest neighbor approach can be successfully used. Finally two checks are carried out: first it is checked if the peak displacement does not exceed a predetermined limit. The second check is whether two peaks have merged and became the same peak. If either of these two events occurs, the tracking of that particular peak is terminated.

When the current peaks cease to contain the global maximum, the newly identified peak corre-

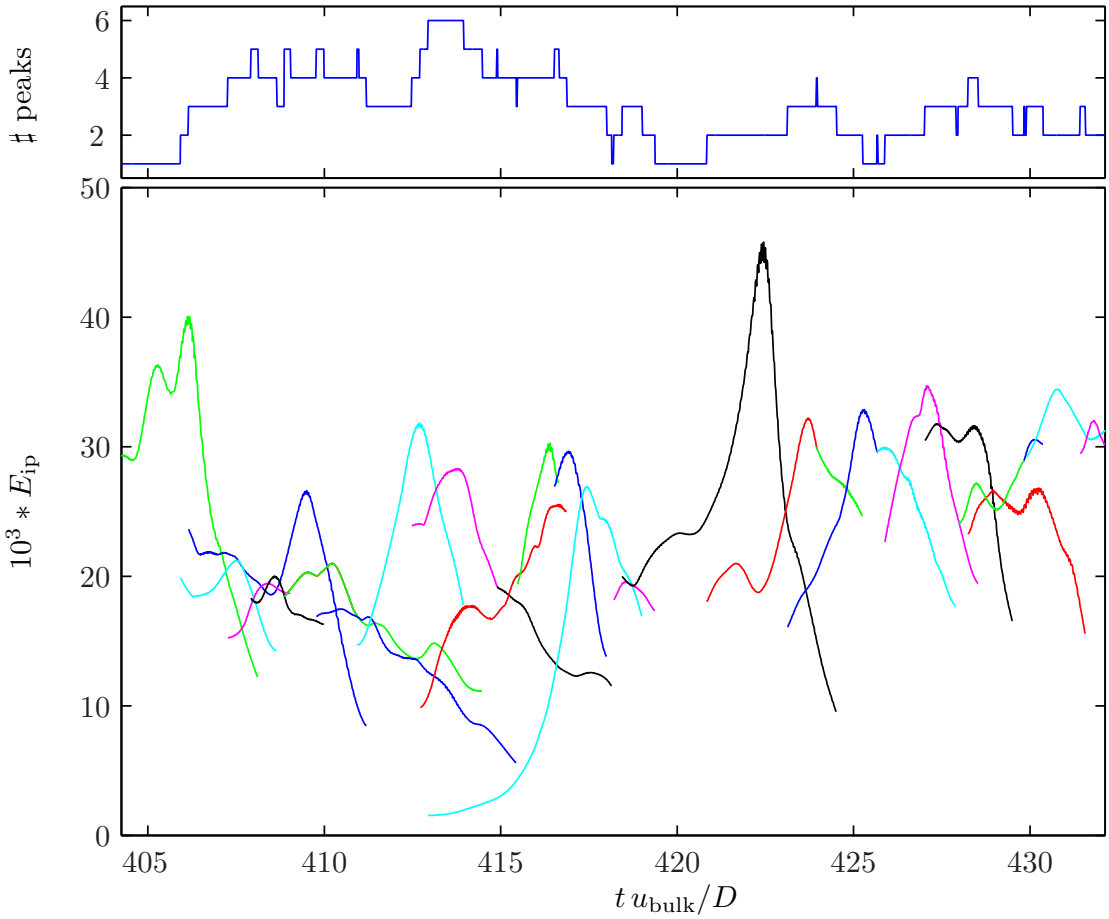

Figure 5.12: The development of the amplitude of a peak over time. Only the peaks that once become the global maximum are taken into account *Top* the number of identified peaks that are simultaneously present over time.

sponding to the global maximum is followed too. This procedure was implemented as a post-processing step. Therefore it was possible to apply the procedure both forward *and* backward in time. This allowed for tracking the entire lifetime of these peaks. A drawback of the currently used method is that the total number of peaks may be underestimated. This is because a peak that never becomes the global maximum over time is not identified, and therefore is not tracked. Despite this drawback, the clear and robust definition is preferred.

5.7.2 Peak characteristics

In the present simulation both the location and the amplitude of the peaks are available over time. In this section the characteristics of the peaks themselves are presented.

In figure 5.12 the amplitude variation of all peaks within a short time interval are presented. Each line in this figure represents the evolution of an individual peak. The horizontal axis gives the progress in time. On the vertical axis the amplitude of the peak is shown. Over time, the

amplitude of a single peak does not only increase monotonically, and after its maximum has been reached decreases monotonically, until it is not present anymore. Instead, the amplitude shows large variations over the lifetime of a peak. Look for example at the first peak, i.e. the one present at $tu_{\text{bulk}}/D = 405$, in figure 5.12. The amplitude of the peak first increases, then decreases for a very short time and finally increases to reach its global maximum before decreasing again. Next to the very dynamic behavior, it shows that the energy contained in a single peak can change tremendously. The amplitude of a single peak can increase up to a factor 20 over its lifetime.

In the top part of figure 5.12 the number of peaks is given that are simultaneously present in the pipe. This value has been determined by counting the number of identified peaks at every time instant. Inherent to the tracking method, always at least one peak is present, which corresponds to the global maximum. In the central part of figure 5.8 the number of peaks are given over a much longer integration time. The *average* number of peaks that are present over time in the puff given in figure 5.8 is equal to three. In the single experimental observation, van Doorne and Westerweel (2009) identified the same number of peaks. These two results combined give on the one hand confidence in the method that is used here to identify the most significant peaks; On the other hand it shows that the results found in the experiments by van Doorne and Westerweel (2009) are a good representation of what happens in the puff during its lifetime and should not be considered as exceptional.

From the data of the simulation not only the amplitude variation over time is available, but also the location of the peak. In order to visualize the behavior of the peaks relative to the puff, a space-time plot is given in figure 5.13. In this figure the horizontal axis represents the axial pipe coordinate. The flow direction corresponds to the positive z direction. Note that in this figure the *actual* position in the pipe is given instead of the position with respect to a convective reference frame, as was shown in figure 5.8. Again the time increases in vertical direction.

In figure 5.13, the bold curves show the result of tracking a single peak, with a different color for each peak.For every peak that was observed in this time interval its location is given as a function of time. Be aware that the data given here are over a much shorter time interval than the data in figure 5.12. To get an idea of the location of the peaks relative to the puff, the location of the puff is also given together with its length. In section 5.4 it was shown how the location of the puff was determined. The length has been determined by the method described in section 5.6.3. The location of the puff is given by a blue dashed line, and the front and back of the puff are indicated by red dashed lines. The front and back are determined by taking the location of the puff and subtracting and adding half the puff length to that location respectively. Recall that the length of the puff did vary over time, but it is clear from figure 5.13 that the length does not change very rapidly.

The inset in this figure shows the distribution of the in plane kinetic energy over the pipe at time $t\,u_{\text{bulk}}/D = 598$ (indicated by the dashed black line in the main figure). The peaks that were tracked at this time are indicated by dots, and the color of each dot corresponds to the color of the peak-location traces in the main figure. The detection method used clearly does not track all peaks present in the in-plane kinetic energy distribution, as was predicted when discussing the detection method. This is confirmed by the two peaks between the blue dashed line and the

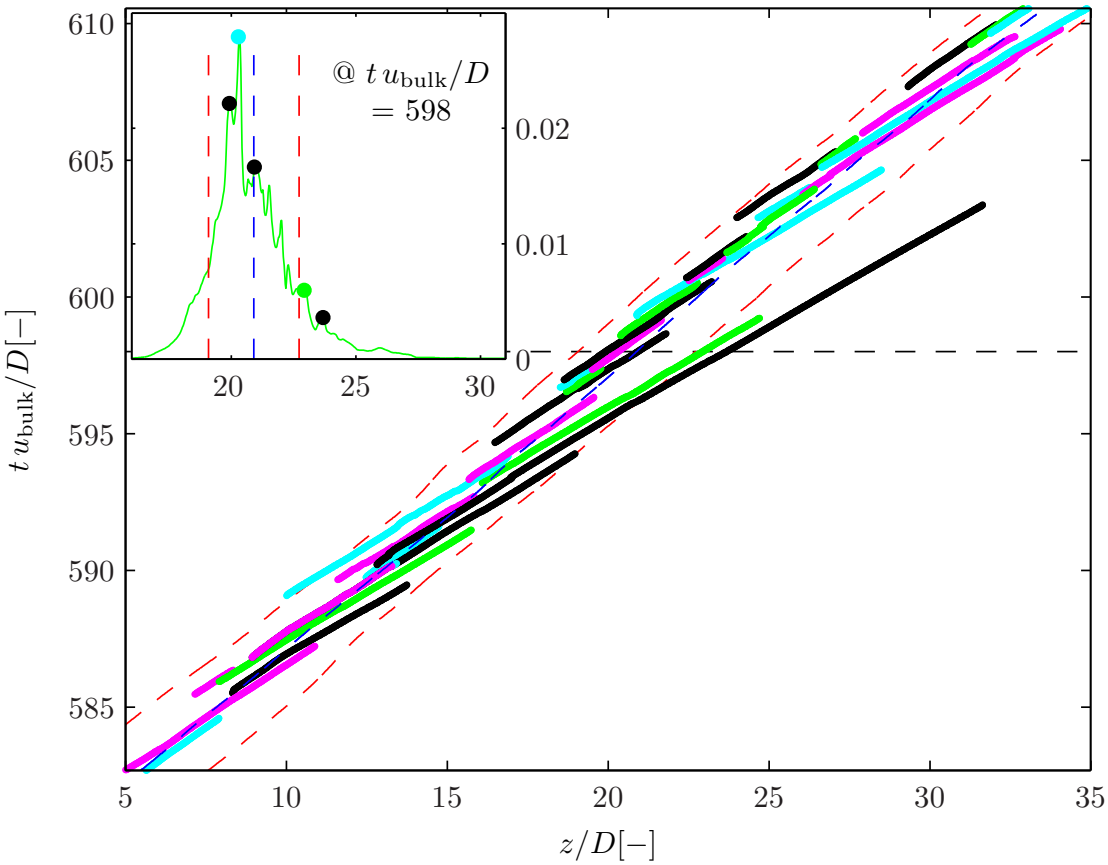

Figure 5.13: Location of puff and the peaks over time. Only peaks of which the amplitude becomes the global maximum at least once in their lifetime are tracked. The red dashed lines give an indication of the two fronts of the puff, the blue dashed line gives the current location of the central moment for the in-plane kinetic energy distribution. *Inset* The in-plane kinetic energy distribution at $t\,u_{\mathrm{bulk}}/D = 598$. Dots in the peaks indicate that these peaks were tracked and at least once became the global maximum peak. Note that the time frame presented here is *not* the same as in figure 5.12.

downstream red dashed line in the inset of figure 5.13, which are not being tracked.

From the distribution given in the inset of figure 5.13, it is clear that the in-plane kinetic energy distribution is skewed. This was already observed when considering the effect of using a different resolution on the behavior of a puff in section 5.3 and similar behavior is found for almost all realizations. On the upstream side of the center of the distribution a higher contribution is found. Therefore it is not surprising that the concentration of peaks is higher in the upstream half of the puff, also when taking the detection method into account. Since only peaks are tracked that once become the global maximum, it is more likely to find peaks in the upstream part than in the downstream part of the in-plane kinetic energy distribution. Nevertheless, on the upstream side peaks do not extend over the boundary indicated by the red dashed line. On the downstream side there is occasionally a peak that survives for a long time and extends over the boundary that indicates the length of the puff. This implies that structures associated with these peaks are created at the upstream side of the puff. Occasionally they are able to survive through the entire puff and are 'ejected' at the downstream side. These structures might be the seeds from which a new puff is created, and hence a new puff can be created downstream. Lindgren (1969) already observed that new structures are generated on the downstream side of the parent puffs, but did not comment on the process that was involved.

From the slope of the traces given in figure 5.13 it is possible to get the velocity of the peaks. The velocity is determined by applying a least square fit to the data for each peak, as presented in figure 5.13. By eye it is already clear that the velocity of the peaks is significantly higher than the velocity of the puff, hence the peaks travel 'forward' *through* the puff.

The velocity distribution of the most significant peaks is given in figure 5.14, for puffs at different Reynolds numbers. In the top part of the figure the peak velocity is normalized by the bulk velocity. The bottom part shows the peak velocity when it is normalized by the average puff velocity as given in figure 5.9.

First consider the velocity distribution of the peaks with respect to the bulk velocity. As the Reynolds number increases, the velocity of the peaks *decreases*. The difference between the distributions at $Re = 1800$ and $Re = 1900$ is larger than the difference between $Re = 2000$ and $Re = 2100$. This indicates that the velocity distribution would be approaching an asymptotic distribution and that there is a lower limit for the peak velocity. In section 5.6.1 it was shown that the puff velocity depends on Reynolds number. The velocity of the puff continues to decrease for increasing Reynolds number. This means that the peaks will travel faster with respect to the *puff* when the Reynolds number is increased.

This is confirmed when the peak velocity is normalized by the *average* puff velocity, shown in the bottom part of figure 5.14. The peak velocity *increases* with respect to the puff velocity for increasing Reynolds number.

For a single simulation at a variable Reynolds number, Shimizu and Kida (2009) observed small scale structures that had a higher velocity than the puff velocity. These structures were found by considering only the centerline velocity distribution over time. The velocity fluctuations observed in the centerline velocity distributions were considered to be caused by a Kelvin-

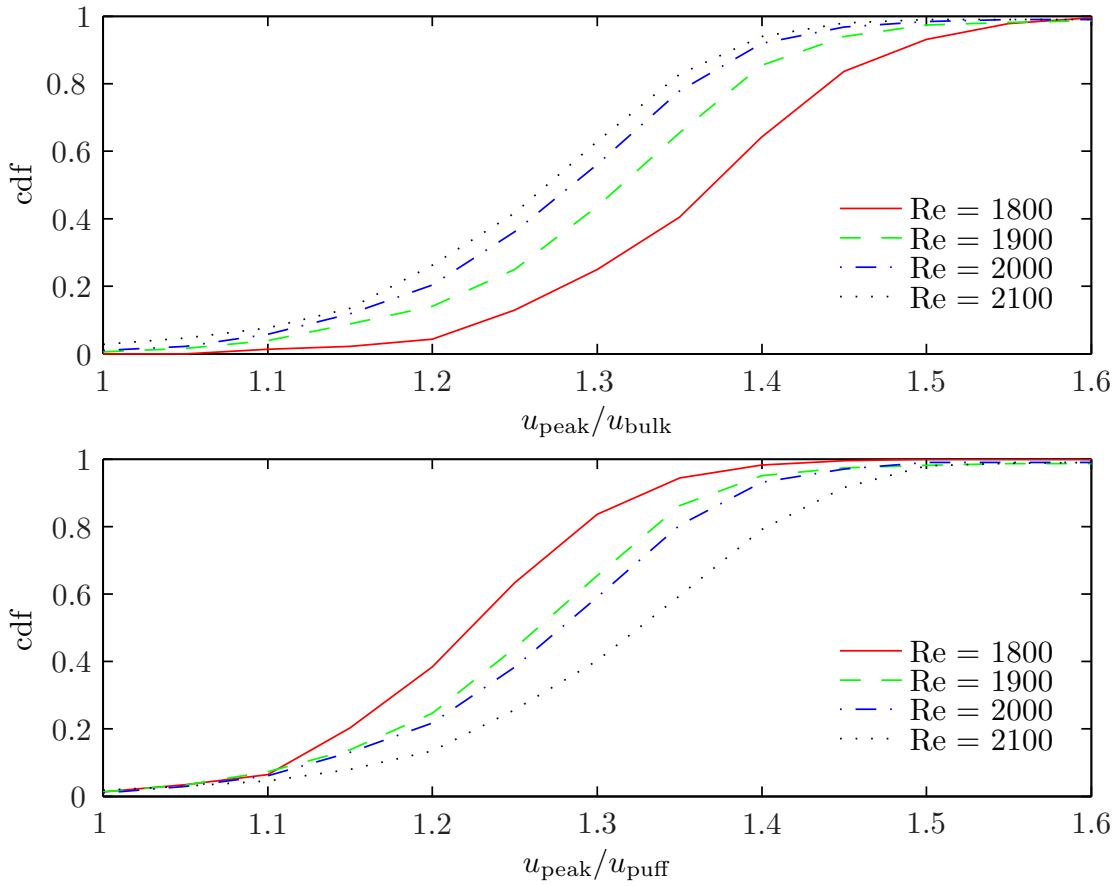

Figure 5.14: Cumulative distribution of the velocity of a peak for different Reynolds numbers, relative to the bulk velocity (*Top*) and to the puff velocity (*Bottom*). The peaks move slower with respect to the bulk velocity for increasing Reynolds number. The opposite behavior is observed with respect to the puff velocity.

Helmholtz instability at the upstream side of the puff. They concluded that this Kelvin-Helmholtz instability was essential in the regeneration process of a puff.

Later, Duguet et al. (2010) also found that at the rear of the puff structures were formed that were caused by a Kelvin-Helmholtz-like instability. They identified these structures by tracking a local maximum in azimuthal vorticity in an axial cross section of the pipe. These structures were carried downstream relative to the slug they considered. The velocities observed for these structures coincide with the velocities of the peaks found in the present investigation. If the structures observed in the present investigation are the same as the structures observed by Duguet et al. (2010), it is not surprising that the majority of the structures is observed at the upstream side of the puff, since this is the location where they are initiated. More details on the structures responsible for a peak in in-plane kinetic energy is given in section 5.7.3.

A question that emerges is whether the distance traveled by a peak depends on the Reynolds number. Since the velocity of the peaks with respect to the puff increases for increasing Reynolds number, the peaks would travel a longer distance through the puff if the survival time of the peaks is constant. The probability distribution of the distance a peak travels relative to the puff is given in figure 5.15. Hence, a negative distance in this figure means that the peak travelled slower than the puff. This shows that the distribution is independent of Reynolds number, which means that the life*time* of a peak *decreases* for increasing Reynolds number.

5.7.3 The structure responsible for a peak

Up to now it is unclear if there is a single coherent structure that is responsible for the high energetic peaks in in-plane kinetic energy. If the high energetic peak is generated by a single structure, the question remains what kind of structure it is. Van Doorne and Westerweel (2009) found in their measurement hairpin vortices close to these peaks. Therefore they concluded that hairpin vortices are responsible for the generation of the high energetic peaks. However, these observations were based on a few observations in a single realization. In the previous section the velocity distribution for the peaks in in-plane kinetic energy was given. When this velocity distribution is considered and compared to the velocity distributions of structures found by others, a range of possible flow structures responsible for these structures can be obtained. Both Shimizu and Kida (2009) and Duguet et al. (2010) found localized structures with a similar velocity as was found for the peaks in in-plane kinetic energy. They related these structures to vortices that were induced by a Kelvin-Helmholtz instability. Furthermore, when comparing the convection velocity of the peaks and the phase velocities of the traveling waves found by Pringle and Kerswell (2007) a similar magnitude is observed. Pringle and Kerswell (2007) found that the phase velocity of the traveling waves ranges from 1.1 to 1.5 times the bulk velocity. It might be that the observed structures are in fact traveling waves. This is not considered likely, because of the spatial extend of the traveling wave solutions that were found and the very localized nature of the currently observed peaks.

From these observations it is not clear what the structures are that cause a peak in in-plane kinetic energy. A first approach to reveal the underlying structure was to conditionally average

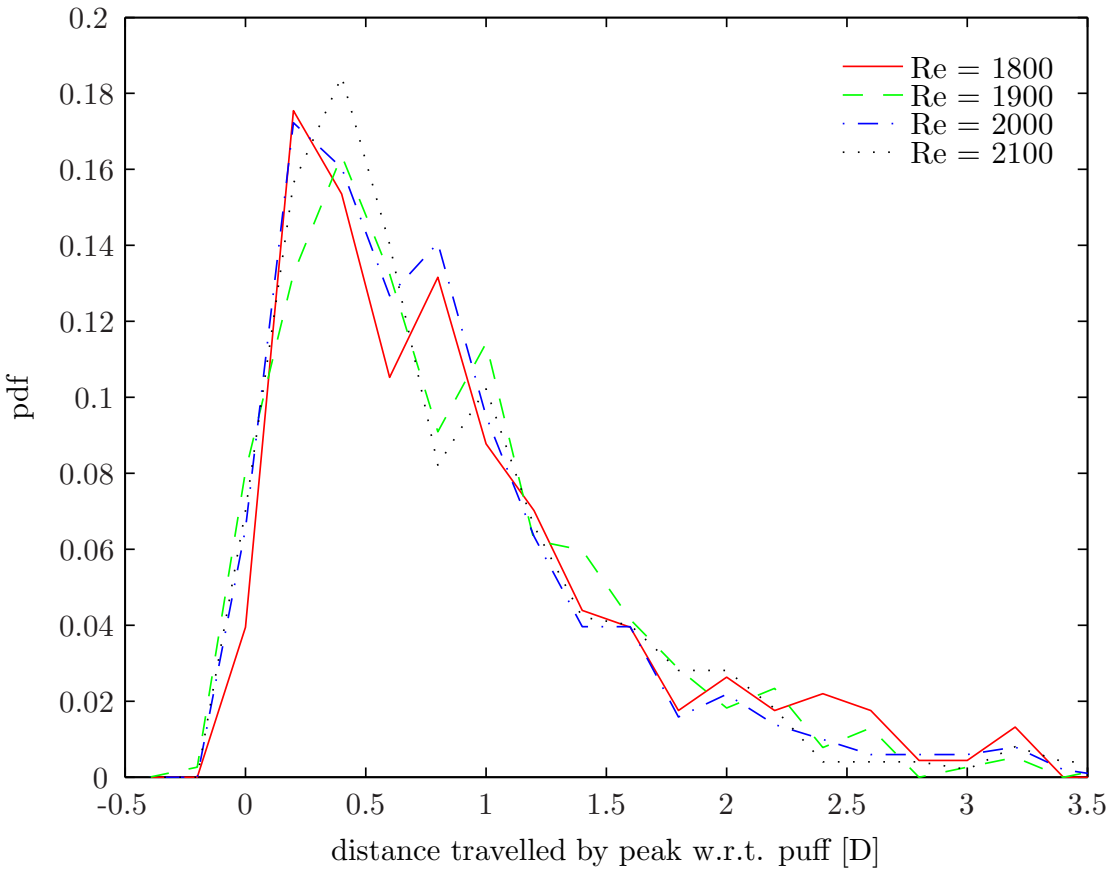

Figure 5.15: The distance covered by the peaks with respect to the puff. The distance that is travelled with respect to the puff seems to be independent of the Reynolds number.

the velocity field. This results in a single cross sectional velocity distribution. When the velocity difference with respect to laminar flow was considered, the velocity field contained three to five high speed regions close to the wall, depending on the peak. This method did not reveal a clear unique structure that could be considered responsible for the generation of the peak in in-plane kinetic energy.

A second approach was to follow the structures in a convective reference frame that moves along with a single peak. The results for a single event are shown in figure 5.16. In this figure the flow is from right to left. In each subfigure iso-contours for a positive value of Q are given. Here Q is the second invariant of $\nabla\mathbf{u}$ (Jeong and Hussain 1995). The same quantity has been used by van Doorne (2004) to identify coherent structures in experimental data. As a reference the in-plane kinetic energy distribution is plotted on the bottom of each subfigure-box.

The time evolution of the structures underneath a single peak is illustrated by three snapshots in figure 5.16. In each subfigure a volume spanning two pipe diameters in the axial direction of the entire domain is shown, taken symmetrically around the currently followed peak. Starting at the top, the time between two consecutive images is equal to $t\,u_{\text{bulk}}/D = 0.7$. It is clear that the structures found in this way are slowly evolving structures that are convected downstream without major changes. In these figures the classical picture of a hairpin vortex could not be detected. Other methods of visualization and different thresholds for Q did not reveal hairpin-like structures either. By tracking six different structures given in figure 5.16 over time, the relative motion of structures inside the puff are explained.

In figure 5.16 these six vortical structures are labeled A to F. The observed vortices can be divided into three categories based on their velocity. The first category contains structures that have the same velocity as the peak (C and D). These structures are the most likely candidates to be responsible for the peak that is currently followed. The second category contains structures that move faster than the peak (A,B and F). Since the average fluid velocity is higher near the center of the pipe, it is expected that these structures can be found closer to the pipe axis. Consequently, structures with a lower velocity (the third category) are expected to reside closer to the pipe wall (E).

In order to find the structures that are responsible for the generation of the high peak in in-plane kinetic energy, only the structures that move at the same velocity as the peak are considered. Because the domain is selected symmetrically around the peak, the structures responsible for this particular peak are expected to be close to the middle of the pipe sections given in figure 5.16. The structure that is labelled C is present close to the middle of the pipe in each of the subfigures and is therefore considered responsible for the generation of the high peak. Note that the structure is always upstream of the peak, which is in accordance to the findings of van Doorne and Westerweel (2009). The structure is orientated normal to pipe axis and is aligned in azimuthal sense with the wall of the pipe. It has a length of approximately one pipe diameter. A vortex which is orientated normal to the pipe axis is able to generate a large amplitude contribution to the in-plane velocity components, which results in a high peak in in-plane kinetic energy. Moreover, a structure with this orientation will contribute to the azimuthal vorticity component, which was used by Duguet et al. (2010) to identify and track Kelvin-Helmhotz vortices generated at

the trailing edge of the puff. Because of its orientation normal to the pipe axis, a relative high resolution in axial direction is needed to resolve this structure properly. This might be a reason why the high energetic peaks were not observed by others, see also table 5.1.

The structure indicated by *D* has approximately the same velocity as the peak. However, it extends over almost half the domain (axially) and can therefore not be considered responsible for the creation of the very localized peak.

In figure 5.16 three structures are labelled that move faster than the peak. These structures are labelled *A*,*B* and *F*. Two structures (*A* & *B*) are present downstream of the structure responsible for the peak in in-plane kinetic energy. Since the velocity is higher, hardly any interaction is expected between these structures and the vortex labeled *C*. The vortex indicated by *A* remains approximately constant in size as it moves downstream and out of the domain. The size of the structure that is labelled *B* increases as time progresses, the velocity of this structure is approximately equal to the velocity of structure *A*. Since the velocity is higher than the peak velocity, it is expected that this structure would be present close to the center of the pipe. However, as can be seen in the bottom part of figure 5.16, the structure is attached to the wall. The propagation velocity of vortical structures clearly does not have to be the same as the local fluid velocity. The third structure that is moving faster than the peak (*F*) is present in the center of the pipe and upstream of the structure *C*. Its velocity is considerable higher than the velocity of the peak, but its velocity is also higher than the velocity of the structures labeled *A* and *B*. Due to its higher velocity, it gets closer to the structure responsible for the peak in in-plane kinetic energy. The approach of structure *F* contributes to the change in orientation of structure *C*. As this structure loses its orientation normal to the pipe axis, the contribution to the in-plane velocity components reduces. As a result the peak in in-plane kinetic energy diminishes.

Finally there is a single structure, indicated by *E*, that moves slower than the peak. This structure is close to the wall and moving slowly in the upstream direction, i.e. relative to the peak. It seems to be a very stable structure, which is hardly influenced by the presence of the structures surrounding it.

This figure shows the richness of structures present in a turbulent puff. By considering only a small fraction of the simulation time a large number of large-scale structures can be identified that survive for a significant time. Furthermore, the high energetic peaks in in-plane kinetic energy were *not* found to be caused by hairpin like vortices. Instead, the peaks seem to be generated by vortical structures that have an orientation normal to the pipe axis. One might argue that the head of a hairpin vortex is also normal to the pipe axis and is therefore responsible for the high peak. This might be the reason why van Doorne and Westerweel (2009) found structures close to the high energetic peaks that could be associated to hairpin vortices. However, from the result shown in figure 5.16 it is clear that the peaks are generated by large scale structures that span almost the entire diameter of the pipe. The same analysis has been applied to numerous other peaks in which a similar behavior is found: A large scale structure that has an orientation normal to the pipe axis generates the large peak in in-plane kinetic energy. In all cases, the classical picture of a hairpin vortex could not directly be associated to vortical structures observed in a puff.

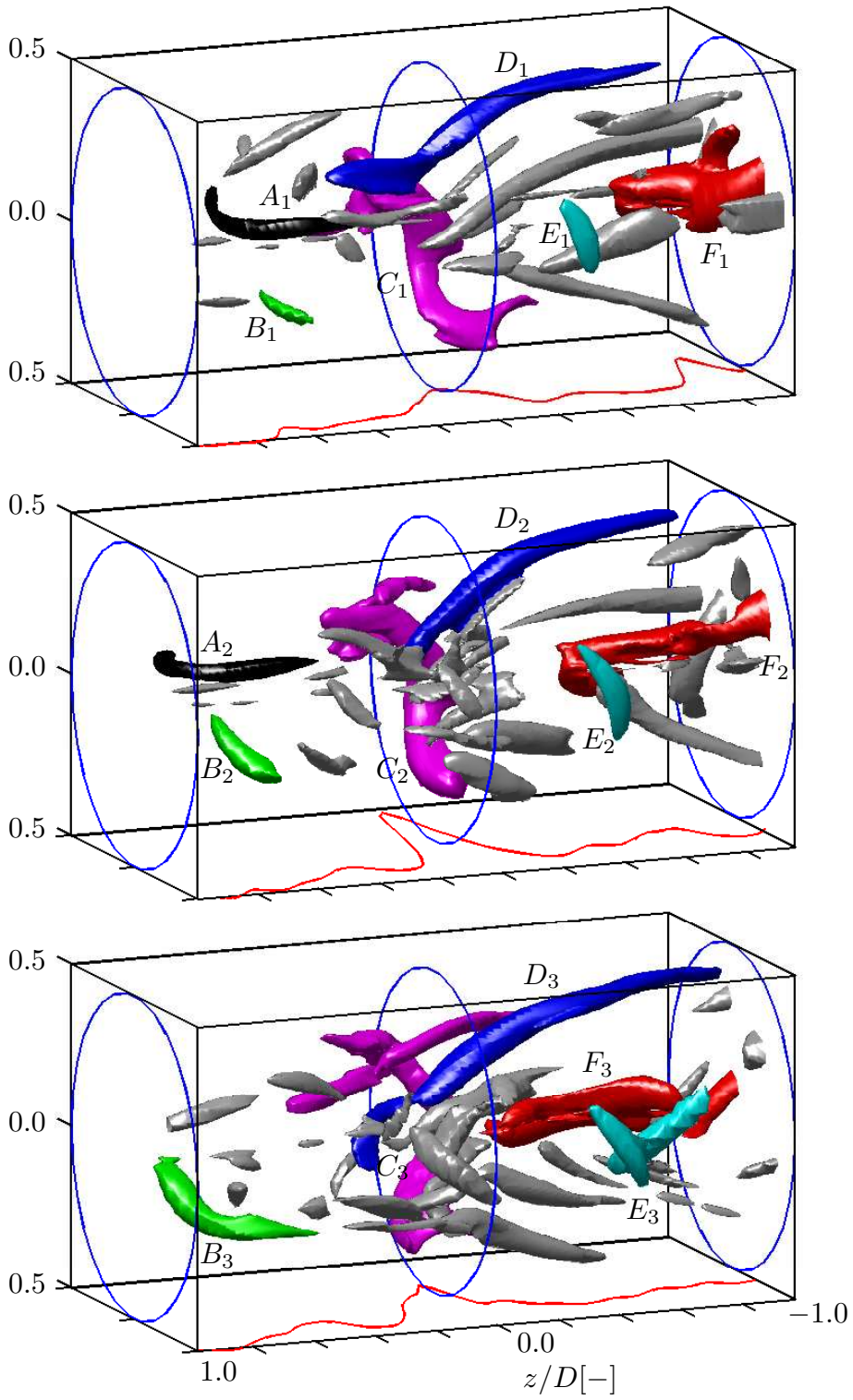

Figure 5.16: Coherent structures in a puff in a convective reference frame that moves along with a peak. The time between consecutive images is $t\,u_{\text{bulk}}/D = 0.7$ timescales. Coherent structures are visualized using iso-contours of Q. On the bottom of each figure the in-plane kinetic energy distribution is shown as a reference.

5.8 Conclusion

In this chapter the results of a direct numerical simulation of transitional pipe flow are presented. The velocity field of a puff measured by PIV was used as an initial condition. It was shown that the requirements on the domain are very demanding for simulating transitional pipe flow. Not only the necessary length of the domain causes a challenge. The high resolution required in axial direction to obtain a puff that behaves similar to puffs observed in experiments, makes the simulation of transitional pipe flow computational intensive.

In order to validate the numerical procedure, fully developed turbulent pipe flow at $Re = 5300$ is simulated. The obtained velocity statistics are then compared to the average flow field of a turbulent puff. Surprisingly, the interior of the puff does not reveal a region that shows the same flow statistics as observed in fully developed turbulent pipe flow. This opposes conclusions in earlier works, e.g. Wygnanski et al. (1975), Bandyopadhyay (1986). At the location in which the average velocity profile has the closest match to the velocity profile for fully developed turbulent pipe flow, the velocity fluctuations show a more homogeneous distribution across the pipe. This location also corresponds to the position with the strongest inflection point in the mean velocity profile, which is considered the source of vorticity by Hof et al. (2010). In the relaminarization region, the maximum intensity for the velocity fluctuations moves towards the center of the pipe, which is in accordance with the classical image of the conical tail characteristic for a puff (Bandyopadhyay 1986).

The instantaneous velocity of the simulated puffs was not constant. This is in agreement with the findings of Kuik et al. (2010). However, Wygnanski et al. (1975) and De Lozar and Hof (2009) found constant propagation velocities for the puffs in their experiments. The average velocity found by in the present simulations agree excellent with the velocities reported by Hof et al. (2006), De Lozar and Hof (2009) and Kuik et al. (2010). This suggests that the distance over which the velocity of a structure was measured by De Lozar and Hof (2009) was already sufficiently long to hide the instantaneous velocity behavior of a puff as observed in the present study and in the experiments by Kuik et al. (2010).

The instantaneous velocity is strongly correlated with the total in-plane kinetic energy present in the puff: A high total in-plane kinetic energy content correlates to a low puff velocity. It is unclear which of these two quantities is the driving factor and is responsible for the behavior of the other.

For Reynolds numbers below 2100, the length of the puff is found to be independent of Reynolds number *and* the velocity of the puff. The length of the puff has been determined by taking the second order moment of the in-plane kinetic energy distribution. At higher Reynolds numbers ($Re \gtrsim 2100$), the length occasionally shows a dramatic increase. This increase is caused by a small patch of fluid containing velocity fluctuations that was 'shed' from the main puff. At lower Reynolds numbers, the puff is not able to shed these patches and its length remains more or less constant.

In the in-plane kinetic energy distribution, van Doorne and Westerweel (2009) found, in a single

measurement, narrow large-amplitude contributions. By extensively studying the corresponding velocity fields, they deduced that a hairpin vortex was responsible for the generation of these energetic peaks. Since it was a single observation, the dynamics of these structures could not be revealed. De Lozar and Hof (2009) showed the in-plane kinetic energy distribution of two different measurements. Similar peaks were observed, however they were not present at the same location. Therefore it was expected that the structures associated to these peaks did not reside at a fixed location in the puff. Up to now, these peaks were not observed in simulations of transitional pipe flow. In hindsight the resolution in axial direction of the simulations was too low (van Doorne and Westerweel 2009). This was the major motivation to perform the current simulations. In these simulations, the high energetic peaks were also observed. The structures were generated at the trailing edge of the puff and travelled downstream with respect to the puff. Hence, their velocity is higher than the puff velocity. Some persisted for very long times and could travel up to $20D$ before disintegrating. For increasing Reynolds number the velocity of these structures decreases with respect to the bulk velocity. However, the velocity of the puff decreases even faster, hence the velocity of the peaks increases with respect to the puff. The distance covered with respect to the puff is found to be independent of the Reynolds number. The majority of the peaks travel from the upstream side of the puff to the downstream side, by which some survive through the entire puff.

A hairpin vortex, as suggested by van Doorne and Westerweel (2009), was not found to be present near a peak in in-plane kinetic energy. Instead, vortical structures were found with an orientated normal to the pipe axis. They were about one diameter long and aligned along the azimuthal direction.

Up to now it is unclear what the exact driving mechanism of a puff is. Several scenarios are proposed, in which the majority of studies support the idea of Kelvin-Helmholtz type of instabilities generated at the upstream side of the turbulent puff (Shimizu and Kida 2009, Duguet et al. 2010, Hof et al. 2010). However, it remains complicated to deduce the causality of events.

By using a lower resolution it was shown that it is not possible anymore to resolve these very localized structures. The question remains if this has a major impact on the behavior of a turbulent puff. It was already shown that the velocity of the puff is slightly increased by reducing the resolution, which could be related as if a turbulent puff is simulated at a lower Reynolds number. For future work one might use a forcing method to influence the high amplitude peaks in in-plane kinetic energy, in order to assess their significance in the survival of a turbulent puff. If the behavior of the puff changes dramatically, it is clear that it is important to resolve these structures accurately in order to understand long-lived transients of localized turbulence and their sudden disintegration.

Acknowledgments

This thesis reflect a significant part of the work that I did over the past four years at the laboratory for Aero & Hydrodynamics at Delft University of Technology. Although on the cover of this thesis only my name is presented, it would never have been here without the guidance, support and help of a large number of people. It is inevitable that I will forget to mention someone in the list below. To cover for this in advance, I would like to thank you all for your invaluable contributions.

First of all I would like to thank my doctoral advisor professor Jerry Westerweel for giving me the opportunity to pursue a PhD degree. You always gave me the freedom to do any experiments or approach I believed in, which has resulted in a large number of experiments of which the results are not included in this thesis. What I really appreciate is that you always came with plenty of new ideas of how I could advance if I had the feeling I was on a dead end road. In 2008, professor Bruno Eckhardt got appointed a part-time position in the laboratory for Aero & Hydrodynamics. I am very grateful that you were willing to become my doctoral advisor. I always enjoyed the conversations we had during your visits to the laboratory. They have contributed significantly to my understanding of the topic. Thank you for your unbiased views and the structured approach you provided.

Further thanks are due to the scientific staff of the laboratory. I really appreciate the fact that all of you always made time to answer questions. I think it is a unique feature of the Aero & Hydrodynamics laboratory and it is something that should be cherished. Christian Poelma, thank you for returning the endless number of pages I put on your desk and providing me incredibly quickly with feedback. Furthermore I really appreciate your pragmatic approach in solving issues encountered during experiments and with matlab. Regarding the help with any fluid mechanical problem, either theoretical or experimental, I always appreciated the help of René. Although you say that you are very busy, you always make time to explain any problem in a very clear and detailed manner. On the numerics side, I have to thank Bendiks Jan and Mathieu for developing and providing the code for the simulation. Without you chapter 5 of this thesis would not have existed. Of course I should not forget to thank both Wim-Paul and Gerrit.

Doing research in a laboratory is not possible without the great support of technical and administrative staff. Therefore I would like to express my gratitude to, Joop, Cor, Simon, Jasper, Caroline and Ria. A special thank you to Edwin, for the nice discussion during the many hours of experimenting.

Without my roommates, my time at the laboratory would have been completely different. I really enjoyed our discussions and I apologize for the many hours I distracted you from your work. Because of you, Marc, Vincent and Jeanette, our room was the most convivial of the laboratory.

After having a very nice time with Gosse and Marcel in 'de kelder' of Aerospace engineering, it was a pleasant experience being colleagues again. The weekly 'buddy updates' really helped me in the last few months to maintain momentum.

Furthermore, I have to thank the bachelor and master students that chose to do their final theses on pipe flow. Renzo, Frans-Jan, Stefano and Evelien, thank you for your time and effort.

At least as important as the people mentioned up to now are those that contributed to atmosphere in the laboratory. I would like to thank Arnoud, Astrid, Carole, Harmen, Maarten, Marieke, Mark, Norbert, Sebastian, Uli, Valentina and all the PhD students and postdocs that were present during my time at the laboratory. I really liked the discussions at the coffee table, during barbecues and during outings.

I also would like to thank my family and friends for their support during these four years. Finally, I also like to thank Anna Joke, for motivating me during difficult times, for your unconditional support and the enormous amount of fun we had during these years. Words cannot describe how grateful I am. I am looking forward to our future together!

Bibliography

Avila, K., Moxey, D., de Lozar, A., Avila, M., Barkley, D. and Hof, B.: 2011, The onset of turbulence in pipe flow, *Science* **333**, 192–196.

Avila, M., Willis, A. P. and Hof, B.: 2010, On the transient nature of localized pipe flow turbulence, *Journal Of Fluid Mechanics* **646**, 127–136.

Bandyopadhyay, P. R.: 1986, Aspects of the equilibrium puff in transitional pipe-flow, *J. Fluid Mech.* **163**, 439–458.

Barkley, D.: 2011, Simplifying the complexity of pipe flow, *Physical Review E* .

Ben-Dov, G. and Cohen, J.: 2007, Critical reynolds number for a natural transition to turbulence in pipe flows, *Physical Review Letters* **98**(6), 064503.

Borrero-Echeverry, D., Schatz, M. F. and Tagg, R.: 2010, Transient turbulence in taylor-couette flow, *Physical Review E* **81**(2), 025301.

Bottin, S. and Chate, H.: 1998, Statistical analysis of the transition to turbulence in plane couette flow, *European Physical Journal B* **6**(1), 143–155.

Bottin, S., Daviaud, F., Manneville, P. and Dauchot, O.: 1998, Discontinuous transition to spatiotemporal intermittency in plane couette flow, *Europhysics Letters* **43**(2), 171–176.

Brosa, U.: 1989, Turbulence without strange attractor, *Journal Of Statistical Physics* **55**(5-6), 1303–1321.

Coles, D.: 1981, Prospects for useful research on coherent structure in turbulent shear flow, *Sadhana* **4**, 111–127.

Crutchfield, J. P. and Kaneko, K.: 1988, Are attractors relevant to turbulence, *Physical Review Letters* **60**(26), 2715–2718.

Darbyshire, A. G. and Mullin, T.: 1995, Transition to turbulence in constant-mass-flux pipe-flow, *Journal Of Fluid Mechanics* **289**, 83–114.

Dauchot, O. and Daviaud, F.: 1995, Finite-amplitude perturbation and spots growth-mechanism in plane couette-flow, *Physics Of Fluids* **7**(2), 335–343.

Dauchot, O. and Manneville, P.: 1997, Local versus global concepts in hydrodynamic stability theory, *Journal De Physique Ii* **7**(2), 371–389.

De Lozar, A. and Hof, B.: 2009, An experimental study of the decay of turbulent puffs in pipe flow, *Philosophical Transactions Of The Royal Society A-Mathematical Physical And Engineering Sciences* **367**(1888), 589–599.

denToonder, J. M. J. and Nieuwstadt, F. T. M.: 1997, Reynolds number effects in a turbulent pipe flow for low to moderate re, *Physics Of Fluids* **9**(11), 3398–3409.

Draad, A.: 1996, *Laminar-turbulent transition in pipe flow for Newtonian and non-Newtonian fluids.*, PhD thesis, Delft University of Technology.

Drazin, P. and Reid, W.: 2004, *Hydrodynamic Stability*, 2^{nd} edn, Cambridge University Press.

Duguet, Y., Willis, A. P. and Kerswell, R.: 2010, Slug genesis in cylindrical pipe flow., *Journal of Fluid Mechanics* **663**, 180–208.

Duguet, Y., Willis, A. P. and Kerswell, R. R.: 2008, Transition in pipe flow: the saddle structure on the boundary of turbulence, *Journal Of Fluid Mechanics* **613**, 255–274.

Durst, F., Ray, S., Unsal, B. and Bayoumi, O. A.: 2005, The development lengths of laminar pipe and channel flows, *Journal of Fluids Engineering-Transactions Of The Asme* **127**(6), 1154–1160.

Durst, F. and Unsal, B.: 2006, Forced laminar-to-turbulent transition of pipe flows, *Journal Of Fluid Mechanics* **560**, 449–464.

Eckhardt, B. and Schneider, T. M.: 2008, How does flow in a pipe become turbulent?, *European Physical Journal B* **64**(3-4), 457–462.

Eckhardt, B., Schneider, T. M., Hof, B. and Westerweel, J.: 2007, Turbulence transition in pipe flow, *Annual Review Of Fluid Mechanics* **39**, 447–468.

Eggels, J. G. M., Unger, F., Weiss, M. H., Westerweel, J., Adrian, R. J., Friedrich, R. and Nieuwstadt, F. T. M.: 1994, Fully-developed turbulent pipe-flow - a comparison between direct numerical-simulation and experiment, *Journal Of Fluid Mechanics* **268**, 175–209.

Eliahou, S., Tumin, A. and Wygnanski, I.: 1998, Laminar-turbulent transition in poiseuille pipe flow subjected to periodic perturbation emanating from the wall, *Journal Of Fluid Mechanics* **361**, 333–349.

Faisst, H. and Eckhardt, B.: 2003, Traveling waves in pipe flow, *Physical Review Letters* **91**(22), 224502.

Faisst, H. and Eckhardt, B.: 2004, Sensitive dependence on initial conditions in transition to turbulence in pipe flow, *Journal Of Fluid Mechanics* **504**, 343–352.

Gavarini, I.: 2004, *Initial stage of transition and optimal control of streaks in Hagen-Poiseuille flow*, PhD thesis, Delft University of Technology.

Grossmann, S.: 2000, The onset of sheer flow turbulence, *Reviews Of Modern Physics* **72**(2), 603–618.

Hof, B., de Lozar, A., Avila, M., Tu, X. Y. and Schneider, T. M.: 2010, Eliminating turbulence in spatially intermittent flows, *Science* **327**(5972), 1491–1494.

Hof, B., Juel, A. and Mullin, T.: 2003, Scaling of the turbulence transition threshold in a pipe, *Physical Review Letters* **91**(24), 244502.

Hof, B., Lozar, A., Kuik, D. J. and Westerweel, J.: 2008, Repeller or attractor? Selecting the dynamical model for the onset of turbulence in pipe flow, *Physical Review Letters* **101**(21), 214501.

Hof, B., van Doorne, C. W. H., Westerweel, J. and Nieuwstadt, F. T. M.: 2005, Turbulence regeneration in pipe flow at moderate reynolds numbers, *Physical Review Letters* **95**(21), 214502.

Hof, B., van Doorne, C. W. H., Westerweel, J., Nieuwstadt, F. T. M., Faisst, H., Eckhardt, B., Wedin, H., Kerswell, R. R. and Waleffe, F.: 2004, Experimental observation of nonlinear traveling waves in turbulent pipe flow, *Science* **305**(5690), 1594–1598.

Hof, B., Westerweel, J., Schneider, T. M. and Eckhardt, B.: 2006, Finite lifetime of turbulence in shear flows, *Nature* **443**(7107), 59–62.

Hof, B., Westerweel, J., Schneider, T. M. and Eckhardt, B.: 2007, Comment on Willis and Kerswell, *PRL* 98, 014501 (2007)., *ArXiv:0707.2642* .

Huang, L. M. and Chen, T. S.: 1974a, Stability of developing laminar pipe-flow, *Physics Of Fluids* **17**(1), 245–247.

Huang, L. M. and Chen, T. S.: 1974b, Stability of developing pipe-flow subjected to non-axisymmetric disturbances, *Journal Of Fluid Mechanics* **63**(MAR18), 183–193.

Jeong, J. and Hussain, F.: 1995, On the identification of a vortex, *Journal Of Fluid Mechanics* **285**, 69–94.

Kadanoff, L. P. and Tang, C.: 1984, Escape from strange repellers, *Proceedings Of The National Academy Of Sciences Of The United States Of America-Physical Sciences* **81**(4), 1276–1279.

Kerswell, R. R. and Tutty, O. R.: 2007, Recurrence of travelling waves in transitional pipe flow, *Journal Of Fluid Mechanics* **584**, 69–102.

Kuik, D. J., Poelma, C. and Westerweel, J.: 2010, Quantitative measurement of the lifetime of localized turbulence in pipe flow, *Journal Of Fluid Mechanics* **645**, 529–539.

Kundu, P. and Cohen, I.: 2004, *Fluid Mechanics*, 3^{rd} edn, Elsevier Academic Press.

Lagha, M. and Manneville, P.: 2007, Modeling transitional plane couette flow, *European Physical Journal B* **58**(4), 433–447.

Lathrop, D. P.: 2006, Fluid dynamics - turbulence lost in transience, *Nature* **443**(7107), 36–37.

Laufer, J.: 1954, The structure of turbulence in fully developed pipe flow, *NACA Report* **1174**, 1–18.

Leite, R. J.: 1959, An experimental investigation of the stability of poiseuille flow, *Journal Of Fluid Mechanics* **5**(1), 81–&.

Lindgren, E. R.: 1969, Propagation velocity of turbulent slugs and streaks in transition pipe flow, *Physics of Fluids* **12**(2), 418–425.

Mellibovsky, F., Meseguer, A., Schneider, T. M. and Eckhardt, B.: 2009, Transition in localized pipe flow turbulence, *Physical Review Letters* **103**(5), 054502.

Meseguer, A. and Trefethen, L. N.: 2003, Linearized pipe flow to reynolds number 10(7), *Journal Of Computational Physics* **186**(1), 178–197.

Moxey, D. and Barkley, D.: 2010, Distinct large-scale turbulent-laminar states in transitional pipe flow, *Proceedings Of The National Academy Of Sciences Of The United States Of America* **107**(18), 8091–8096.

Mullin, T. and Peixinho, J.: 2006, Transition to turbulence in pipe flow, *Journal of Low Temperature Physics* **145**(1-4), 75–88.

Nishi, M., Unsal, B., Durst, F. and Biswas, G.: 2008, Laminar-to-turbulent transition of pipe flows through puffs and slugs, *Journal of Fluid Mechanics* **614**, 425–446.

Peixinho, J. and Mullin, T.: 2006, Decay of turbulence in pipe flow, *Physical Review Letters* **96**(9), 094501.

Peixinho, J. and Mullin, T.: 2007, Finite-amplitude thresholds for transition in pipe flow, *J. Fluid Mech.* **582**, 169–178.

Pomeau, Y.: 1986, Front motion, metastability and subcritical bifurcations in hydrodynamics, *Physica D* **23**(1-3), 3–11.

Pringle, C. C. T. and Kerswell, R. R.: 2007, Asymmetric, helical, and mirror-symmetric traveling waves in pipe flow, *Physical Review Letters* **99**(7), 074502.

Priymak, V. G. and Miyazaki, T.: 2004, Direct numerical simulation of equilibrium spatially localized structures in pipe flow, *Physics Of Fluids* **16**(12), 4221–4234.

Ptasinski, P.: 2002, *Turbulent flow of polymer solutions near maximum drag reduction*, PhD thesis, Delft University of Technology.

Ptasinski, P. K., Boersma, B. J., Nieuwstadt, F. T. M., Hulsen, M. A., Van den Brule, B. H. A. A. and Hunt, J. C. R.: 2003, Turbulent channel flow near maximum drag reduction: simulations, experiments and mechanisms, *Journal Of Fluid Mechanics* **490**, 251–291.

Reynolds, O.: 1883, An experimental investigation of the circumstances which determine whether the motion of water shall be direct or sinuous, and of the law of resistance in parallel channels, *Philosophical Transactions of the Royal Society of London* **174**, 935–982.

Robert, C., Alligood, K. T., Ott, E. and Yorke, J. A.: 2000, Explosions of chaotic sets, *Physica D-Nonlinear Phenomena* **144**(1-2), 44–61.

Rotta, J.: 1956, Experimenteller Beitrag zur Entstehung turbulenter Strömung im Rohr, *Ingenieur Archiv* **24**, 258–281.

Sarpkaya, T.: 1975, Note on stability of developing laminar pipe-flow subjected to axisymmetric and non-axisymmetric disturbances, *Journal Of Fluid Mechanics* **68**(MAR25), 345–352.

Schlichting, H.: 1968, *Boundary-Layer Theory*, sixth edn, McGraw-Hill.

Schmiegel, A.: 1999, *Transition to turbulence in linearly stable shear flows*, PhD thesis, Philipps Universität Marburg.

Schneider, T. M., Eckhardt, B. and Vollmer, J.: 2007, Statistical analysis of coherent structures in transitional pipe flow, *Physical Review E* **75**(6), 066313.

Schneider, T. M., Eckhardt, B. and Yorke, J. A.: 2007, Turbulence transition and the edge of chaos in pipe flow, *Phys. Rev. Lett.* **99**, 034502–.

Shan, H., Ma, B., Zhang, Z. and Nieuwstadt, F. T. M.: 1999, Direct numerical simulation of a puff and a slug in transitional cylindrical pipe flow, *Journal Of Fluid Mechanics* **387**, 39–60.

Shimizu, M. and Kida, S.: 2008, Structure of a turbulent puff in pipe flow, *Journal Of The Physical Society Of Japan* **77**(11), 114401.

Shimizu, M. and Kida, S.: 2009, A driving mechanism of a turbulent puff in pipe flow, *Fluid Dynamics Research* **41**(4), 045501.

Skufca, J. D., Yorke, J. A. and Eckhardt, B.: 2006, Edge of chaos in a parallel shear flow, *Phys. Rev. Lett.* **96**(17), 174101.

Tatsumi, T.: 1952a, Stability of the laminar inlet-flow prior to the formation of poiseuille regime .1., *Journal Of The Physical Society Of Japan* **7**(5), 489–495.

Tatsumi, T.: 1952b, Stability of the laminar inlet-flow prior to the formation of poiseuille regime .2., *Journal Of The Physical Society Of Japan* **7**(5), 495–502.

Tél, T. and Lai, Y. C.: 2008, Chaotic transients in spatially extended systems, *Physics Reports-Review Section Of Physics Letters* **460**(6), 245–275.

Trefethen, L., Chapman, S., Henningson, D., Meseguer, A., Mullin, T. and Nieuwstadt, F. T. M.: 2000, Threshold amplitudes for transition to turbulence in a pipe, *arxiv:physics/0007092v1* .

van Doorne, C.: 2004, *Stereoscopic PIV on transition in pipe flow*, PhD thesis, Delft University of Technology.

van Doorne, C. W. H. and Westerweel, J.: 2007, Measurement of laminar, transitional and turbulent pipe flow using stereoscopic-piv, *Exp. Fluids* **42**(2), 259–279.

van Doorne, C. W. H. and Westerweel, J.: 2009, The flow structure of a puff, *Philosophical Transactions of The Royal Society A-Mathematical Physical and Engineering Sciences* **367**(1888), 489–507.

Waleffe, F.: 1995, Transition in shear flows - nonlinear normality versus nonnormal linearity, *Physics Of Fluids* **7**(12), 3060–3066.

Wedin, H. and Kerswell, R. R.: 2004, Exact coherent structures in pipe flow: travelling wave solutions, *Journal Of Fluid Mechanics* **508**, 333–371.

Westerweel, J., Draad, A. A., vanderHoeven, J. C. T. and vanOord, J.: 1996, Measurement of fully-developed turbulent pipe flow with digital particle image velocimetry, *Experiments In Fluids* **20**(3), 165–177.

Willis, A. P. and Kerswell, R. R.: 2007a, Critical behavior in the relaminarization of localized turbulence in pipe flow, *Physical Review Letters* **98**(1), 014501.

Willis, A. P. and Kerswell, R. R.: 2007b, Reply to comment on 'Critical behaviour in the relaminarization of localized turbulence in pipe flow', *ArXiv:0707.2684v1* .

Willis, A. P. and Kerswell, R. R.: 2008, Coherent structures in localized and global pipe turbulence, *Phys. Rev. Lett.* **100**, 124501.

Willis, A. P. and Kerswell, R. R.: 2009, Turbulent dynamics of pipe flow captured in a reduced model: puff relaminarization and localized 'edge' states, *Journal Of Fluid Mechanics* **619**, 213–233.

Wu, X. H. and Moin, P.: 2008, A direct numerical simulation study on the mean velocity characteristics in turbulent pipe flow, *Journal Of Fluid Mechanics* **608**, 81–112.

Wygnanski, I. and Champagne, F.: 1973, Transition in a pipe. part 1. origin of puffs and slugs and flow in a turbulent slug, *Journal of Fluid Mechanics* **59**, 281–335.

Wygnanski, I., Sokolov, M. and Friedman, D.: 1975, Transition in a pipe .2. equilibrium puff, *Journal Of Fluid Mechanics* **69**, 283–&.

Curriculum Vitae

October 5, 1981	Born in Franeker, the Netherlands.
1994-2000	Secondary Education (VWO) at 'Dockinga College" in Dokkum
2000-2007	Bachelor and Master of Science in Aerospace Engineering at Delft University of technology. For the final thesis experimental work was done on the turbulent boundary layer. Title of the thesis: "Tomographic PIV investigation of a turbulent boundary layer".
2007-2011	PhD research at the Laboratory for Aero and Hydrodynamics, which is part of the Process & Energy department, faculty of Mechanical, Maritime and Material sciences (3ME), Delft University of Technology.

Appendix A

Derivation of the energy budgets in a cylindrical coordinate system

In this section the derivation of the mean and turbulent kinetic energy is given. The steps involved are very similar to the steps involved in the derivation of the turbulent kinetic energy for fully developed turbulent channel flow. Textbooks are usually limited to channel flow, which allows for using the Navier-Stokes equations in a cartesian coordinate system. Moreover, fully developed flow is often considered since it simplifies the equations tremendously. For localized turbulent pipe flow these assumptions cannot be applied. This is because the mean velocity distribution is not independant of the axial direction.

Unfortunately the full equations for the mean and turbulent kinetic energy in cylindrical coordinates were not found in existing literature.

The following procedure is used to derive the turbulent kinetic energy budget equations:

1. start with the Navier-Stokes equations in cylindrical coordinates
2. apply Reynolds decomposition, i.e. assume the velocities to consist of an average and a fluctuation: $\mathbf{u} = \overline{\mathbf{u}} + \mathbf{u}'$.
3. average the equation to obtain the Reynolds Averaged Navier-Stokes (RANS) equations in cylindrical coordinates.
4. by multiplying each component of the RANS with its mean velocity and adding the equations for each direction, results in the equation for the mean kinetic energy.
5. subtract the RANS from the equation obtained in step 2. Only the fluctuating part remains.
6. multiply each component with the corresponding velocity fluctuation and averaging results in the equation for turbulent kinetic energy in each direction.

7. adding the equations for each direction results in the equation for the turbulent kinetic energy.

In this section not every step is given in detail. As a reference a number of essential equations are given below, starting with the Navier-Stokes equations in cylindrical coordinates. These equations can be found in books that introduce fluid dynamics, e.g. Kundu and Cohen (2004). In the following sections, the RANS equations, the mean kinetic energy equation and the turbulent kinetic energy equations are given. After the full equations are obtained, it is indicated how these equations can be simplified when the flow of a turbulent puff is considered. Finally, the equations are simplified even more to obtain the equations for fully developed turbulent pipe flow, which are identical to the equations given in exisiting literature.

A.0.1 Navier Stokes equation

As a starting point, the Navier-Stokes equations are given below for each velocity component. These equations are given as a reference and can be found in most textbooks introducing fluid dynamics.

For the radial direction:

$$\begin{aligned} \frac{\partial u_r}{\partial t} + u_r\frac{\partial u_r}{\partial r} + \frac{u_\theta}{r}\frac{\partial u_r}{\partial \theta} + u_z\frac{\partial u_r}{\partial z} - \frac{u_\theta^2}{r} = \\ -\frac{1}{\rho}\frac{\partial p}{\partial r} + \nu\left[\frac{1}{r}\frac{\partial}{\partial r}\left(r\frac{\partial u_r}{\partial r}\right) + \frac{1}{r^2}\frac{\partial^2 u_r}{\partial \theta^2} + \frac{\partial^2 u_r}{\partial z^2} - \frac{u_r}{r^2} - \frac{2}{r^2}\frac{\partial u_\theta}{\partial \theta}\right] \end{aligned} \tag{A.1}$$

For the azimuthal direction:

$$\begin{aligned} \frac{\partial u_\theta}{\partial t} + u_r\frac{\partial u_\theta}{\partial r} + \frac{u_\theta}{r}\frac{\partial u_\theta}{\partial \theta} + u_z\frac{\partial u_\theta}{\partial z} + \frac{u_r u_\theta}{r} = \\ -\frac{1}{\rho r}\frac{\partial p}{\partial \theta} + \nu\left[\frac{1}{r}\frac{\partial}{\partial r}\left(r\frac{\partial u_\theta}{\partial r}\right) + \frac{1}{r^2}\frac{\partial^2 u_\theta}{\partial \theta^2} + \frac{\partial^2 u_\theta}{\partial z^2} + \frac{2}{r^2}\frac{\partial u_r}{\partial \theta} - \frac{u_\theta}{r^2}\right] \end{aligned} \tag{A.2}$$

For the axial direction:

$$\begin{aligned} \frac{\partial u_z}{\partial t} + u_r\frac{\partial u_z}{\partial r} + \frac{u_\theta}{r}\frac{\partial u_z}{\partial \theta} + u_z\frac{\partial u_z}{\partial z} = \\ -\frac{1}{\rho}\frac{\partial p}{\partial z} + \nu\left[\frac{1}{r}\frac{\partial}{\partial r}\left(r\frac{\partial u_z}{\partial r}\right) + \frac{1}{r^2}\frac{\partial^2 u_z}{\partial \theta^2} + \frac{\partial^2 u_z}{\partial z^2}\right] \end{aligned} \tag{A.3}$$

A.0.2 Reynolds Averaged Navier Stokes equation

After substituting each velocity component by an average velocity and a fluctuation, i.e. using Reynolds decomposition, the resulting equations are averaged. This results in the Reynolds

Averaged Navier-Stokes equations or RANS. For the radial direction:

$$\begin{aligned}\frac{\partial \overline{u_r}}{\partial t}+\overline{u_r}\frac{\partial \overline{u_r}}{\partial r}+\frac{\overline{u_\theta}}{r}\frac{\partial \overline{u_r}}{\partial \theta}+\overline{u_z}\frac{\partial \overline{u_r}}{\partial z}-\frac{\overline{u_\theta}^2}{r}=\\ -\frac{1}{\rho}\frac{\partial \overline{p}}{\partial r}-\frac{1}{r}\frac{\partial r\overline{u_r'u_r'}}{\partial r}-\frac{1}{r}\frac{\partial \overline{u_r'u_\theta'}}{\partial \theta}-\frac{\partial \overline{u_r'u_z'}}{\partial z}\\ +\frac{\overline{u_\theta'^2}}{r}+\nu\left[\frac{1}{r}\frac{\partial}{\partial r}\left(r\frac{\partial \overline{u_r}}{\partial r}\right)+\frac{1}{r^2}\frac{\partial^2 \overline{u_r}}{\partial \theta^2}+\frac{\partial^2 \overline{u_r}}{\partial z^2}-\frac{\overline{u_r}}{r^2}-\frac{2}{r^2}\frac{\partial \overline{u_\theta}}{\partial \theta}\right]\end{aligned} \tag{A.4}$$

For the azimuthal direction:

$$\begin{aligned}\frac{\partial \overline{u_\theta}}{\partial t}+\overline{u_r}\frac{\partial \overline{u_\theta}}{\partial r}+\frac{\overline{u_\theta}}{r}\frac{\partial \overline{u_\theta}}{\partial \theta}+\overline{u_z}\frac{\partial \overline{u_\theta}}{\partial z}-\frac{\overline{u_r}\,\overline{u_\theta}}{r}=\\ -\frac{1}{\rho r}\frac{\partial \overline{p}}{\partial \theta}-\frac{1}{r}\frac{\partial r\overline{u_r'u_\theta'}}{\partial r}-\frac{1}{r}\frac{\partial \overline{u_\theta'u_\theta'}}{\partial \theta}-\frac{\partial \overline{u_\theta'u_z'}}{\partial z}\\ +\frac{\overline{u_r'u_\theta'}}{r}+\nu\left[\frac{1}{r}\frac{\partial}{\partial r}\left(r\frac{\partial \overline{u_\theta}}{\partial r}\right)+\frac{1}{r^2}\frac{\partial^2 \overline{u_\theta}}{\partial \theta^2}+\frac{\partial^2 \overline{u_\theta}}{\partial z^2}-\frac{\overline{u_\theta}}{r^2}-\frac{2}{r^2}\frac{\partial \overline{u_r}}{\partial \theta}\right]\end{aligned} \tag{A.5}$$

For the axial direction:

$$\begin{aligned}\frac{\partial \overline{u_z}}{\partial t}+\overline{u_r}\frac{\partial \overline{u_z}}{\partial r}+\frac{\overline{u_\theta}}{r}\frac{\partial \overline{u_z}}{\partial \theta}+\overline{u_z}\frac{\partial \overline{u_z}}{\partial z}=\\ -\frac{1}{\rho}\frac{\partial \overline{p}}{\partial z}-\frac{1}{r}\frac{\partial r\overline{u_r'u_z'}}{\partial r}-\frac{1}{r}\frac{\partial \overline{u_\theta'u_z'}}{\partial \theta}-\frac{\partial \overline{u_z'u_z'}}{\partial z}\\ +\nu\left[\frac{1}{r}\frac{\partial}{\partial r}\left(r\frac{\partial \overline{u_z}}{\partial r}\right)+\frac{1}{r^2}\frac{\partial^2 \overline{u_z}}{\partial \theta^2}+\frac{\partial^2 \overline{u_z}}{\partial z^2}\right]\end{aligned} \tag{A.6}$$

A.0.3 Mean kinetic energy equation

Each component of the RANS is multiplied by its mean velocity compenent. After combining the three resulting equations, the equation for the mean kinetic energy is obtained: equation A.7.

$$
\begin{aligned}
&\frac{\partial Q}{\partial t}+\overline{u_r}\frac{\partial Q}{\partial r}+\frac{\overline{u_\theta}}{r}\frac{\partial Q}{\partial \theta}+\overline{u_z}\frac{\partial Q}{\partial z}= \\
&-\frac{1}{\rho}\left(\frac{1}{r}\frac{\partial r\overline{u_r}\,\overline{p}}{\partial r}+\frac{1}{r}\frac{\partial \overline{u_\theta}\,\overline{p}}{\partial \theta}+\frac{\partial \overline{u_z}\,\overline{p}}{\partial z}\right) \\
&-\frac{1}{r}\frac{\partial}{\partial r}r\left(\overline{u_r'u_r'}\overline{u_r}+\overline{u_r'u_\theta'}\overline{u_\theta}+\overline{u_r'u_z'}\overline{u_z}\right) \\
&-\frac{1}{r}\frac{\partial}{\partial \theta}\left(\overline{u_r'u_\theta'}\overline{u_r}+\overline{u_\theta'u_\theta'}\overline{u_\theta}+\overline{u_z'u_\theta'}\overline{u_z}\right) \\
&-\frac{\partial}{\partial z}\left(\overline{u_r'u_z'}\overline{u_r}+\overline{u_\theta'u_z'}\overline{u_\theta}+\overline{u_z'u_z'}\overline{u_z}\right) \\
&+\overline{u_r'u_r'}\frac{\partial \overline{u_r}}{\partial r}+\overline{u_r'u_\theta'}\frac{\partial \overline{u_\theta}}{\partial r}+\overline{u_r'u_z'}\frac{\partial \overline{u_z}}{\partial r} \\
&+\frac{\overline{u_r'u_\theta'}}{r}\frac{\partial \overline{u_r}}{\partial \theta}+\frac{\overline{u_\theta'u_\theta'}}{r}\frac{\partial \overline{u_\theta}}{\partial \theta}+\frac{\overline{u_z'u_\theta'}}{r}\frac{\partial \overline{u_z}}{\partial \theta} \\
&+\overline{u_r'u_z'}\frac{\partial \overline{u_r}}{\partial z}+\overline{u_\theta'u_z'}\frac{\partial \overline{u_\theta}}{\partial z}+\overline{u_z'u_z'}\frac{\partial \overline{u_z}}{\partial z} \\
&+\overline{u_\theta'u_\theta'}\frac{\overline{u_r}}{r}-\overline{u_r'u_\theta'}\frac{\overline{u_\theta}}{r} \\
&+\nu\left[\frac{1}{r}\frac{\partial}{\partial r}\left(r\frac{\partial Q}{\partial r}\right)+\frac{1}{r^2}\frac{\partial^2 Q}{\partial \theta^2}+\frac{\partial^2 Q}{\partial z^2}\right. \\
&-\left\{\left(\frac{\partial \overline{u_r}}{\partial r}\right)^2+\left(\frac{\partial \overline{u_\theta}}{\partial r}\right)^2+\left(\frac{\partial \overline{u_z}}{\partial r}\right)^2\right\} \\
&-\frac{1}{r^2}\left\{\left(\frac{\partial \overline{u_r}}{\partial \theta}\right)^2+\left(\frac{\partial \overline{u_\theta}}{\partial \theta}\right)^2+\left(\frac{\partial \overline{u_z}}{\partial \theta}\right)^2\right\} \\
&-\left\{\left(\frac{\partial \overline{u_r}}{\partial z}\right)^2+\left(\frac{\partial \overline{u_\theta}}{\partial z}\right)^2+\left(\frac{\partial \overline{u_z}}{\partial z}\right)^2\right\} \\
&\left.-\frac{2\overline{u_r}}{r^2}\frac{\overline{u_\theta}}{\partial \theta}+\frac{2\overline{u_\theta}}{r^2}\frac{\overline{u_r}}{\partial \theta}-\left(\frac{\overline{u_r}}{r}\right)^2-\left(\frac{\overline{u_\theta}}{r}\right)^2\right]
\end{aligned}
\tag{A.7}
$$

Here Q is the mean kinetic energy of the flow: $Q=(\overline{u_r}^2+\overline{u_\theta}^2+\overline{u_z}^2)/2$.

Mean kinetic energy equation for a puff

For a turbulent puff the following assumptions are made in order to simplify equation A.7:

- The solution is considered steady state (hence $\partial/\partial t = 0$)
- The flow is considered axisymmetric, without swirl ($\partial/\partial\theta = 0$ & $\overline{u_\theta} = 0$), only for mean quantities.

$$\begin{aligned}
\overline{u_r}\frac{\partial Q}{\partial r} + \overline{u_z}\frac{\partial Q}{\partial z} = &-\frac{1}{\rho}\left(\frac{1}{r}\frac{\partial r\overline{u_r}\,\overline{p}}{\partial r} + \frac{\partial \overline{u_z}\,\overline{p}}{\partial z}\right) \\
&-\frac{1}{r}\frac{\partial}{\partial r}r\left(\overline{u_r'u_r'}\overline{u_r} + \overline{u_r'u_z'}\overline{u_z}\right) - \frac{\partial}{\partial z}\left(\overline{u_r'u_z'}\overline{u_r} + \overline{u_z'u_z'}\overline{u_z}\right) \\
&+\overline{u_r'u_r'}\frac{\partial \overline{u_r}}{\partial r} + \overline{u_r'u_z'}\frac{\partial \overline{u_z}}{\partial r} + \overline{u_r'u_z'}\frac{\partial \overline{u_r}}{\partial z} + \overline{u_z'u_z'}\frac{\partial \overline{u_z}}{\partial z} + \overline{u_\theta'u_\theta'}\frac{\overline{u_r}}{r} \\
&+\nu\left[\frac{1}{r}\frac{\partial}{\partial r}\left(r\frac{\partial Q}{\partial r}\right) + \frac{\partial^2 Q}{\partial z^2}\right. \\
&\left.-\left\{\left(\frac{\partial \overline{u_r}}{\partial r}\right)^2 + \left(\frac{\partial \overline{u_z}}{\partial r}\right)^2 + \left(\frac{\partial \overline{u_r}}{\partial z}\right)^2 + \left(\frac{\partial \overline{u_z}}{\partial z}\right)^2 + \left(\frac{\overline{u_r}}{r}\right)^2\right\}\right]
\end{aligned} \tag{A.8}$$

Mean kinetic energy equation for fully developed turbulent flow

The mean kinetic energy equation obtained for the puff can be simplified even more when considering fully developed turbulent pipe flow. The following assumptions are used to obtain the equation for fully developed turbulent pipe flow:

- statistically the flow does not vary in axial direction ($\partial/\partial z = 0$)
- there is no mean flow in radial direction ($\overline{u_r} = 0$)

$$\begin{aligned}
0 = &-\frac{1}{\rho}\left(\frac{\partial \overline{u_z}\,\overline{p}}{\partial z}\right) - \frac{1}{r}\frac{\partial}{\partial r}r\left(\overline{u_r'u_z'}\overline{u_z}\right) + \overline{u_r'u_z'}\frac{\partial \overline{u_z}}{\partial r} \\
&+\nu\left[\frac{1}{r}\frac{\partial}{\partial r}\left(r\frac{\partial Q}{\partial r}\right) - \left\{\left(\frac{\partial \overline{u_z}}{\partial r}\right)^2 + \left(\frac{\partial \overline{u_z}}{\partial z}\right)^2\right\}\right]
\end{aligned} \tag{A.9}$$

A.0.4 Turbulent kinetic energy equation

A similar procedure is used for the turbulent kinetic energy equation as was used for the mean kinetic energy equation. Only the equation for the turbulent kinetic energy is presented. This equation is obtained by first subtracting the RANS equation for each component from the Navier-Stokes equation in which the Reynolds decomposition is substituted (i.e. $u = \overline{u} + u'$). The resulting equations are then multiplied by the their corresponding velocity fluctuation. After rewriting

this results in the turbulent kinetic energy equation.

$$
\begin{aligned}
\frac{\partial q}{\partial t}+\overline{u_r}\frac{\partial q}{\partial r}+\frac{\overline{u_\theta}}{r}\frac{\partial q}{\partial \theta}+\overline{u_z}\frac{\partial q}{\partial z}= \\
-\frac{1}{\rho}\left(\frac{1}{r}\frac{\partial r\overline{u_r' p'}}{\partial r}+\frac{1}{r}\frac{\partial \overline{u_\theta' p'}}{\partial \theta}+\frac{\partial \overline{u_z' p'}}{\partial z}\right) \\
-\overline{u_r' u_r'}\frac{\partial \overline{u_r}}{\partial r}-\frac{\overline{u_\theta' u_\theta'}}{r}\frac{\partial \overline{u_\theta}}{\partial \theta}-\overline{u_z' u_z'}\frac{\partial \overline{u_z}}{\partial z} \\
-\overline{u_r' u_\theta'}\left(\frac{\partial \overline{u_\theta}}{\partial r}+\frac{1}{r}\frac{\partial \overline{u_r}}{\partial \theta}\right)-\overline{u_r' u_z'}\left(\frac{\partial \overline{u_z}}{\partial r}+\frac{\partial \overline{u_r}}{\partial z}\right) \\
-\overline{u_\theta' u_z'}\left(\frac{1}{r}\frac{\partial \overline{u_z}}{\partial \theta}+\frac{\partial \overline{u_\theta}}{\partial z}\right)+\frac{\overline{u_r' u_\theta'}\,\overline{u_\theta}}{r}-\frac{\overline{u_\theta' u_\theta'}\,\overline{u_r}}{r} \\
-\frac{1}{r}\frac{\partial r\overline{u_r' q}}{\partial r}-\frac{1}{r}\frac{\partial \overline{u_\theta' q}}{\partial \theta}-\frac{\partial \overline{u_z' q}}{\partial z} \\
+\nu\left[\frac{1}{r}\frac{\partial}{\partial r}\left(r\frac{\partial q}{\partial r}\right)+\frac{1}{r^2}\frac{\partial^2 q}{\partial \theta^2}+\frac{\partial^2 q}{\partial z^2}\right. \\
-\left\{\overline{\left(\frac{\partial u_r'}{\partial r}\right)^2}+\overline{\left(\frac{\partial u_\theta'}{\partial r}\right)^2}+\overline{\left(\frac{\partial u_z'}{\partial r}\right)^2}\right\} \\
-\frac{1}{r^2}\left\{\overline{\left(\frac{\partial u_r'}{\partial \theta}\right)^2}+\overline{\left(\frac{\partial u_\theta'}{\partial \theta}\right)^2}+\overline{\left(\frac{\partial u_z'}{\partial \theta}\right)^2}\right\} \\
-\left\{\overline{\left(\frac{\partial u_r'}{\partial z}\right)^2}+\overline{\left(\frac{\partial u_\theta'}{\partial z}\right)^2}+\overline{\left(\frac{\partial u_z'}{\partial z}\right)^2}\right\} \\
\left.-\frac{\overline{2u_r'}}{r^2}\frac{\partial u_\theta'}{\partial \theta}+\frac{\overline{2u_\theta'}}{r^2}\frac{\partial u_r'}{\partial \theta}-\frac{\overline{u_r' u_r'}}{r^2}-\frac{\overline{u_\theta' u_\theta'}}{r^2}\right]
\end{aligned}
\tag{A.10}
$$

Here q is the turbulent kinetic energy: $q=\left(\overline{u_r'^2}+\overline{u_\theta'^2}+\overline{u_z'^2}\right)/2$

Turbulent kinetic energy equation for a puff

By applying the same assumptions given in appendix A.0.3, the turbulent kinetic energy relation reduces to:

$$\begin{aligned}
\overline{u_r}\frac{\partial q}{\partial r}+\overline{u_z}\frac{\partial q}{\partial z} &= -\frac{1}{\rho}\left(\frac{1}{r}\frac{\partial r\overline{u_r' p'}}{\partial r}+\frac{\partial \overline{u_z' p'}}{\partial z}\right) \\
-\overline{u_r' u_r'}\frac{\partial \overline{u_r}}{\partial r}-\overline{u_z' u_z'}\frac{\partial \overline{u_z}}{\partial z}-\overline{u_r' u_z'}\left(\frac{\partial \overline{u_z}}{\partial r}+\frac{\partial \overline{u_r}}{\partial z}\right)&-\frac{\overline{u_\theta' u_\theta'}\,\overline{u_r}}{r} \\
-\frac{1}{r}\frac{\partial r\overline{u_r' q}}{\partial r}-\frac{\partial \overline{u_z' q}}{\partial z}+\nu\left[\frac{1}{r}\frac{\partial}{\partial r}\left(r\frac{\partial q}{\partial r}\right)\right.&+\frac{\partial^2 q}{\partial z^2} \\
-\left\{\overline{\left(\frac{\partial u_r'}{\partial r}\right)^2}+\overline{\left(\frac{\partial u_\theta'}{\partial r}\right)^2}+\overline{\left(\frac{\partial u_z'}{\partial r}\right)^2}\right\}& \\
-\frac{1}{r^2}\left\{\overline{\left(\frac{\partial u_r'}{\partial \theta}\right)^2}+\overline{\left(\frac{\partial u_\theta'}{\partial \theta}\right)^2}+\overline{\left(\frac{\partial u_z'}{\partial \theta}\right)^2}\right\}& \\
-\left\{\overline{\left(\frac{\partial u_r'}{\partial z}\right)^2}+\overline{\left(\frac{\partial u_\theta'}{\partial z}\right)^2}+\overline{\left(\frac{\partial u_z'}{\partial z}\right)^2}\right\}& \\
\left.-\overline{\frac{2u_r'}{r^2}\frac{\partial u_\theta'}{\partial \theta}}+\overline{\frac{2u_\theta'}{r^2}\frac{\partial u_r'}{\partial \theta}}-\overline{\frac{u_r' u_r'}{r^2}}-\overline{\frac{u_\theta' u_\theta'}{r^2}}\right]&
\end{aligned} \tag{A.11}$$

This equation is almost identical to the equation given by Wygnanski et al. (1975), equation A.11 contains two viscous dissipation terms that were not given by Wygnanski et al. (1975). These terms are: $\overline{\frac{2u_r'}{r^2}\frac{\partial u_\theta'}{\partial \theta}}$ and $\overline{\frac{2u_\theta'}{r^2}\frac{\partial u_r'}{\partial \theta}}$. It is unclear why these terms were neglected by Wygnanski et al. (1975).

Turbulent kinetic energy equation for fully developed turbulent flow

When the same assumptions are applied to the turbulent kinetic energy relation as was done for the mean kinetic energy relation in section A.0.3, the turbulent kinetic energy relation reduces

too.

$$\begin{aligned} 0 = & -\frac{1}{\rho}\left(\frac{1}{r}\frac{\partial r\overline{u_r' p'}}{\partial r} + \right) \\ & -\overline{u_r' u_z'}\frac{\partial \overline{u_z}}{\partial r} \\ -\frac{1}{r}\frac{\partial r\overline{u_r' q}}{\partial r} + \nu\left[\frac{1}{r}\frac{\partial}{\partial r}\left(r\frac{\partial q}{\partial r}\right) + \right. & -\left\{\overline{\left(\frac{\partial u_r'}{\partial r}\right)^2} + \overline{\left(\frac{\partial u_\theta'}{\partial r}\right)^2} + \overline{\left(\frac{\partial u_z'}{\partial r}\right)^2}\right\} \\ & -\frac{1}{r^2}\left\{\overline{\left(\frac{\partial u_r'}{\partial \theta}\right)^2} + \overline{\left(\frac{\partial u_\theta'}{\partial \theta}\right)^2} + \overline{\left(\frac{\partial u_z'}{\partial \theta}\right)^2}\right\} \\ & -\left\{\overline{\left(\frac{\partial u_r'}{\partial z}\right)^2} + \overline{\left(\frac{\partial u_\theta'}{\partial z}\right)^2} + \overline{\left(\frac{\partial u_z'}{\partial z}\right)^2}\right\} \\ & \left. -\overline{\frac{2u_r'}{r^2}\frac{\partial u_\theta'}{\partial \theta}} + \overline{\frac{2u_\theta'}{r^2}\frac{\partial u_r'}{\partial \theta}} - \overline{\frac{u_r' u_r'}{r^2}} - \overline{\frac{u_\theta' u_\theta'}{r^2}}\right] \end{aligned} \tag{A.12}$$

This equation is identical to the equation given for fully developed turbulent pipe flow by Laufer (1954).

Names for each term

Convection Term:

$$\overline{u_r}\frac{\partial q}{\partial r} + \overline{u_z}\frac{\partial q}{\partial z} = \tag{A.13}$$

Pressure diffusion term (VPG):

$$-\frac{1}{\rho}\left(\frac{1}{r}\frac{\partial r\overline{u_r' p'}}{\partial r} + \frac{\partial \overline{u_z' p'}}{\partial z}\right) \tag{A.14}$$

Production term (PR):

$$-\overline{u_r' u_r'}\frac{\partial \overline{u_r}}{\partial r} - \overline{u_z' u_z'}\frac{\partial \overline{u_z}}{\partial z} - \overline{u_r' u_z'}\left(\frac{\partial \overline{u_z}}{\partial r} + \frac{\partial \overline{u_r}}{\partial z}\right) - \frac{\overline{u_\theta' u_\theta'}\overline{u_r}}{r} \tag{A.15}$$

Turbulent diffusion terms (TD):

$$-\frac{1}{r}\frac{\partial r\overline{u_r' q}}{\partial r} - \frac{\partial \overline{u_z' q}}{\partial z} \tag{A.16}$$

Visous diffusion term (VD):

$$+\nu\left[\frac{1}{r}\frac{\partial}{\partial r}\left(r\frac{\partial q}{\partial r}\right) + \frac{\partial^2 q}{\partial z^2}\right. \tag{A.17}$$

Viscous dissipation term (DS)

$$\begin{aligned}
&-\left\{\overline{\left(\frac{\partial u_r'}{\partial r}\right)^2}+\overline{\left(\frac{\partial u_\theta'}{\partial r}\right)^2}+\overline{\left(\frac{\partial u_z'}{\partial r}\right)^2}\right\}\\
&-\frac{1}{r^2}\left\{\overline{\left(\frac{\partial u_r'}{\partial \theta}\right)^2}+\overline{\left(\frac{\partial u_\theta'}{\partial \theta}\right)^2}+\overline{\left(\frac{\partial u_z'}{\partial \theta}\right)^2}\right\}\\
&-\left\{\overline{\left(\frac{\partial u_r'}{\partial z}\right)^2}+\overline{\left(\frac{\partial u_\theta'}{\partial z}\right)^2}+\overline{\left(\frac{\partial u_z'}{\partial z}\right)^2}\right\}\\
&\left.-\overline{\frac{2u_r'}{r^2}\frac{\partial u_\theta'}{\partial \theta}}+\overline{\frac{2u_\theta'}{r^2}\frac{\partial u_r'}{\partial \theta}}-\overline{\frac{u_r'u_r'}{r^2}}-\overline{\frac{u_\theta'u_\theta'}{r^2}}\right]
\end{aligned} \tag{A.18}$$

Some general comments on the equations

First of all, when these equations were derived, the definition of the averaging operator is not stated. If the averaging operator means a time average, then obviously the result is that the time derivative of the average velocity distribution is equal to zero by definition. However, a different averaging operation can be defined as long as it complies to the following definitions and rules. A bar above the variable, or collection of variables, indicate an averaging operation. In the following equations, α is a constant, f and g are velocity components, n can either be a spacial direction or a temporal indication.

- $\overline{\alpha f}=\alpha\overline{f}$
- $\overline{\overline{f}}=\overline{f}$
- $\overline{f+g}=\overline{f}+\overline{g}$
- $\overline{f\overline{g}}=\overline{f}\,\overline{g}$
- $\overline{\partial f/\partial n}=\partial\overline{f}/\partial n$
- $\overline{\int f\,\mathrm{d}n}=\int\overline{f}\,\mathrm{d}n$
- $\overline{f-\overline{f}}=0$